Michael S. Triantafyllou
Antoine Bliek
Hyunkyoung Shin

Static and Fatigue Analysis of Multi-leg Mooring System

MIT Sea Grant
College Program

Massachusetts
Institute of Technology
Cambridge, MA 02139

MITSG 86-21

Static and Fatigue Analysis of Multi-leg Mooring System

Report No: MITSG 86-21

Michael S. Triantafyllou: Associate Professor
Antoine Bliek: Post-doctoral Associate
Hyunkyoung Shin: Graduate Student

Massachusetts Institute of Technology
Cambridge, Massachusetts

Table of Contents

List of Figures

List of Tables

Acknowledgments

This research was supported by the M.I.T. Sea Grant Program through the National Oceanic and Atmospheric Administration in the U.S. Department of Commerce and a consortium of companies including Chevron Oil Field Research Co., Conoco Inc., Exxon Production Research Co., and Shell Development Company.

The authors are indebted to the representatives of the offshore companies, Dr. Dirceu L. Botelho and Mr. Paul Aagaart of Chevron; Dr. Peter Wybro, Dr.Richard Van Hoof, Mr. Paul Erb and Dr. Joao de Oliveira of Conoco; Dr. Constantine G. Caracostis of Shell; and Dr. W. C. Kan and Dr. Pejarer of Exxon, who discussed the project of the research, offered suggestions and shared their experience, and information that was available to them

Authors ;

The authors are all affiliated with the M.I.T. Department of Ocean Engineering and held the following positions of the time this report was completed

Michael S. Triantafyllou, Associate Professor

Antoine Bliek, post-Doctoral Associate [now with Shell, Holland]

Hyunkyoung Shin, Graduate Student

1. INTRODUCTION

The present report describes all theoretical developments for evaluating the fatigue life of multi-leg mooring systems. The project was supported by the MIT Sea Grant Program and a consortium of offshore companies consisting of Chevron Oil Field Research Co., Conoco Inc., Exxon Production Research Co. and Shell Development Company. The study was a continuation of a previous year's effort [Triantafyllou 86] during which the statics and dynamics of a moring line were studied in detail.

One of the major developments of the previous year effort [Triantafyllou 86] was the discovery of the mechanism creating very large dynamic tensions in deeper water mooring systems: It was found that the fluid drag exerts such a large lateral restraint to a vibrating cable that externally imposed motions, particularly along the tangential direction, are accommodated almost entirely by stretching, which in turn causes very high dynamic tensions with imposed displacements only of the order of a few feet.

This development drew our attention to the fact that the quasi-static approach, as described for example in the American Petroleum Institute (A.P.I.) rules for spread mooring systems [API 84a], becomes increasingly inapplicable in deeper waters, since the dynamic tension, although caused by small amplitude motions, is as important as the quasi-static tension caused by the large amplitude, slowly varying excursions of the vessel. This is due to the fact that the dynamic tension is caused by stretching, which involves the very large elastic stiffness, while the static tension is caused by readjustment of the cable configuration, i.e. involving its catenary stiffness, which is by orders of magnitude smaller than the elastic stiffness [Triantafyllou 85].

The possibility of a direct failure of the cable always exists therefore in deeper water, if the cable is designed only on the basis of quasi-static criteria. Safety factors may or may not eliminate this danger, since the mechanism of dynamic tension is more or less irrelevant to quasi-static considerations.

What is even more important, however, is the distinct possibility for *cable fatigue*,

given the large, fast varying tension variations. This need for efficiently assessing the fatigue life of cables led to the present study and the development of the cable fatigue methodology. The developments of the present, second phase of the study were based to a major degree on the previous phase results, providing very efficient computer procedures as described in the sequel.

One major decision was made at the beginning of the study: The drag nonlinearity was to be linearized stochastically and the cable dynamic code was to employ frequency domain techniques by iterating with respect to the nonlinear drag effect until convergence was achieved. Substantial time was devoted to compare the predictions of this procedure with a fully nonlinear, time-domain methodology derived during the previous phase of this study. This decision led to the development of very efficient computationally methods to treat the very complex problem of long term cable fatigue.

2. Overview of Static and Dynamic Analysis for Multi-Leg Systems

2.1 Introduction

Solution methods in the frequency domain for the danamic response of a mooring line, are reviewed to provide the basis for good understanding of the complex behaviour of multi-leg mooring systems [Bliek 84], [Shin 85] and [Triantafyllou 86].

In this chapter, all the theoretical and practical procedures necessary to develop a multi-leg system analysis method are studied. We pay also particular attention to the statics of multi-leg systems, using as basic tool the single line statics, which was studied in the previous year's effort [Triantafyllou 86].

2.2 Review - Solution Methods in the Frequency Domain for a Single Cable

2.2.1 Nonlinear Dynamic Equations

The dynamic equations, obtained from the dynamic equilibrium of forces acting on a mooring line in the moving coordinate system (x,y), including the nonlinear hydrodynamic forces are as follows :

$$m\left[\frac{\partial v_t}{\partial t} - v_n \frac{\partial \phi}{\partial t}\right] = \frac{\partial T_e}{\partial s} - w_0 \sin\phi + F_t$$

$$m\left[\frac{\partial v_n}{\partial t} + v_t \frac{\partial \phi}{\partial t}\right] = T_e \frac{\partial \phi}{\partial s} - w_0 \cos\phi + F_n - m_a \frac{\partial v_n}{\partial t} \qquad (2.1)$$

with :

$$F_t = 0.5\,\pi\,\rho_w\,C_{Dt}\,D_0\,(U\cos\phi - v_t)\,|\,U\cos\phi - v_t\,|\,(1+e/2)$$

$$F_n = 0.5\,\rho_w\,C_{Dt}\,D_0\,(-U\sin\phi - v_n)\,|-U\sin\phi - v_n\,|\,(1+e/2)$$

$$v_t = \frac{\partial p}{\partial t} \cos \phi_1 + \frac{\partial q}{\partial t} \sin \phi_1$$

$$v_n = -\frac{\partial p}{\partial t} \sin \phi_1 + \frac{\partial q}{\partial t} \cos \phi_1$$

where :

m = Mass per unit unstretched length

m_a = Added mass per unit unstretched length

T_e = Effective tension

e = Strain

p = Tangential displacement relative to the static configuration

q = Normal displacement relative to the static configuration

v_t = Tangential velocity of cable in the moving coordinate system

v_n = Normal velocity of cable in the moving coordinate system

ϕ = Angle between horizontal line and cable ($\phi = \phi_0 + \phi_1$)

ϕ_1 = Dynamic angle

ϕ_0 = Static angle

F_t = Tangential drag force

F_n = Normal drag force

The compatibility equations for the mooring lines must be satisfied. :

$$\frac{\partial v_t}{\partial s} - \frac{\partial \phi}{\partial s} v_n = \frac{\partial e}{\partial t}$$

$$\frac{\partial v_n}{\partial s} + \frac{\partial \phi}{\partial s} v_t = (1+e) \frac{\partial \phi}{\partial t} \qquad (2.2)$$

Finally, a constitutive equation for the cable must be added :

$$T_e = f(e, \frac{\partial e}{\partial t}, s) \tag{2.3}$$

Equations (2.1), (2.2) and (2.3) constitute the complete set of the nonlinear two-dimensional dynamic equations (5 equations with 5 unknowns).

An important simplification of the dynamic problem is obtained when the solution is assumed to consist of a quasi-static part, which is slowly varying in time and represents a change in the mean configuration of the mooring line, and a dynamic part, which constitutes small harmonic oscillations around the mean position. The governing equations can then be separated in nonlinear static and linearized dynamic equations. In this section, we investigate the linearization of the nonlinear dynamic equations

2.2.2 Linearization

We derive the equations governing the dynamics of small deviations (p,q) from the static configuration along the tangential and normal directions respectively, by expanding the set of nonlinear equations (2.1), (2.2) and (2.3) written in the moving coordinate system about the static configuration and neglecting higher order terms, i.e. we set :

$$T_e = T_0 + T_1 \tag{2.4}$$

$$\phi = \phi_0 + \phi_1$$

Finally, we obtain the following set of equations in the (p,q) coordinate system :

$$m \frac{\partial^2 p}{\partial t^2} = \frac{\partial T_1}{\partial s} + F_{t1} - T_0 \frac{d\phi_0}{ds} \phi_1$$

$$M \frac{\partial^2 q}{\partial t^2} = \frac{d\phi_0}{ds} T_1 + \frac{\partial \phi_1}{\partial s} T_0 + F_{n1} + \frac{dT_0}{ds} \phi_1$$

$$\frac{\partial p}{\partial s} - q \frac{d\phi_0}{ds} = \frac{T_1}{EA} \tag{2.5}$$

$$\frac{\partial q}{\partial s} + p \frac{d\phi_0}{ds} = \phi_1 (1+e_0)$$

with

$$F_{t1} = F_t - F_{t0} \simeq 0$$

$$F_{n1} = F_n - F_{n0}$$

where ; F_{t0} and F_{n0} are static drag forces, respectively

Also it can be shown that the equations for the in-plane dynamics (p,q) including the compatibility equations, are completely decoupled from the equation for the out-of-plane motion (r), for the case of a static two- dimensional configuration. For a proof, see [Bliek 84].

2.2.3 Numerical Solution of the Linearized Problem

The governing equations (2.5) can be solved using numerical methods. The governing equations written in the Fourier domain are:

$$-m\omega^2 p_a = \frac{dT_{1a}}{ds} - T_0 \frac{d\phi_0}{ds} \phi_{1a}$$

$$-M\omega^2 q_a = \frac{d\phi_0}{ds} T_{1a} + \frac{d\phi_{1a}}{ds} T_0 + ib\omega q_a + \frac{dT_0}{ds} \phi_{1a}$$

$$\frac{dp_a}{ds} - q_a \frac{d\phi_0}{ds} = \frac{T_{1a}}{EA} \qquad (2.6)$$

$$\frac{dq_a}{ds} + p_a \frac{d\phi_0}{ds} = \phi_{1a} (1+e_0)$$

where subscript 'a' in the equations denotes the amplitude of the corresponding dynamic quantity.

The problem is reduced to a set of four ordinary differential equations with two boundary conditions at each end.

Different methods can be used to solve the problem numerically. Using the linearity of the equations, shooting techniques can be used to reduce it to an initial value problem, which can be solved by classical integration techniques.

Another possible method is the use of implicit differences, to reduce the problem to a set of linear algebraic equations. Unfortunately, when a realistic grid length is used, the number of equations becomes very large.

An explicit centered difference scheme was selected to solve this problem. The centered difference scheme allows a transfer matrix formulation of the problem. The boundary conditions can easily be handled in this formulation [Keller 69].

The linearized dynamic equations are rewritten in matrix form.

$$\begin{bmatrix} \frac{dT_{1a}}{ds} \\ \frac{d\phi_{1a}}{ds} \\ \frac{dp_a}{ds} \\ \frac{dq_a}{ds} \end{bmatrix} = \begin{bmatrix} 0 & T_0 \frac{d\phi_0}{ds} & -m\omega^2 & 0 \\ -\frac{1}{T_0}\frac{d\phi_0}{ds} & -\frac{1}{T_0}\frac{dT_0}{ds} & 0 & -\frac{(M\omega^2 + ib\omega)}{T_0} \\ \frac{1}{EA} & 0 & 0 & \frac{d\phi_0}{ds} \\ 0 & 1+e_0 & -\frac{d\phi_0}{ds} & 0 \end{bmatrix} \begin{bmatrix} T_{1a} \\ \phi_{1a} \\ p_a \\ q_a \end{bmatrix}$$

where, b is the equivalent damping coefficient.

We rewrite this as:

$$\frac{dy}{ds} = A(s)\, y(s) \tag{2.7}$$

with: $y^T(s) = (T_{1a}\ \phi_{1a}\ p_a\ q_a)$

Using centered differences, the following difference scheme is obtained:

$$y_{i+1} = [I - \frac{\Delta s_{i,i+1}}{2} A(s_{i+1})]^{-1} [I + \frac{\Delta s_{i,i+1}}{2} A(s_i)] y_i$$

$$= B_i y_i \tag{2.8}$$

Due to the fact that the static variables are slowly changing with respect to the spatial coordinate, the difference scheme will give acceptable results, except when the wave length becomes of the same order as the grid length. The overall error is $O(\Delta s^2)$. To find the expression relating the two ends, we can write:

$$y_n = (\prod_{i=1}^{n-1} B_i) y_i \tag{2.9}$$

We write:

$$\prod_{i=1}^{n-1} B_i = \begin{bmatrix} \alpha_{11} & \alpha_{12} \\ \alpha_{21} & \alpha_{22} \end{bmatrix} \tag{2.10}$$

If motions are imposed at the upper end of the cable, the following relation is obtained:

$$\begin{bmatrix} T_{top} \\ \phi_{top} \\ p_{top} \\ q_{top} \end{bmatrix} = \begin{bmatrix} \alpha_{11} & \alpha_{12} \\ \alpha_{21} & \alpha_{22} \end{bmatrix} \begin{bmatrix} T_{bot} \\ \phi_{bot} \\ 0 \\ 0 \end{bmatrix}$$

Therefore,

$$\begin{bmatrix} p_{top} \\ q_{top} \end{bmatrix} = \alpha_{21} \alpha_{11}^{-1} \begin{bmatrix} T_{top} \\ \phi_{top} \end{bmatrix} \tag{2.11}$$

This provides a direct relation between the imposed motions at the top and the

unknown dynamic angle and tension at the top. The matrices α_{11} and α_{21} are obtained from the matrix multiplication

$$\prod_{i=1}^{n-1} B_i$$

These matrices can be calculated explicitly and they are functions of the static quantities, the frequency and the grid length.

The difference scheme can also be used to calculate the dynamic variables along the cable. When the displacements and the dynamic tension and angle at the top are known, the problem is an initial value problem which can be integrated directly.

The eigenfrequencies for the cable can be found by imposing zero motion boundary conditions at the top, and by searching for the frequencies which give the governing equations a non-trivial solution. This can be written according to (2.11) as:

$$\text{Det} [\, \alpha_{21} (\omega)] = 0 \tag{2.12}$$

A search of the roots of (2.12) is done by a root-finding method which locates the eigenfrequencies within a desired accuracy.

2.3 Terminal Impedances

2.3.1 Introduction

The concept of termination impedances has been widely used in the design of guyed masts (See for example [Davenport 65]). In mooring line design, the termination impedances can also be useful. In this section we will discuss some introductory concepts about terminal impedances. This will allow us to calculate the eigenfrequencies and the linear response for multi-leg systems. The concept discussed here is only valid for linear systems. In the case where equivalent drag damping is used, the superposition principle is not valid anymore, so that the combined response can only be obtained by adding the equivalent impedance coefficients with the correct motion for each leg of a multi-leg system.

2.3.2 Terminal Impedances in Two-Dimensions

The upper end of the cable is excited by an externally imposed harmonic motion. The mooring line termination impedances are defined in the following way:

$$\begin{bmatrix} S_{xx}(\omega) & S_{xy}(\omega) \\ S_{yx}(\omega) & S_{yy}(\omega) \end{bmatrix} \begin{bmatrix} x \\ y \end{bmatrix} = \begin{bmatrix} F_x \\ F_y \end{bmatrix} \tag{2.13}$$

where: x: complex amplitude motion, horizontal direction

y: complex amplitude motion, vertical direction

F_x: complex amplitude force, horizontal direction

F_y: complex amplitude force, vertical direction

The resonance frequencies are the poles of the impedance transfer functions. The mooring line admittance matrix can be calculated as the inverse of the impedance matrix. In practical applications, the above transfer matrices can be used to find body motions and dynamic tensions.

At the top of the cable, sinusoidal motions in the x direction and the y direction are imposed. The dynamic forces at the top are obtained as:

$$S_{xx} = [\, T_{11} \cos\phi_o - T_o \sin\phi_o \, \phi_{11} \,]/A_x$$

$$S_{yx} = [\, T_{11} \sin\phi_o + T_o \cos\phi_o \, \phi_{11} \,]/A_x \tag{2.14}$$

where: T_{11}, ϕ_{11} are the dynamic tension and the dynamic angle, respectively, caused by external motion in the x direction

$$S_{xy} = [\, T_{12} \cos\phi_o - T_o \sin\phi_o \, \phi_{12} \,]/A_y$$

$$S_{yy} = [\, T_{12} \sin\phi_o + T_o \cos\phi_o \, \phi_{12} \,]/A_y \tag{2.15}$$

where: T_{12}, ϕ_{12} are the dynamic tension and the dynamic angle, respectively, caused by external motion in the y direction

The dynamic tension at the top due to unit motion in the x or the y direction is also a very important transfer function. It indicates how much dynamic tension is generated in the cable by a unit amplitude motion, and can be used directly in fatigue analysis. The dynamic tension transfer functions are defined as;

$$S_{Tx} = T_{11}/A_x$$

$$S_{Ty} = T_{12}/A_y \qquad (2.16)$$

The solutions of the above equations can be obtained by solving the linearized dynamic equations in the frequency domain. Solutions were obtained by using a finite difference scheme.

2.4 OVERVIEW OF STATIC AND DYNAMIC ANALYSIS FOR MULTI-LEG MOORING SYSTEMS

The principal properties of a mooring line were studied in the previous year's effort as described in [Triantafyllou 86]. In order to develop a multi-leg fatigue analysis methodology the following steps were necessary:

1. Development of a multi-leg static solution handling several multi-segment lines of arbitrary configuration.

2. Development of a stochastic drag linearization methodology for a single line excited at the top in both directions, with random imposed motions of given power spectral density.

3. Development of a statistical methodology to evaluate from calculated power spectra of the dynamic tension the resulting fatigue damage.

The complexity of the overall solution is due to the substantial processing of a large number of input and output data. Indeed, a number of storms must be considered in order to adequately describe the long-term environmental statistical properties. Each

storm is described by a power sea spectrum, prevalent weather direction, current velocity and direction and associated probability of occurrence.

For each storm the power spectrum of the tension is derived, based on the storm characteristics, the six-degree-of freedom Response Amplitude Operators (R.A.O.s) of the moored vessel, and the drift forces acting on the vessel, since these define the slowly varying positions of the vessel, about which the fast varying oscillations will occur.

The vessel is drifting slowly about a position of rest due to wind, current and (especially) the second order wave forces. The subject of wave drift forces is by no means completely understood, especially as to their statistical distribution and magnitude content. As a result, it was deemed appropriate to specify, for each storm, a number of drift force combinations, together with their probability of occurrence, so that one can completely describe the drift force distributrion, without the limitations of a specific theoretical formulation. This increases the computational effort somewhat and requires the preparation of the second order force combinations before hand.

Table 2-1: Required Data for The Moored Vessel

1. Six degree of freedom Response Amplitude Operators (Amplitude and Phase) as a function of frequency and relative wave direction. The operators are input for a number of discrete frequencies and for a number of discrete angles.

2. External loads, including wind loads, current loads and drift forces acting on the vessel for each storm specified. More than one combination can be specified for each storm to adequately describe the statistics of the second order forces. An associated probability of occurrence is required for each drift force combination.

3. Fairlead positions to be used for the multi-leg static program and to evaluate the imposed motions at the end of each mooring line, based on the R.A.O.s of the vessel.

Table 2-2: Required Data for The Mooring Lines

1. Number of mooring lines.

2. Direction of each mooring line relative to a fixed X,Y system.

3. Characteristics of each mooring line: Number of segments. For each segment the unstretched length, weight in water, mass and added mass per unit length, drag and frictional coefficient, drag diameter, Young's modulus, area are required.

4. Pretension for each line. Based on the fairlead positions (vessel data, Table 2-1), the directions of the lines and the static results the anchor positions are fixed and hence the overall mooring characteristics can be derived. One complication is the current whose direction may vary, hence altering the static characteristics of the mooring system from storm to storm.

Table 2-3: Required Data for The Storms

1. Total number of storms for each storm.

2. Probability of occurrence.

3. Significant wave height and modal frequency to describe a Bretschneider spectrum, or alternatively the sea spectrum (point by point) for a discrete set of frequency points.

4. Current direction.

Table 2-4: Required Fatigue Data

1. The coefficients of the S-N curve for each line.

2. If an experimental S-N curve is available, the number of data points in the S-N curve and an S-N data file must be given as input.

2.5 Multi-Leg Static Analysis

The complexity of the multi-leg static problem is due to the nonlinear behavior of each individual line and the effect of current which affects each line differently.

The input required for each line is complicated already, so in a multi-leg case an efficient arrangement of the overall input becomes a necessity. In particular, it makes a substantial computational difference if all lines are identical and the current is zero, versus the (complex) case of having several different lines.

As a result, two different approaches were studied, one to handle identical lines and one to handle completely different lines.

In order to solve for each individual line, we employ the methods developed in the previous phase of the project [Triantafyllou 86]. These methods are very well tested and the algorithms very efficient.

One major assumption is that each static configuration is two- dimensional. For this reason, in the presence of a current only the in-plane component of the current velocity is taken into account. The effect of the out-of-plane current component is very small for metallic lines.

Also, the direct wave load on each line is neglected. Given the large forces transmitted by the vessel on the lines and the exponential decay of the wave loading this assumption is justified for all realistic mooring problems.

The first step in a multi-leg static solution is to position initially the anchors relative to the fairlead positions. This is a very crucial first step because all subsequent solutions are obtained in reference to the position at rest, while the pretensions are fixed for the subsequent static and dynamic analysis.

In order to get the initial position of the system, we should first determine the pretension at the top of each leg (fairlead) and the fixed deployment position of anchors, without external loads and current. The pretensioned position of the multi-leg mooring

system obtained from the static equilibrium condition changes into a different position due to external loads and the effect of the current accompanied by a change in the tension.

Here, the change in static tension is assumed to be a function of only the horizontal distance (l_x) between the anchor position and the fairlead position ($H = H(l_x)$ or $T = T(l_x)$), and the relation between the deviation and external loads represents the stiffness of the multi-leg mooring system. Therefore, the final step of the procedure is to find the spring constants and to derive the functional relation and its derivatives between the horizontal distance l_x and the top tensile force (or top horizontal force).

The differential changes of the total holding loads (equal to the negative of external loads) due to the differential displacements of the system can be obtained easily through the following simple manipulations of derivatives by using the geometry of the system.

2.5.1 The Derivation of The Holding Loads and Spring Constants of Each Leg

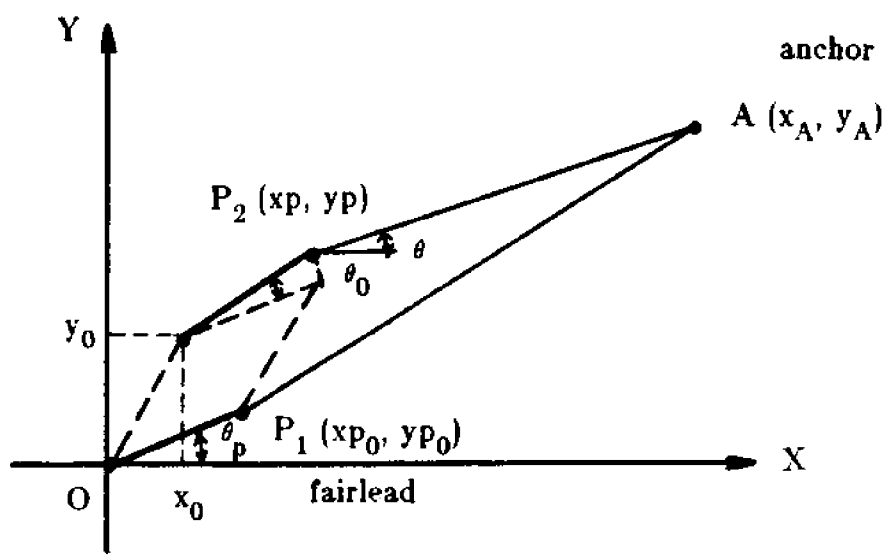

Figure 2-1: Displacement of the Fairlead and the Anchor

The deviation from the initial position of the offshore structure can be expressed by the small vector of motion and rotational angle (x_0, y_0, θ_0) and the resulting fairlead motion from the point P_1 (xp_0, yp_0) to the point P_2 (xp, yp) with respect to the fixed anchor position A (x_A, y_A) can be expressed in terms of this vessel motion. Under the assumption that the holding force in each line is a function of only the horizontal distance from the fairlead to the anchor, we can find the relations $h = h(l_x)$ and the spring constants by using the geometry of each line.

$$
\begin{aligned}
h &= h(l_x) = h[\, l_x(x_0, y_0, \theta_0)\,] \\
f_x &= h \cdot \cos(\theta) \\
f_y &= h \cdot \sin(\theta) \\
rm &= (xp - x_0) \cdot f_y - (yp - y_0) \cdot f_x
\end{aligned}
\tag{2.17}
$$

where :

x_0 = x-component of the displacement of the origin

y_0 = y-component of the displacement of the origin

θ_0 = angle of rotation of OP_1

θ = orientation angle of i-th leg at the moved position

θ_p = angle of OP_1

l_x = the horizontal distance from the fairlead to the anchor

f_x = x-component of the holding force h of i-th leg

f_y = y-component of the holding force h of i-th leg

rm = moment due to the holding force f_x and f_y

From the geometry, we get the following relations:

$$l_x \cos(\theta) = x_A - xp = x_A - x_0 - OP_1 \cos(\theta_p + \theta_0)$$

$$l_x \sin(\theta) = y_A - yp = y_A - y_0 - OP_1 \sin(\theta_p + \theta_0) \tag{2.18}$$

From the equation (2.18), the derivatives are obtained as follows:

$$\frac{\partial}{\partial x_0}(l_x \cos\theta) = \frac{\partial l_x}{\partial x_0}\cos\theta + l_x(-\sin\theta)\frac{\partial\theta}{\partial x_0} = -1$$

$$\frac{\partial}{\partial y_0}(l_x \cos\theta) = \frac{\partial l_x}{\partial x_0}\sin\theta + l_x(\cos\theta)\frac{\partial\theta}{\partial x_0} = 0 \tag{2.19}$$

Therefore,

$$\frac{\partial l_x}{\partial x_0} = -\cos\theta, \qquad \frac{\partial\theta}{\partial x_0} = \frac{\sin\theta}{l_x}$$

Similarly,

$$\frac{\partial l_x}{\partial y_0} = -\sin\theta, \qquad \frac{\partial\theta}{\partial y_0} = \frac{-\cos\theta}{l_x} \tag{2.20}$$

$$\frac{\partial l_x}{\partial\theta_0} = OP_1 \sin(\theta_p + \theta_0 - \theta), \qquad \frac{\partial\theta}{\partial\theta_0} = -\frac{OP_1}{l}\cos(\theta_p + \theta_0 - \theta)$$

The spring constants for the i-th leg are expressed by the following symmetric matrix from equations (2.17) and (2.20):

$$[S]^i = \begin{bmatrix} \frac{\partial f_x}{\partial x_0} & \frac{\partial f_x}{\partial y_0} & \frac{\partial f_x}{\partial\theta_0} \\ \frac{\partial f_y}{\partial x_0} & \frac{\partial f_y}{\partial y_0} & \frac{\partial f_y}{\partial\theta_0} \\ \frac{\partial rm}{\partial x_0} & \frac{\partial rm}{\partial y_0} & \frac{\partial rm}{\partial\theta_0} \end{bmatrix} \tag{2.21}$$

$$S_{11} = -\left(\frac{dh}{dl_x}\cos^2\theta + \frac{h}{l_x}\sin^2\theta\right)$$

$$S_{12} = \left(\frac{h}{l_x} - \frac{dh}{dl_x}\right)\sin\theta\cos\theta$$

$$S_{13} = -OP_1\sin(\theta_p+\theta_0)\frac{\partial f_x}{\partial x_0} + OP_1\cos(\theta_p+\theta_0)\frac{\partial f_x}{\partial y_0}$$

$$S_{21} = \frac{\partial f_x}{\partial y_0} = S_{12}$$

$$S_{22} = -\left(\frac{dh}{dl_x}\sin^2\theta + \frac{h}{l_x}\cos^2\theta\right)$$

$$S_{23} = -OP_1\sin(\theta_p+\theta_0)\frac{\partial f_y}{\partial x_0} + OP_1\cos(\theta_p+\theta_0)\frac{\partial f_y}{\partial y_0}$$

$$S_{31} = \frac{\partial f_x}{\partial \theta_0} = S_{13}$$

$$S_{32} = \frac{\partial f_y}{\partial \theta_0} = S_{23}$$

$$S_{33} = -\left[OP_1\sin(\theta_p+\theta_0)f_y + OP_1\cos(\theta_p+\theta_0)f_x\right]$$
$$\left[OP_1\cos(\theta_p+\theta_0)\frac{\partial f_y}{\partial \theta_0} - OP_1\sin(\theta_p+\theta_0)\frac{\partial f_x}{\partial \theta_0}\right]$$

2.5.2 Spring Constants of the Multi-Leg Mooring System

The spring constants of the whole mooring system are found simply by summing the spring constants of each line.

$$\sum_{i=1}^{N} [S]^i = \begin{bmatrix} \frac{\partial F_x}{\partial x_0} & \frac{\partial F_x}{\partial y_0} & \frac{\partial F_x}{\partial \theta_0} \\ \frac{\partial F_y}{\partial x_0} & \frac{\partial F_y}{\partial y_0} & \frac{\partial F_y}{\partial \theta_0} \\ \frac{\partial RM}{\partial x_0} & \frac{\partial RM}{\partial y_0} & \frac{\partial RM}{\partial \theta_0} \end{bmatrix} \tag{2.22}$$

where : N is the number of lines

$$F_x = \sum_{i=1}^{N} (f_x)_i$$

$$F_y = \sum_{i=1}^{N} (f_y)_i$$

$$RM = \sum_{i=1}^{N} (rm)_i$$

2.5.3 Calculation of the New Position due to External Loads

The relations among external loads, spring constants and the deviations are expressed in the following equations, neglecting higher order terms.

$$F_x = f_1(x,y,\theta) = f_1(x_0,y_0,\theta_0) + \delta\left(\frac{\partial f_1}{\partial x}\right)_0 + \epsilon\left(\frac{\partial f_1}{\partial y}\right)_0 + \gamma\left(\frac{\partial f_1}{\partial q}\right)_0$$

$$F_x = f_2(x,y,\theta) = f_2(x_0,y_0,\theta_0) + \delta\left(\frac{\partial f_2}{\partial x}\right)_0 + \epsilon\left(\frac{\partial f_2}{\partial y}\right)_0 + \gamma\left(\frac{\partial f_2}{\partial q}\right)_0$$

$$RM = f_3(x,y,\theta) = f_1(x_0,y_0,\theta_0) + \delta\left(\frac{\partial f_3}{\partial x}\right)_0 + \epsilon\left(\frac{\partial f_3}{\partial y}\right)_0 + \gamma\left(\frac{\partial f_3}{\partial q}\right)_0$$

$$E_x = -F_x \qquad (2.23)$$

$$E_y = -F_y$$

$$EM = -RM$$

where :

$x = x_0 + \delta$

$y = y_0 + \epsilon$

$\theta = \theta_0 + \gamma$

(x,y,θ) : new position

(x_0,y_0,θ_0) : previous position

From equations (2.22) and (2.23), with known external loads, we can calculate the new position of the offshore structure and the static tension at each line. Usually, the initial position, under pretension only, serves as a starting position for the iterative method which has good convergence qualities. At each intermediate position produced at every iterative step, the spring constants of the whole system are calculated again and the difference between the position at the j-th step and the previous position at the j-1 th step is used in the convergence criterion. Finally, once convergence is achieved. the static tension and the new position which corresponds to the given external loads are calculated.

3. Equivalent Drag Linearization

3.1 Introduction

The core of the overall methodology is the derivation of the spectrum of the dynamic tension for each storm. The difficulties associated with interpreting statistically the output of a nonlinear solution with random input are well known, in particular with respect to estimating the probability of the highest peaks based on a finite time record. An equally important consideration is the computational effort required for sufficiently long simulations, particularly in the present case when the solution must be repeatedly obtained, to derive long-term statistics.

The confidence for using a frequency domain procedure, accounting for the nonlinear drag by using an equivalent linear term and iterating until convergence is achieved, was built from last year's effort [Triantafyllou 86]. Remarkably accurate predictions were achieved in all cases considered. As a result, this approach was followed in constructing the present cable fatigue methodology.

The input for each line is random, but of known spectrum. An extension was necessary, therefore, to derive the equivalent damping coefficient of a cable driven from its upper end in two dimensions randomly, given the spectra and relative correlation of the two random inputs (imposed motions in the x and z directions).

The motions at the fairlead are considered as given by the R.A.O.s of the vessel. This implies that the fastly varying dynamic tension of the lines does not influence significantly the vessel motions. This is indeed the case for all well behaved mooring systems, given the large mass of the vessel. An exception with minor effects is roll, which is influenced by the added damping provided by the mooring lines as they move through water.

The slowly varying motions of the vessel are, of course, substantially influenced by the mooring line tensions, and this is taken fully into account in the present formulation.

In this chapter, therefore, we will show the methodology employed in finding the equivalent damping coefficient to replace the nonlinear drag term, and the iteration scheme needed to converge to the correct result.

This was done in the previous year's effort for monochromatic excitation. Presently this is extended for two random inputs at the top (in the x and z directions respectively) of known spectra and relative correlation.

3.2 Stochastic Linearization of Drag Forces

The drag force plays a major role in the dynamics of mooring lines [Triantafyllou 86]. The drag force is the dominant force on the cable and alters significantly the motions of the cable caused by excitation of the fairlead. The restraining effect on the normal motion causes a build-up of dynamic tension. This increase in dynamic tension is very significant and should be appropriately modeled to obtain accurate tension predictions.

The success of the equivalent linearization in the harmonic case encourages the use of a similar technique for a random excitation at the top. The use of equivalent statistical linearization of the drag forces has been studied extensively in the context of wave forces on a pile. The description of the equivalent drag force will play a major role in the study of the mooring lines under random excitation.

Borgman's work on the subject can be considered the basis for the statistical equivalent linearization [Borgman 65a], [Borgman 65b] and [Borgman 67]. Also, Paulling derived the equivalent drag force in the presence of a current [Paulling 79]. An explicit expression for the drag force in the presence of a current, based on Paulling's formulation, has been given by Triantafyllou [Triantafyllou 82].

3.2.1 Equivalent Linearization of Nonlinear Drag under Random Excitation

The velocity of the mooring line is assumed to be a random function of time and in the presence of a steady current, the relative fluid velocity is assumed to be a Gaussian stationary random process of variance σ and mean value u_0. Then the Gaussian probability density function is the following:

$$u(t) = u_0 + u_1(t) \tag{3.1}$$

$$f_u(\lambda) = \frac{1}{\sigma\sqrt{2\pi}} \exp[-\frac{(\lambda-u_0)^2}{2\sigma^2}] \tag{3.2}$$

Then, $w = u(t)\,|u(t)|$ is a square of the relative velocity and represents the nonlinear drag with an appropriate damping coefficient.

From the density function (3.2), the probability density function of w is obtained and its procedure is given in the following.

First, the cumulative probability function $P_w(\omega)$ is derived. Second, in order to obtain the probaility density function $f_w(\omega)$, we differentiate the cumulative probability function.

$$\begin{aligned} P_w(\omega) &= P[\, w \leq \omega \,] \\ &= P[\, u \leq |\omega|^{1/2} \,] \qquad \text{if } \omega \geq 0 \\ &= P[\, u \leq -|\omega|^{1/2} \,] \qquad \text{if } \omega \leq 0 \end{aligned} \tag{3.3}$$

Therefore,

$$\begin{aligned} P_w(\omega) &= \int_{-\infty}^{\pm|\omega|^{1/2}} f_u(\lambda)\, d\lambda \\ &= \int_{-\infty}^{\pm|\omega|^{1/2}} \frac{1}{\sqrt{2\pi}\sigma} \exp\,[-\frac{(\lambda-u_0)^2}{2\sigma^2}]\, d\lambda \end{aligned} \tag{3.4}$$

$$f_w(\omega) = \frac{dP_w(\omega)}{dw} \tag{3.5}$$

$$= \frac{1}{2|\omega|^{1/2}} \frac{1}{\sqrt{2\pi}\sigma} \exp\left[-\frac{(\,\mathrm{sgn}(\omega)\,|\omega|^{1/2} - u_0\,)^2}{2\sigma^2}\right]$$

where :

$$\mathrm{sgn}(\omega) = 1 \qquad \text{if } \omega \geq 0$$

$$= -1 \qquad \text{if } \omega < 0$$

The drag force is

$$F(t) = C_D\, u(t)|u(t)| \tag{3.6}$$

Its equivalent force can be expressed as the sum of a mean force F_0 plus a time dependent part which is proportional to the velocity $u_1(t)$

$$F_e = F_0 + C_e u_1(t) \tag{3.7}$$

where : $F_0 = C_D\, \overline{u|u|}$

The residue R, which is the difference of the equations (6) and (7), is the following

$$R = F_e - F(t)$$

$$= F_0 + C_e u_1(t) - C_D u(t)|u(t)| \tag{3.8}$$

In order to minimize the mean square of the error between the equivalent drag force and the nonlinear drag force, we differentiate R^2 with respect to the linearized equivalent damping coefficient C_e.

$$\frac{\partial \overline{R^2}}{\partial C_e} = 2F_0\overline{u_1} + 2C_e\overline{u_1^{\,2}} - 2C_D\overline{u_1 u|u|} = 0 \tag{3.9}$$

Since $u_1 = 0$ and $u_1^{\,2} = \sigma^2$, the equivalent damping coefficient

$$C_e = \frac{C_D}{\sigma^2}\,\overline{u_1 u|u|} \tag{3.10}$$

$$= \frac{C_D}{\sigma^2} [\, \overline{u^2|u|} - u_0 \overline{u|u|} \,]$$

According to Paulling [Paulling 79],

$$C_e = \frac{C_D}{\sigma^2} [\, \frac{\sigma^3}{\sqrt{2\pi}} \int_0^\infty \xi^3 \{\exp[-\frac{(\xi-\mu)^2}{2}] + \exp[-\frac{(\xi+\mu)^2}{2}] \} \, d\xi$$

$$- \frac{\sigma^2 u_0}{\sqrt{2\pi}} \int_0^\infty \xi^2 \{\exp[-\frac{(\xi-\mu)^2}{2}] - \exp[-\frac{(\xi+\mu)^2}{2}] \} \, d\xi$$

$$= \frac{1}{\sqrt{8\pi}} \rho_w C_{Dn} D_0 [\, \sigma I_1 - u_0 I_2 \,] \qquad (3.11)$$

where :

$C_D = \frac{1}{2} \rho_w C_{Dn} D_0$

$I_1 =$ the First Integration in Equation (3.11)

$I_2 =$ the Second Integration in Equation (3.11)

$\xi = \frac{\lambda}{\sigma}$

$\mu = \frac{\mu_0}{\sigma}$

Finally,

$$I_1 = \mu I_2 + 2\mu\sqrt{2\pi}\, \mathrm{erf}(\frac{\mu}{\sqrt{2}}) + 4\exp(-\frac{\mu^2}{2})$$

$$I_2 = \sqrt{2\pi}(1+\mu^2)\, \mathrm{erf}(\frac{\mu}{\sqrt{2}}) + 2\mu\exp(-\frac{\mu^2}{2})$$

$$C_e = \sqrt{\frac{2}{\pi}}\,\rho_w C_D D_0\,\sigma\,[\,\exp(-\frac{\mu^2}{2}) + \mu\sqrt{\frac{\pi}{2}}\,\mathrm{erf}(\frac{\mu}{\sqrt{2}})\,] \tag{3.12}$$

where :

$$\mu = \frac{u_0}{\sigma}$$

$$\mathrm{erf}(x) = \frac{2}{\sqrt{\pi}}\int_0^{\infty} e^{-x^2}dx$$

For the case of $u_0 = 0$, we obtain the following expression:

$$C_e = \sqrt{\frac{2}{\pi}}\,\rho_w C_D D_0\,\sigma \tag{3.13}$$

$$= \sqrt{\frac{8}{\pi}}\,\frac{1}{2}\,\rho_w\,C_D\,D_0\,\sigma$$

The application to cables leads to

$$F_d = -\frac{1}{2}\,\rho_w\,C_D\,D_0\,\sqrt{\frac{8}{\pi}}\,\sigma_n\,v_n \tag{3.14}$$

where : v_n is a random normal velocity of the cable and σ is the standard deviation of the normal velocity.

It should be noted here that the linearization theory is based on a random normal velocity. The excitation of the cable, however, is in two directions at the top, each with its own spectrum. As a result, the procedure must be extended to account for a double excitation.

A particular aspect of our problem is that although we have two excitations, they are correlated, because they are the results of the same random input, i.e. the sea elevation.

As a result we can use the procedure outlined in Table 3-3 to achieve equivalent stochastic linearization. We note that the two inputs cause no additional complexity, other than a change in the procedure for iteration. The methodology in Table 3-3 guarantees that the relative phase angle between motions in the x and z directions at the top are taken completely into account.

3.3 Comparison between Stochastic Linearization Results and Nonlinear Simulation Results

Stochastic linearization is achieved by assuming a certain probability density function for the internal variables of the problem. This probability density function for our problem is assumed to be Gaussian.

The assumption of Gaussian distribution has certain limitations for the tension. It is obvious that when the dynamic tension exceeds the value of the static tension, an additional nonlinearity appears, i.e. the enforcement of nonnegative tension by clipping off the large negative peaks. Also, the resulting snap motion may reinforce the positive peaks.

Our findings from investigating realistic mooring configuratins are that the most loaded lines are represented very well by stochastic linearization in most cases, making our fatigue analysis valid. The least loaded lines and extremely rough seas cause peak tensions which may require special treatment, as described in the last chapters of this report.

The basic test, therefore, described herein is that for Gaussian distribution of the tension. In order to consider a realistic mooring case, we considered a semi-submersible in 700 meters of water depth (2,100 ft). The line is wire with $3\frac{1}{2}$ inch diameter, its length is 1,700 m (5,100 ft), the elastic stiffness is EA $= 9.53 \times 10^7$ lb, the drag coefficient is C_n $= 1.2$ and the frictional coefficient has been neglected ($C_t = 0$). The pretension is 157,000 lb.

We studied the dynamic tension in the line when a fairlead random excitation is

imposed in the x-direction only. Figure 3-1 shows the assumed spectrum of the imposed motion, whose standard deviation is 0.628 m (2.06 ft) corresponding roughly to a significant wave height of 2.512 m (8.24 ft).

The dynamic tension was studied by using

- the statistical linearization methodology employing frequency domain techniques

- a fully nonlinear solution for the dynamics of a single line, as described in the first phase of the project [Triantafyllou 86].

Figure 3-2 shows the time trace of the x motion imposed at the cable top, assuming a Gaussian distribution of the motion and using the spectrum of Figure 3-1. The Gaussian assumption is well justified for ship motions. Figure 3-3 shows a detail of Figure 3-2 as an indication of the structure of the input.

Figure 3-4 is the time trace obtained from the nonlinear code for the tension. A detail from Figure 3-4 is shown in Figure 3-5, again to indicate the nature of the response.

Table 3-4 is the statistical analysis of the input motion. The target standard deviation was 0.6286 m and the achieved value in the time realization is 0.6233 m. This is due to the use of a finite record (1050 sec) and the deficiencies of the used pseudo-random number generator to obtain the time realization.

Figure 3-6 compares the normal probability density function (target pdf) with the achieved pdf in the time trace of the x motion shown in Figure 3-2.

The resulting time trace of the tension has a probability density function shown in Figure 3-7, where the normal distribution predicted by the stochastic linearization is also shown. Agreement is very good and it can be said with confidence that for such levels of excitation the tension is normally distributed.

The statistics of the tension trace are shown in Table 3-5 to confirm this result. The predicted standard derivation is

nonlinear program $\sigma = 27{,}925$ N

stochastic linearization $\sigma = 28{,}849$ N

The difference is 3.31%. Actually if it is taken into account that the achieved spectrum of the x motion is slightly lower than the target spectrum (see Figure 3-6), this difference would be actually smaller.

3.4 Comparison between Stochastic and Harmonic Linearization

In both cases of harmonic and stochastic linearization the mean square error between the linear and nonlinear terms is minimized in a certain sense, based on reasonable assumptions.

In the case of harmonic excitation a harmonic response is assumed and the average energy per cycle between the linear and nonlinear terms is minimized.

In the case of stochastic linearization a certain probability density function is assumed for the response (Gaussian in our case) and the variance of the difference between the linear and nonlinear terms is minimized.

The question arises as to whether in the limit the two predictions would agree, i.e. by taking a very narrow band spectrum to have the same prediction from the stochastic linearization and the harmonic response program.

This, although at first seems like a plausible hypothesis, is actually incorrect and it is worth explaining why.

A very narrow band spectrum provides linearizations which resemble the "beat" phenomena. It contains a carrier sinusoidal function of constant frequency equal roughly to the average frequency of the narrow band and the amplitude is modulated from near zero values to a certain maximum value.

Even if we proceed to make the spectrum infinitesimally small in width, but of finite constant area, the realization will always show a modulated time function, i.e. it will never become a perfect, constant amplitude sinusoid.

This is the reason why in a nonlinear solution the predictions using stochastic linearization will never agree with those of a harmonic linearization program. In fact, a constant difference of about 30% will be obtained in the limit: Let C_s denote the equivalent damping coefficient obtained by stochastic linearization and C_h the coefficient obtained for harmonic excitation. If a very narrow band spectrum has variance σ^2, the "equivalent" harmonic has amplitude $\sqrt{2}\,\sigma$, hence, using Table 3-1.

$$\frac{C_s}{C_h} = \sqrt{\frac{8}{\pi}} \Big/ \left(\frac{8}{3\pi}\sqrt{2}\right) = \frac{3}{4}\sqrt{\pi} = 1.33$$

This is important to remember because cross-checking of the two procedures will be always subject to this difference in prediction. Also, the use of a harmonic linearization procedure to obtain an equivalent Response Amplitude Operator (R.A.O.) will be subject to these constraints making the predictions inaccurate.

Table 3-1: Drag Linearization

Approximation:

$$\frac{1}{2}\rho_w C_D D_0 u|u| \simeq F_0(s) + C_e(s) \cdot u$$

where :

ρ_w = water density

C_D = drag coefficient

D_0 = drag diameter

u = cable-fluid relative velocity in the transverse direction
($u=u_0 + u_i(t)$)

$F_0(s)$ = equivalent average force per unit length

$C_e(s)$ = equivalent space dependent damping coefficient

Table 3-1, continued

1. Sinusoidal Response u

$$C_e = \rho_w C_D D_0 \omega q a$$

$$F_0 = \frac{1}{2} \rho_w C_D D_0 \omega^2 q^2 (a^2+1/2) \qquad |a| \geq 1$$

$$C_e = \frac{2}{\pi} \rho_w C_D D_0 \omega q \left[\frac{1}{3}(a^2+2)\sqrt{1-a^2}+a \sin^{-1}a \right]$$

$$F_0 = \frac{1}{\pi} \rho_w C_D D_0 \omega^2 q^2 \left| (a^2+1/2) \sin^{-1}a+ \frac{3}{2} a \sqrt{1-a^2} \right| \qquad |a| < 1$$

where : $a = \frac{u_0 \sin \phi}{\omega q}$

q = amplitude of normal displacement

ϕ = total angle of cable

Table 3-1, concluded

2. Random Response u

$$C_e = \sqrt{\frac{8}{\pi}}\frac{1}{2}\rho_w C_D D_0 \sigma \qquad u_0 = 0$$

$$C_e = \sqrt{\frac{2}{\pi}}\rho_w C_D D_0 \sigma \left[\exp\left(-\frac{\mu^2}{2}\right) + \mu\sqrt{\frac{\pi}{2}}\,\mathrm{erf}\left(\frac{\mu}{\sqrt{2}}\right)\right] \qquad u_0 \neq 0$$

where :

σ = variance of u

u_0 = mean of u

$\mu = u_0/\sigma$

erf(x) = error function of x

$$= \frac{2}{\sqrt{\pi}}\int_0^{\infty} e^{-x^2} dx$$

Table 3-2: Drag Linearization Algorithm for Sinusoidal Input

Excitation at the top

$$x(t) = A \sin(\omega_0 t)$$

$$z(t) = B \sin(\omega_0 t + \psi)$$

where :

A, B = amplitudes of imposed motion in the x,y directions respectively

ω_0 = excitation frequency

ψ = relative phase angle between x and y motions

Table 3-2, concluded

Algorithm

1. Assume an initial damping coefficient b(s) for a discrete set of points s_i along the cable

2. Determine the motion response in the transverse direction at all points s_i, using frequency domain techniques and the damping coefficient b(s)

3. Using the formulae of Table 3-1, determine new damping coefficient b'(s) at all points s_i

4. If $\sum_{i=1}^{N} |b'(s_i) - b(s_i)| < \epsilon$

,where ϵ is the tolerance for accuracy, then convergence has been achieved. Otherwise we employ the new damping b'(s) and proceed to repeat step (2) and so on

Table 3-3: Drag Linearization Algorithm for Random Input

Excitation at the top x(t), z(t) random processes of spectra respectively

$$S_x(\omega) = |H_x(\omega)|^2 S_w(\omega)$$

$$S_z(\omega) = |H_z(\omega)|^2 S_w(\omega)$$

where $H_x(\omega)$, $H_z(\omega)$ the corresponding R.A.O.s of the cable fairlead point, and $S_w(\omega)$ the sea spectrum $S_x(\omega)$, $S_z(\omega)$ are known at a discrete set of frequencies ω_i.

Table 3-3, continued

Algorithm

1. Assume an initial damping coefficient b(s) for a discrete set of points s_i along the cable

2. For each frequency ω_k assume sinusoidal excitation at the top of the form

$$x(t) = H_x(\omega_k)\ e^{i\omega_k t}$$

$$z(t) = H_z(\omega_k)\ e^{i\omega_k t}$$

and determine the transverse velocity at each point s_i, $V(\omega_k,s_i)$, using frequency domain techniques and the damping coefficient b(s).

3. At eah point s_i find the spectrum of the transverse velocity

$$S_{v_i}(\omega_k) = |v(\omega_k,s_i|)^2\ S_w(\omega_k)$$

and hence the variance at each point s_i by numerically integrating the spectrum $S_{v_i}(\omega_k)$ with respect to the frequency

4. Using the results of Table 3-1, find at each point s_i the new damping coefficient $b'(s_i)$ based on the variance $\sigma_{V_i}^2$

5. If $\sum_{i=1}^{N} |b'(s_i)-b(s_i)| < \epsilon$

where ϵ is the tolerance for accuracy, then convergence has been achieved. Otherwise we employ the new damping b'(s) and proceed to repeat step (2) and so on.

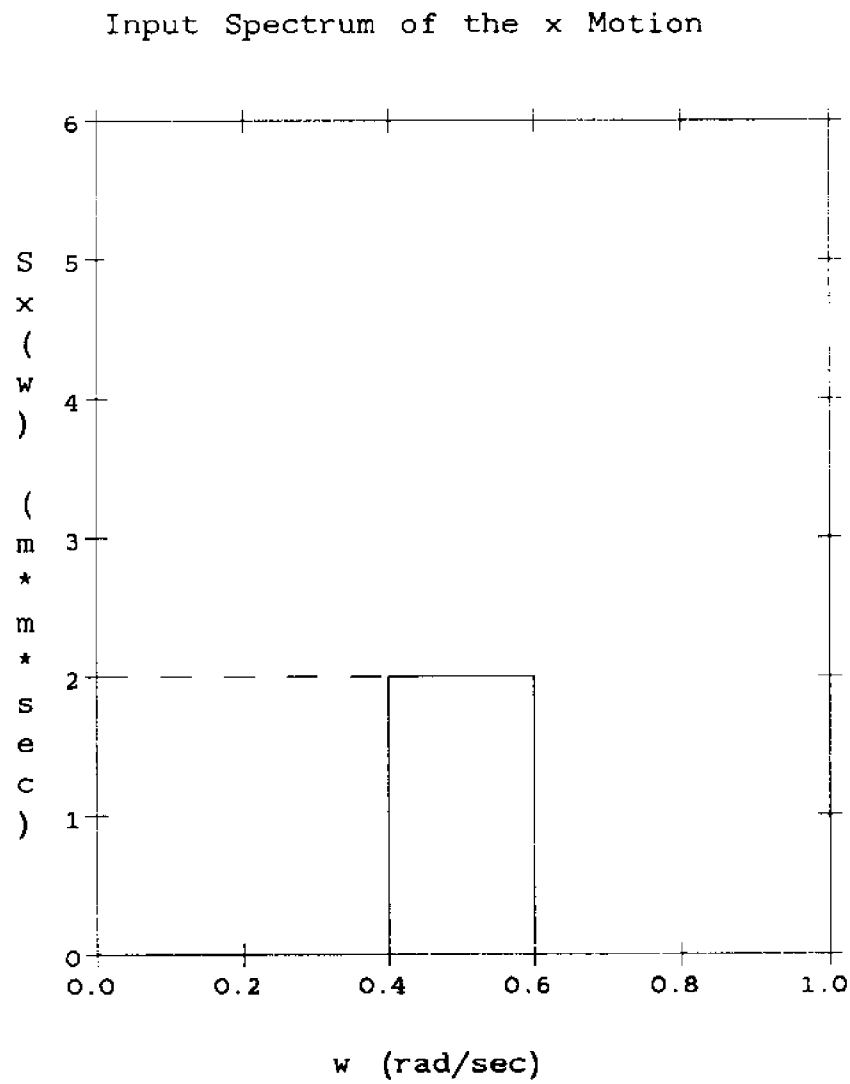

Figure 3-1: Input Spectrum of the x Motion

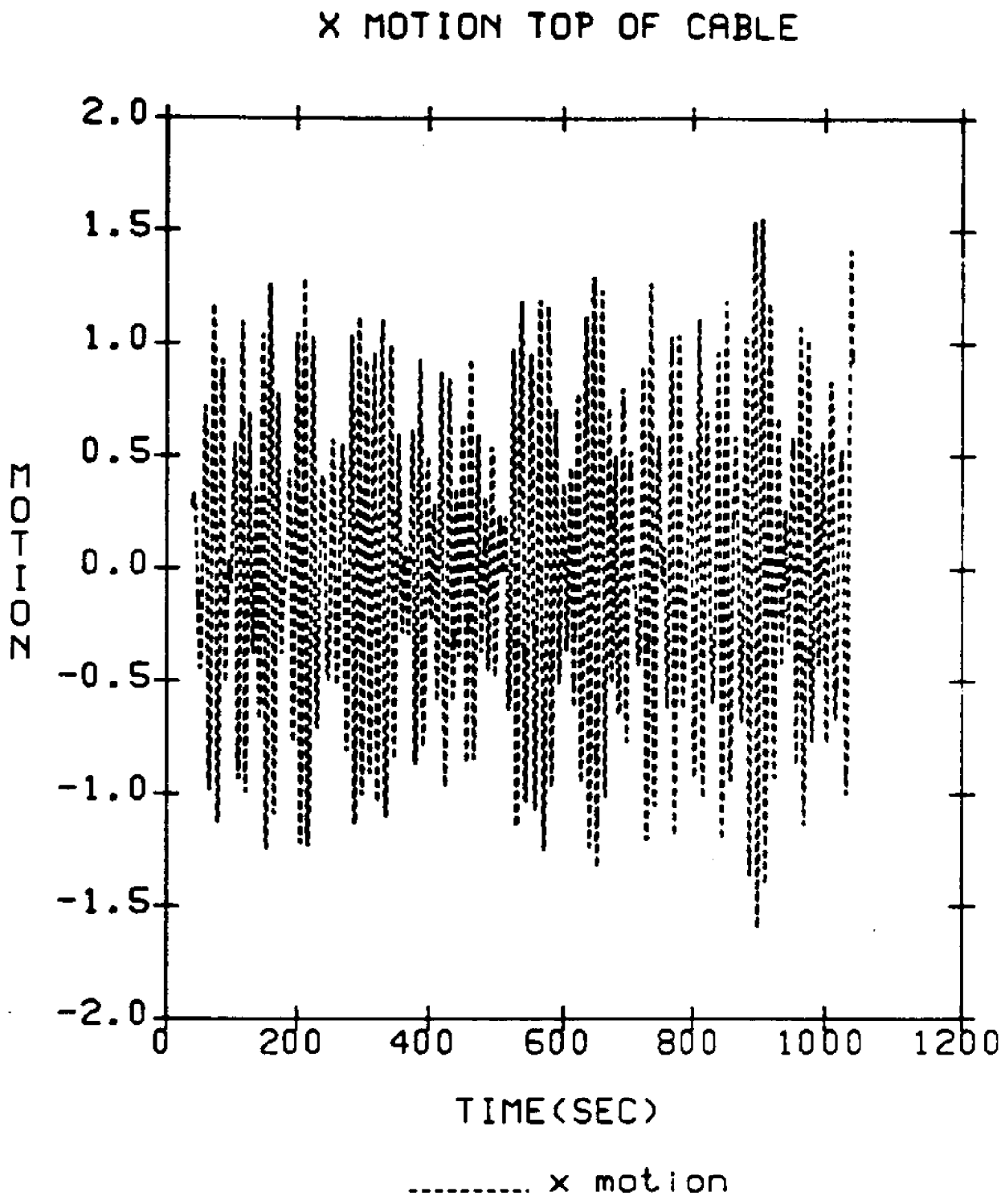

Figure 3-2: Time realization of the x Motion

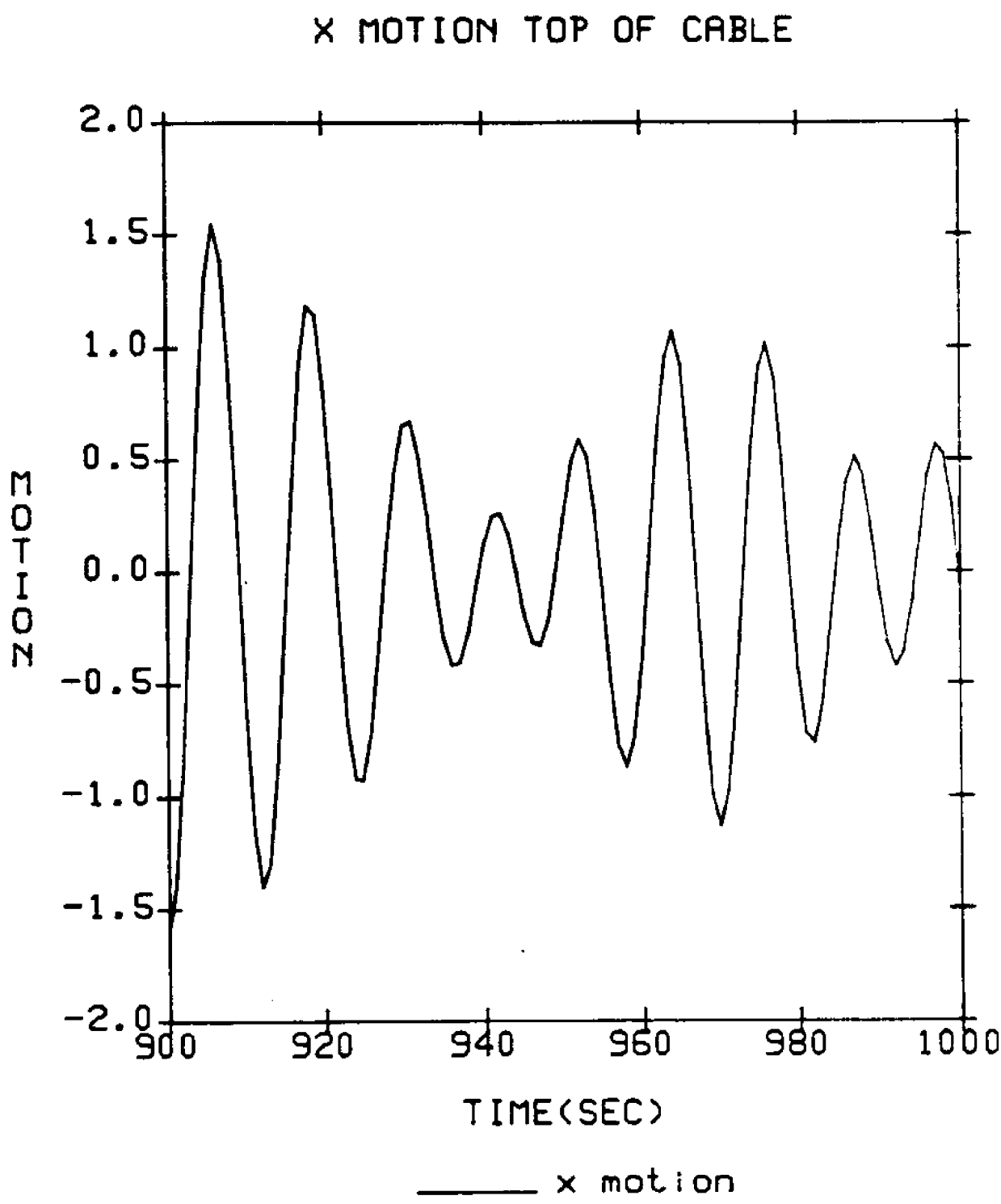

Figure 3-3: Detail of Figure 3-2

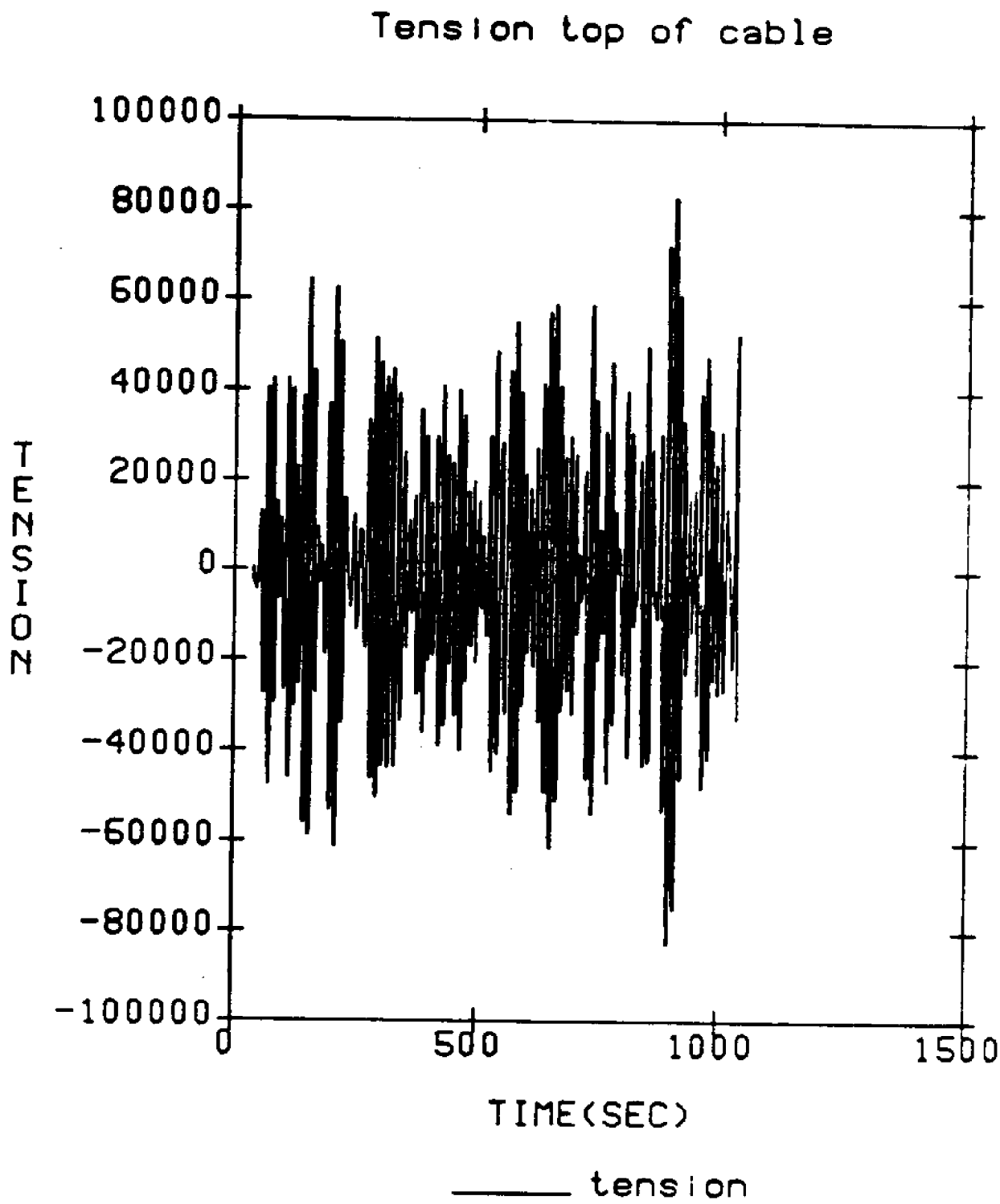

Figure 3-4: Time Trace of Dynamic Tension as Obtained from the Nonlinear Simulation Program

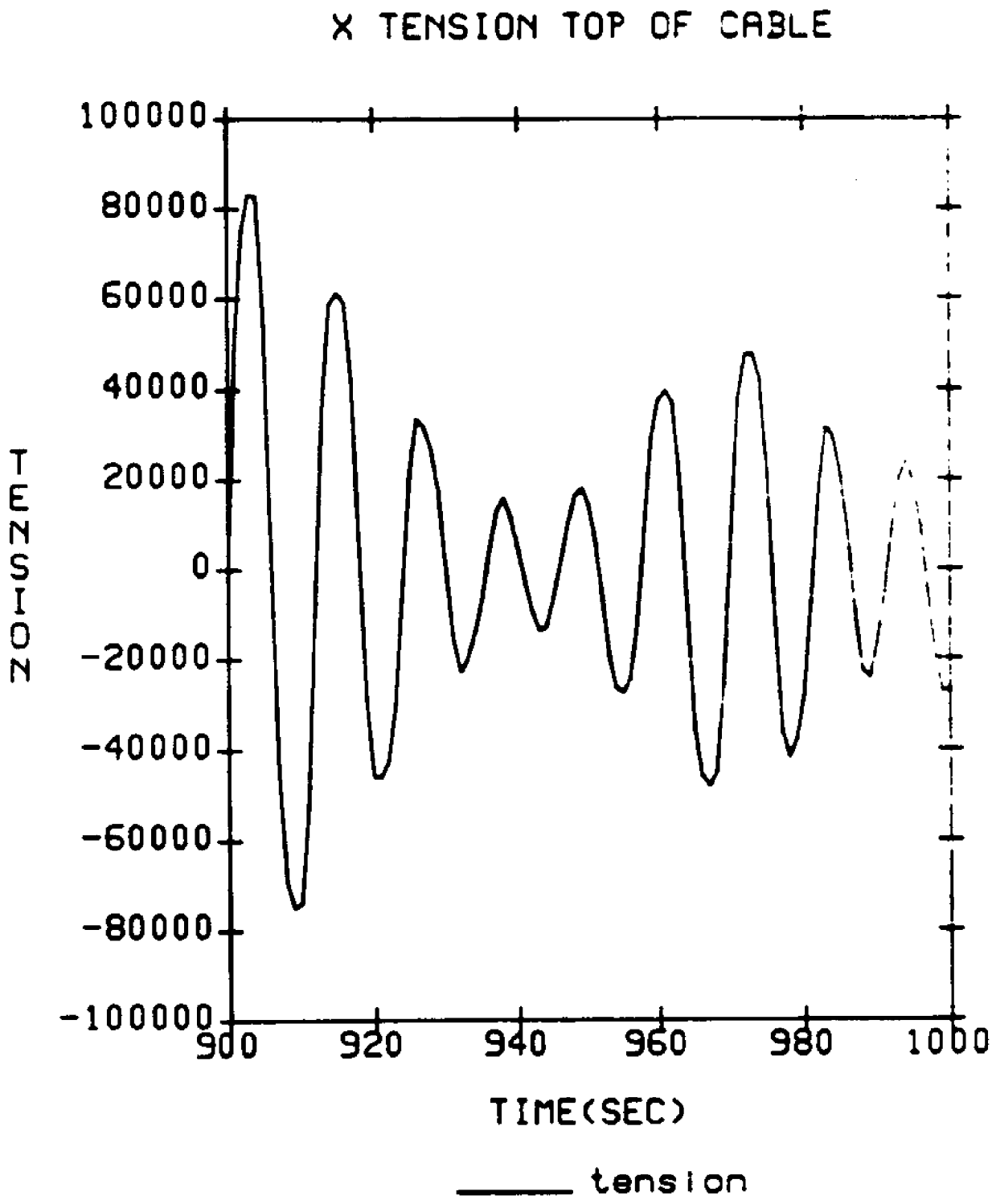

Figure 3-5: Detail of Figure 3-4

Table 3-4: Statistics of Input Motion

0 Statistic	1 Value
1 Count (N)	5001.000000
2 Sum	16.899339
3 Mean	0.003379
4 SEM (s.e. of mean)	0.008814
5 Median	0.002333
6 Variance	0.388516
7 StDev (sd)	0.623311
8 Maximum	1.545785
9 Minimum	-1.598778
10 Range	3.144563
11 Skewness	0.005341
12 Kurtosis	760.812051

Table 3-5: Statistics of Dynamic Tension Trace obtained from the Nonlinear Progrm

0 Statistic	1 Value
1 Count (N)	5000.000000
2 Sum	434927.739056
3 Mean	86.985548
4 SEM (s.e. of mean)	394.820152
5 Median	-51.309820
6 Variance	7.798096e+08
7 StDev (sd)	27925.071751
8 Maximum	0.8491112E+05
9 Minimum	-0.8501763E+05
10 Range	169926.750000
11 Skewness	0.001096
12 Kurtosis	1118.842[illegible]

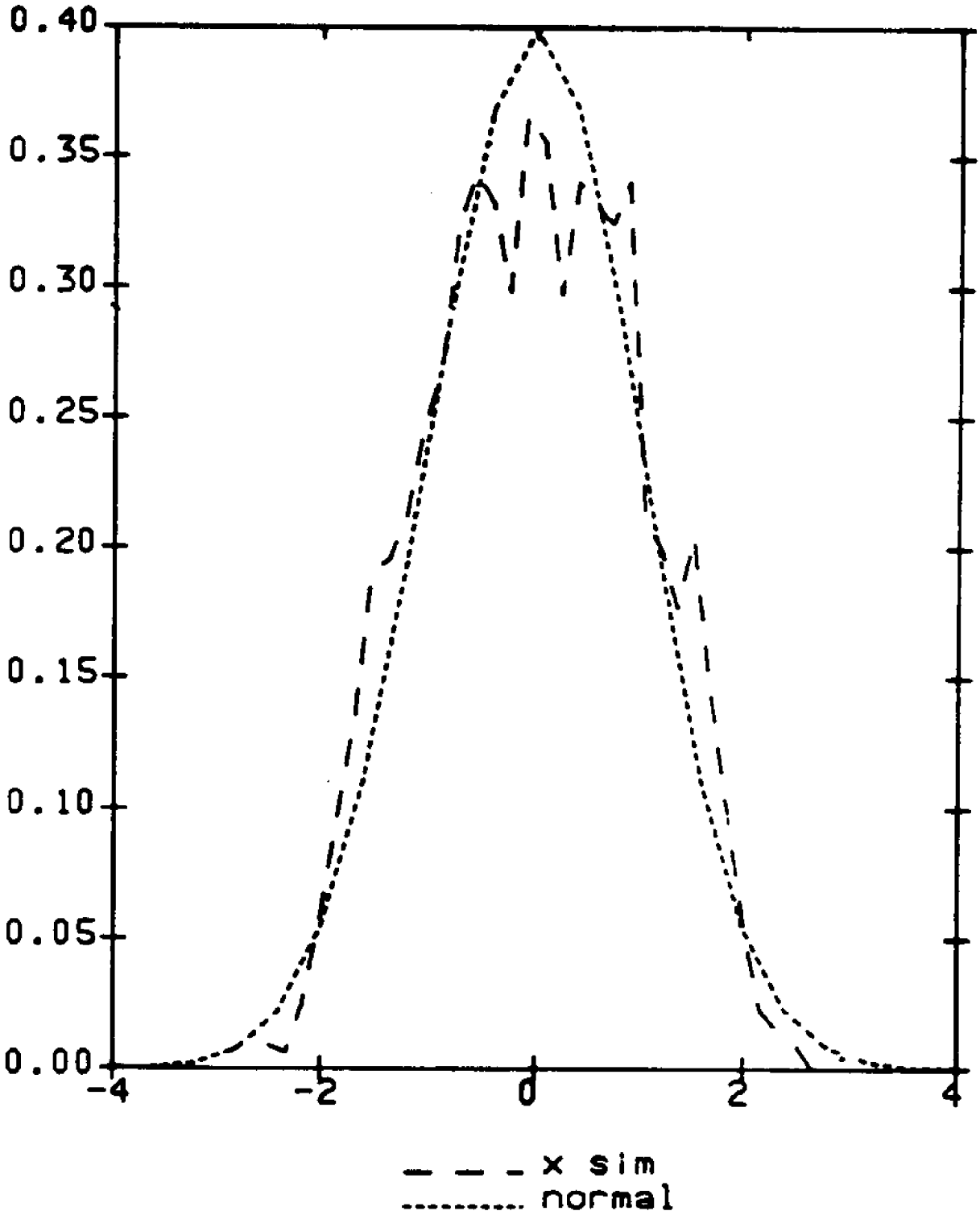

Figure 3-6: Comparison of the Target Probability Distribution (Normal) and the achieved pdf for the x Motion imposed at the top

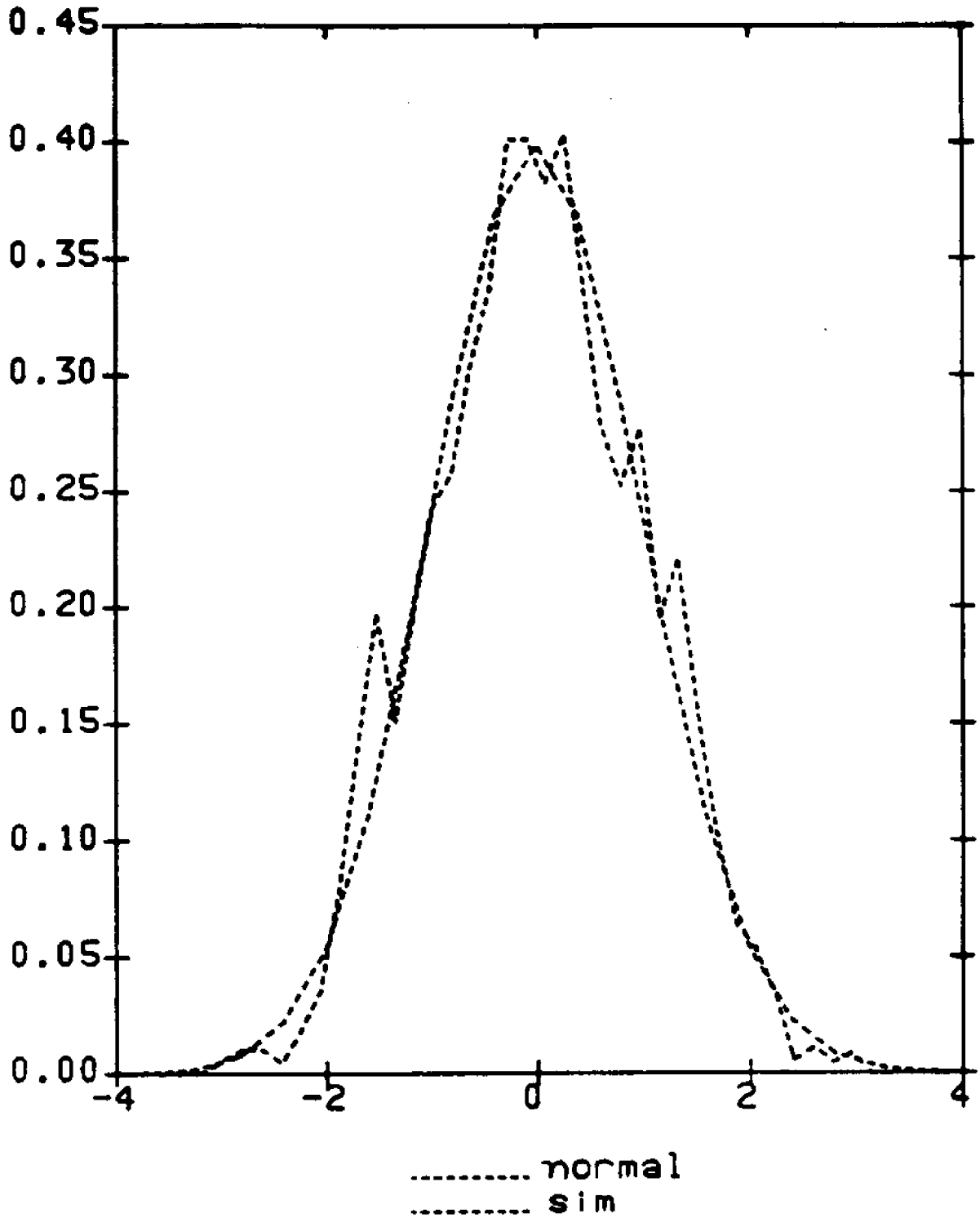

Figure 3-7: Probability Density Function of the Tension as Predicted by Nonlinear Simulation, Compared with the Normal Distribution

4. Methods for Fatigue Analysis

4.1 Introduction

The ocean structures are subject to random loads, so the stress at each point can be modelled as a random process. In this chapter we study the statistics of dynamic response quantities such as stress, tension, displacement, etc. in order to use them to predict the fatigue failure of multi-leg mooring systems, subjected to the dynamic effects of the ocean environment. In order to describe the frequency content and intensity of a random vibration environment it is convenient to use its power spectral density [Crandall 63].

As part of a procedure for the preliminary design of mooring systems, a stochastic cumulative fatigue analysis model is developed using dynamic spectral response analysis techniques. In the fatigue failure approach, it is postulated that each stress cycle imposes on the material an infinitesimal damage, which depends primarily on the peak amplitude of the excursion s(t) and is accumulated over time. Each consecutive cycle inflicts additional damage and the total damage is the sum of each individual damage. Failure is said to occur when the accumulated total damage reaches 100%. Given that the structure is subject to millions of cycles it is possible that the total damage will eventually cause failure to the structure [Triantafyllou 80].

4.2 S-N Curves

The physical mechanism of fatigue is the creation of microscopic cracks which grow slowly until one of them is subject to a random, large, local stress in which case the crack develops rapidly causing fracture. In order to obtain fatigue data experimentally, it is necessary to run tests on specimens of the material, or the system of interest. The major part of fatigue data has been obtained from tests with constant amplitude, in which the mean stress is zero, but some investigators have obtained data regarding the effect of mean stress. The modified Goodman diagram approach is usually used to include the effect of mean stress [Wirsching 80] and [Dowling 83].

From tests of a large number of identical samples the S-N curve can be plotted, which

gives the mean of the statistical distribution of fatigue lives obtained for given stress amplitudes. The curve is assumed to be of the form

$$NS^b = C \tag{4.1}$$

where :

S = the stress level [stress range or stress amplitude, see eq. (4.8)]

N = cycles to failure

b and C are empirical constants

The next chapter provides detailed S-N data for a mooring system which is composed of wires and (or) chains. Also a summary of references for fatigue data is given in a separate appendix.

4.3 The Palmgren-Miner Rule

In the case of a stress which is a random process rather than a sinusoidally changing function, the prediction of fatigue failure is very difficult and is usually based on the linear damage accumulation hypothesis, proposed by Palmgren and Miner as a simple model for a relative criterion.

According to this hypothesis, if n cycles of constant stress amplitude s have been experienced, then the material has used up a fraction of its fatigue life equal to n/N, where N is the number of cycles at which failure occurs under uniform amplitude s. When therefore the structure is subject to n_1 cycles of a sinusoidal stress requiring N_1 cycles for failure, and then to n_2 cycles requiring N_2 cycles for failure, and so on, then the total cumulative damage is ;

$$D = \sum_{i=1}^{M} \frac{n_i}{N_i} \tag{4.2}$$

If $D \geq 1$ then the structure is considered to be failed, otherwise it is safe against fatigue. Note that under this hypothesis there is no restriction regarding the order of

application of the various stress levels. Several hypotheses different from the Palmgren-Miner rule, were presented for the fatigue model in [Wirsching 73].

4.4 Fatigue Failure due to a Stationary Random Stress Process

Suppose that the dynamic response s(t) is a stationary random process described by a spectrum S(ω). In order to determine the spectrum of stress in a structure, we need to find the relation of the stress to the source of excitation, such as the wave elevation. When this relation is linear, standard techniques can be used that make the calculations very easy.

In a narrow band process, individual cycles can be easily identified and by using the Palmgren-Miner hypothesis one can ascribe an incremental damage to each cycle. Accumulating these damages leads to a total damage D(T) for a time period T.

In a wide band process, the first step in estimating the fatigue life is to represent the history by a reasonable number of stress blocks where each block is composed of a number of cycles of constant stress. The most widely accepted method of cycle counting for fatigue performance evaluation, is the Rainflow method, which identifies all cycles, including cycles which occur within larger cycles [Kenley 82]. Also P.H. Wirsching has presented several papers on the fatigue design procedure for structural elements subjected to a stress process, modeled as stationary wide band Gaussian. He estimated fatigue damage easily by considering an equivalent gaussian narrow band process, which gives conservative but reasonable results, relative to the rain-flow algorithm [Wirsching 80].

4.4.1 The Analysis for the Mean Values of the Damage

Let λ be the average number of zero-up crossings per second. In a time period T we expect :

$$M = \lambda T \tag{4.3}$$

number of cycles.

The possibility of these cycles having stress amplitudes between s_0 and s_0+ds_0 is $p(s_0)ds_0$, where $p(s_0)$ is the probabilty density of the peaks. The expected number $n(s_0)$ of such peaks is :

$$n(s_0) = \lambda T\, p(s_0)ds_0 \tag{4.4}$$

Let us denote by $N(s_0)$ the number of cycles required for the material to break, at the stress amplitude s_0. Then the damage on the material due to all cycles having peaks between s_0 and s_0+ds_0 is :

$$\frac{n(s_0)}{N(s_0)} = \lambda T \frac{p(s_0)}{N(s_0)} ds_0 \tag{4.5}$$

The total expected damage E(D) according to the postulate mentioned above is :

$$\begin{aligned} E(D) &= \lambda\, T \int_0^\infty \frac{p(s_0)}{N(s_0)} ds_0 \\ &= \lambda T \cdot E\left[\frac{1}{N(s_0)}\right] \end{aligned} \tag{4.6}$$

If the random response s(t) is normal, then the peaks have a Rayleigh distribution.

$$p(s_0) = \frac{s_0}{\sigma_s^{\,2}} \exp\left(-\frac{s_0^{\,2}}{2\sigma_s^{\,2}}\right) \tag{4.7}$$

When we use the S-N curve of eq. (4.1) as the fatigue model, the expected damage can be expressed as :

$$E[D(T)] = \frac{\lambda T}{C\sigma_s^{\,2}} \int_0^\infty s_0^{\,b+1} \exp\left(-\frac{s_0^{\,2}}{2\sigma_s^{\,2}}\right) ds_0 \tag{4.8}$$

where the S-N curve is based on the stress amplitude s_0. ($S_0N^b=C$)

$$= \frac{\lambda T}{C_1} (2\sqrt{2}\sigma)^b \Gamma(1+b/2) \tag{4.9}$$

where $\Gamma(x)$ denotes the Gamma function of x, and
the S-N curve is based on the stress range s_r.

$$(S_r N^b = C, \; s_r = 2 s_0)$$

This result gives the expected damage from an ensemble of narrow band stress histories of duration T.

4.4.2 the Application to the Multi-leg System

The sea state is not stationary for long periods of time and is modelled as a piecewise stationary Gaussian process [Karadeniz 82]. We are given the probability of each sea state through the statistics of $H^{1/3}$, T_m.

Then we can define a damage for each combination $H^{1/3}$, T_m :

$$D(H^{1/3},T_m) = T\,\lambda(H_0,T_0)\cdot P(H^{1/3}=H_0,T_m=T_0) \tag{4.10}$$

$$\times \int_0^\infty \frac{p(s = s_0/H_0,T_0)}{N(s_0)}\, ds_0$$

where T is the life period of the structures in sec. The total damage is defined as :

$$D = T \int_0^\infty \int_0^\infty P(H^{1/3}=H_0,T_m=T_0)\,\lambda(H_0,T_0) \tag{4.11}$$

$$\times \int_0^\infty \frac{p(s=s_0/H_0,T_0)}{N(s_0)}\, ds_0\, dH_0\, dT_0$$

In a similar way equations (4.7) and (4.1) can give the following expression for long term applications.

$$D = \frac{T\,\Gamma(1+b/2)}{C} \sum_i \sum_j P(H^{1/3}=H_i, T_m=T_j)\,\lambda_{ij}\,[\,2\,M_{0\,ij}\,]^{b/2} \tag{4.12}$$

$$\text{with } \lambda_{ij} = \frac{1}{2\pi}\sqrt{\frac{M_{2\,ij}}{M_{0\,ij}}} \tag{4.13}$$

where :

M_0 is the area of the spectrum $S(\omega)$

M_2 is the second moment of the spectrum $S(\omega)$

5. Fatigue Data

5.1 Introduction

Wire ropes and chains are increasingly used for deep water applications when dynamic tension can be substantial. This trend makes it necessary to improve our understanding of the long term behaviour of wire ropes and chains under cyclic loading.

Comprehensive laboratory tests for a variety of ropes have been carried out, but the number of cyclic tensile load testing of metallic ropes for marine use is very small compared with that of cyclic bending tests, especially for large diameter ropes.

Tests on single wires [Thorpe 83] have been carried out to gain a better understanding of the fatigue failure process in wire ropes. Data for small diameter wire ropes (less than 50mm) are available. [Matanzo 72], [Lucht 77], [Stange 83], [Thorpe 83], [Waters 85] and others. Recently developed systems, such as the Tethered Buoyant platform, the Guyed Tower, Water Energy devices and OTEC systems require large diameter wire ropes for the mooring system.

A method for predicting the service life of large diameter wire ropes from small rope tests would be beneficial because of the relatively high cost of testing large diameter wire ropes.

5.2 Summary of Important Data

5.2.1 Wire Rope

Results of fatigue tests on single wires [Thorpe 83] provided the following facts.

- Fretting in air has the most deleterious effect on fatigue life. This is supported by the single datum for air testing from the NEL wire rope tests, which lies on the extrapolation of the single wire fretting line (Fig.6).*

- Synergistic interaction between corrosion and fretting can cause a substantial reduction in fatigue life for wire ropes in seawater (Fig.7).*

* see Appendix

- Fatigue endurance has a strong dependence on stress range, but no effect of the mean stress has been observed in air (Fig.3)* Also [Matanzo 72], [Lucht 77] and [Ronson 80] derive the same conclusion.

- Corrosion-Fatigue endurance is decreased with increasing mean stress (Fig.4).* This observed trend is contradictory to the results of wire ropes reported in [Hanzawa 81].

Fatigue Data for small diameter wire ropes can be obtained from several references. Data for a specific wire rope with 1/4" diameter is illustrated in [Stange 83]. Matanzo presents data for 1/2" diameter wire ropes in air and in seawater [Matanzo 72]. He studied the effect of core and corrosion and concluded that Lang, IWRC wire rope appeared to be the best for marine applications, although it suffered the greatest loss in fatigue life due to corrosion (Fig.4).*This conclusion is, however, not in agreement with the API SPECIFICATION [API 84b] and results from [Acaster 72].

Acaster and API SPECIFICATION recommend right lay, regular lay, IWRC, preformed, galvanized or bright (bare) wire ropes for mooring systems [API 84a, 6.23].

The U.S. Steel Corporation has performed a series of tests on small wire ropes with 1/2" to 2-11/16" diameter in axial tension fatigue [Lucht 77]. Lucht suggests that there may be a fatigue limit for wire ropes in axial tension fatigue (Fig.4).*From the data obtained in the Seacon experiment (Table 3) and Woods Hole Buoy Farm (Fig.5),*they concluded that plastic jacketed, drawn galvanized, torque balanced wire ropes with booted terminations provide performance superior to any other wire rope configuration. The superiority of plastic jacketed wire ropes over bare wire ropes is also exhibited in fatigue data of Bergen Wire Rope [Savastano 67].

Hanzawa [Hanzawa 81] shows the possibility of extrapolation of fatigue data for small diameter wire ropes in order to predict the service life of large diameter wire ropes. He developed a new wire breakage detector for the internal wire breakage, making use of acoustic emission and an accelerometer.

---

* see Appendix

In that paper, the 85mm diameter Hanger rope exhibited a superior fatigue endurance than the 50mm diameter hanger rope made with similar rope constrution (Fig.4).*The Battelle North West Laboratory also concluded that under certain conditions the performance of large diameter wire ropes in bending could be predicted from tests on small diameter samples [Waters 85] and [Alzheimer 81]. However, Waters concluded through his collection of fatigue data from several published papers that the extrapolaton of data is inappropriate [Waters 85] (Fig.1).*

5.2.2 Chain

Unstable failure of a brittle manner is found to be the major failure mechanism preceeded by little or no fatigue cracking. Conventional fatigue failure terminated by a ductile final fracture is far less frequently reported for marine structures such as drilling units or for similar short term uses. This is supported by the records from DNV in [Berg 80] and [Taraldsen 85] and from ABS in [Stern 78].

Fatigue tests by SHELL in Netherlands show the relative fatigue life of the different types of chain subjected to alternating load between 800-1200 KN [Helvoirt 82]. As for connecting elements, the Kenter-type connecting link has been found to be the weakest part in each mooring line and hence the use of continuous chain is recommended for permanent mooring systems (Table 1).*This inferiority of connecting links is also shown in ABS records [Stern 78] (Table VI).*The veritas Joint Industry research project was performed on 76mm and 40mm diameter chains of common links and connecting links at 3 cyclic load levels in air [Lereim 85] (Fig.3).*Although these fatigue results are not representative of real fatigue strength in corrosive environment, the data suggest that connecting links of Kenter type should be avoided in lines used for long term permanent moorings, where fatigue considerations may become critical.

The effects of corrosion and preload on chains with different grades were examined at the laboratories of Domnarvete Jernverk in Sweden [Celander 72]. The fatigue tests show the negative effect of corrosion and favourable effect of preload, as expected (Fig.4)* The proof load, or preload, stiffens up the material and changes the stress picture in a favourably way, because a repeated load on a proof-loaded link must first overcome the negative stress at the most exposed point of the link (Fig.2).

* see Appendix

Wear failure of the Mantiloc 4 leg anchor chain has been reported [Shoup 84]. During the storm two chains failed by excessive interlink wear and the remaining two chains were worn about 50% through. Comparative wear tests on U3 and U4 steels and Model basin tests were carried out and investigations from both tests revealed that the cause of wear failure was excessive wear generated by large values of interlink force and motion induced by the dynamic behavior of the antisymmetric 4 leg mooring pattern (Fig.11).*

5.3 Comments about Fatigue Data for Marine Use

Published papers about the fatigue behaviour of large diameter wire rope are rarely found, especially in the case of cyclic tensile load test. Most summaries of papers written in the previous chapter are made from small data base and reveal sometimes disagreement between conclusions of different investigators. Although these results and conclusions do not represent completely the real trends in a corrosive environment, as required for marine applications, the data presented here can be used to derive useful suggestions in developing test programs in future. In conclusion, it appears advisable to plan and conduct systematic test programs of cyclic tensile load testing for large diameter wire ropes and chains.

6. Geometric - Material Nonlinearity

6.1 Introduction

The cable is a mechanism, i.e. its shape changes for any change in the externally imposed load, causing a nonlinear load-response relation of the stiffening type.

Also, there are materials, such as the synthetic ones (Kevlar, polyethylene), which demonstrate a nonlinear, hysteretic stress-strain relation.

Since the building block of the fatigue package developed in this study is an equivalent linearization procedure, it is essential that we consider in this chapter the effects of these two nonlinearities.

6.2 Modeling of Geometric and Material Nonlinearities

For moderate load conditions the tension-extension relation is approximated by a linear euation [Prescott 46]:

$$T = \delta \cdot e \tag{6.1}$$

where : δ is equal to EA with E expressing Young's modulus and A the cable cross-sectional area, if the cable is modelled as a single wire. Since cables consist of several strands multiplexed in various configurations, it is necessary to determine an equivalent Young's modulus E, which is, usually, roughly equal to half the material modulus. For accuracy, data from cable fabricators should be normally used.

In the case of chains, the calculation is even more complicated, because the extension of each link is related to bending of the curved rod that makes up the link. If a stud is inserted in the link, the equivalent Young's modulus is about one-fourth of the material modulus. Again, constructor's data should be used.

Once the load becomes extreme, though, the linear relation does not adequately represent the extensional properties of the cable. There are two reasons for nonlinear behavior of the tension-displacement relation:

1. Material nonlinearity which causes a stiffening of the curve of tension versus extension for high tension and a weakening for low tensions eventually knowing that the cable cannot carry compression. "Material nonlinearity refers to the properties of the helical structure of a wire, or of the link of a chain, rather than the material itself (steel).

2. Geometric nonlinearity of the extension-displacement relation resulting from large amplitude motions.

In the case of mooring systems, we have shown that the effect of nonlinear drag is so drastic that makes amplification (resonance) of motions impossible. We are certain, therefore, that the amplitude of motion is at most equal to the motion at the top, which for the wave frequency range is very small compared to the cable length.

Large tensions, however, can be obtained even for small motions, due to the effect of drag. Hence, the stiffening of the relation and, especially, the leveling-off to ensure non-zero tensions may be important. Let us denote by

$$T = N(e) \tag{6.2}$$

the relation between tension and extension.

We will not consider geometric nonlinearity because it becomes important for very taut (practically impossible) cables or for large motions (compared to the mooring line length), which do not occur in mooring systems within the wave frequency range.

In order to approximate the effect of the nonlinearity, we consider a linear relation

$$T = \Delta \cdot e \tag{6.3}$$

Since the nonlinearity is memoryless and time-invariant, the equivalent linear system is a simple constant. It should be noted here that hysteresis effects known to occur in synthetic lines can also be represented through a frequency dependent term.

The assumption here is that both e and T are stationary random processes. Then we wish to have the optional linear approximation in the mean-square sense; i.e. [Vidyasagar 78]

$$\min_{\Delta \geq 0} E\{ [N(e) - \Delta \cdot e]^2 \} \tag{6.4}$$

The condition is easy to derive; i.e.

$$E\{ e[N(e) - \Delta \cdot e] \} = 0 \tag{6.5}$$

or, if p(e) is the probability density function of e

$$\int_{-\infty}^{\infty} e\, N(e)\, p(e)\, de = \Delta \int_{-\infty}^{\infty} e^2\, p(e) de$$

$$\Delta = \int_{-\infty}^{\infty} e\, N(e)\, p(e)\, de \,/\, \sigma_e^{\,2} \tag{6.6}$$

where, σ_e is the standard deviation of e

Application :

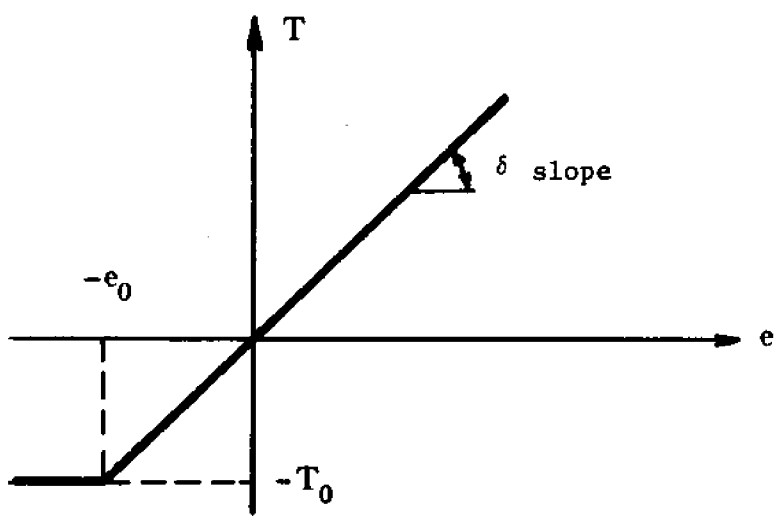

Figure 6-1: Relation between Tension and Extension

The tension T denotes the dynamic tension and e the dynamic extension. Let T_0, e_0 denote the static tension and extension respectively. Then the relation is assumed to be that of a perfect limit, as shown in Figure 6-1.

Let us further assume that e is Gaussian distributed, and zero mean; i.e.

$$p(e) = \frac{1}{\sigma_e \sqrt{2\pi}} e^{-\frac{e^2}{2\sigma_e^2}} \tag{6.7}$$

where σ_e is the standard deviation of e.

Then

$$\Delta = \frac{1}{\sigma_e^2} \{T_0 \int_{-\infty}^{-e_0} e\, p(e)\, de + \delta \int_{-e_0}^{\infty} e^2\, p(e)\, de\} \tag{6.8}$$

Discussion :

The issues in such approximations are: How good is the optimal fit and what is the probability density function of T. The first question can be answered usually through agreement with exact solutions, while the second one has further repercussions, because T is the outcome of a system of partial differential equations affecting also e and hence the motions.

The assumption of a normal distribution, therefore, may not be a good one if the level e_0 is frequently exceeded, when a severe distortion of the distribution of the tension will result. Such a case, however, has much more severe impliations, becuse frequent loss of tension implies snap phenomena, which require by their own nature, a time domain analysis. In addition, the response cannot be assumed to be stationary.

As a result, we use this approximation to include the stiffening-weakening effects of the tension-extension relation for cables and not to study pathological cases. The Gaussian assumption is then justified.

7. Cable - Bottom Interaction

7.1 Introduction

The lower part of a mooring line lies partly on the floor and is heavy enough to keep the anchor under horizontal load at all times.

As the line oscillates under the influence of wave excitation, part of the line lifts off and then touches down. This motion can be smooth and quasi-static, or quite violent [Suhara 81].

When a clump weight is used, the dynamics of the weight are quite important and may cause drastic changes in the dynamic tension [Fylling 82].

Here we consider a line partly lying on the bottom, which represents the majority of exciting mooring lines. We will consider the proper modelling of this cable-bottom interaction within our scope of a fatigue investigation.

7.2 Bottom boundary condition

A mooring line that lies partly on the floor will be subjected to a dynamic cable-bottom interaction. This is a nonlinear phenomenon because it causes a variation in the length, and a contact force, which acts only when geometry implies that part of the line lies on the bottom. This force may be a single quasi-static, distributed force simply supporting the weight of the cable, or an impact force acting at the point of lift-off (or touch down).

Let y(t,x) describe the cable configuration very close to be the touchdown point C, whose distance from the origin is denoted by $\xi(t)$. Since the elevation of the (movable) point C is always zero, we conclude

$$\frac{\partial y}{\partial t} + \frac{d\xi}{dt}\frac{\partial y}{\partial x} = 0 \qquad \text{at } x=\xi \tag{7.1}$$

Also, Newton's law applied to a segment ds at the touchdown point provides to first order

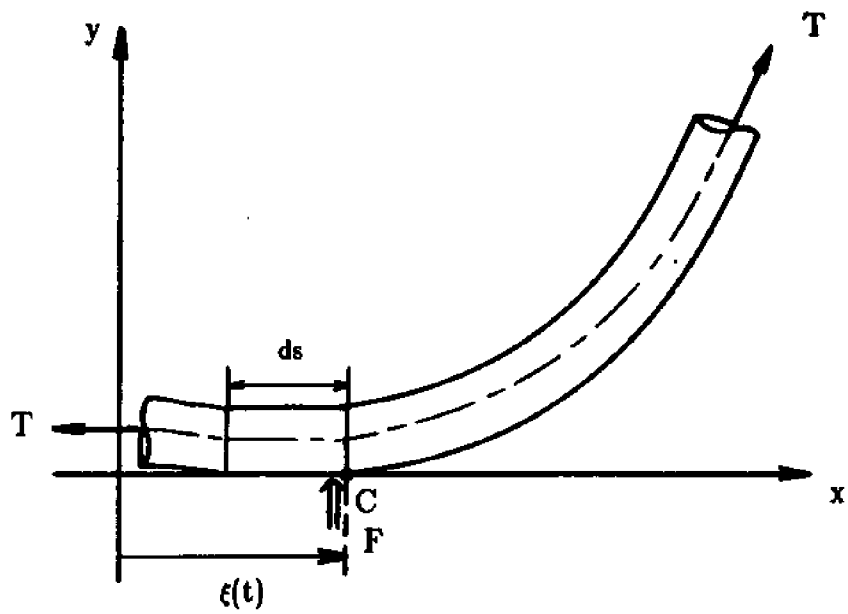

Figure 7-1: a Segment of the Cable around the Touchdown point

$$-M \frac{\partial y}{\partial t} \frac{d\xi}{dt} = T_0 \frac{\partial y}{\partial x} + F \tag{7.2}$$

where F is the impulsive force acting at C, and M is the mass augmented by the added mass per unit length. It should be noted that the effect of the distributed forces is nil in Equation (7.2).

By introducing (7.1) in (7.2) we conclude

$$\{ M (\frac{d\xi}{dt})^2 - T_0 \} \frac{\partial y}{\partial x} = F \qquad \text{at } x=\xi \tag{7.3}$$

with the restrictions

$$\frac{\partial y}{\partial x} \geq 0 \qquad \text{(geometric)} \tag{7.4}$$

$$F \geq 0 \qquad \text{(resistive force)} \tag{7.5}$$

As a result of restrictions (7.4) and (7.5) we find

$$\text{(a) for } \left|\frac{d\xi}{dt}\right| > \sqrt{\frac{T_0}{M}} \tag{7.6}$$

the slope can be positive as well as the resistive force F

$$\text{(b) for } \left|\frac{d\xi}{dt}\right| < \sqrt{\frac{T_0}{M}} \tag{7.7}$$

the left hand side of (7.3) is negative by virtue of (7.4), which violates (7.5). Then the only possible solution is that the slope and the resistive force F are zero.

The criterion (7.6) and (7.7) can be easily identified with a comparison between the speed of lift-off and the phase velocity of the transverse waves of an equivalent taut string. Because the configuration of the cable is tangent to the bottom at rest, there is no first order coupling between transverse and longitudinal dynamics (at that point); hence transverse motions are transmitted like those of a taut string.

7.3 Representation of the Bottom Boundary Condition

In the previous section we showed what the proper form of the bottom boundary condition is. In this section we select a representation that is both correct and convenient for our numerical implementation.

For this purpose we consider a cable of length L whose static configuration is tangent at the bottom. We consider the lower end supported by two springs, one vertical with constant θ and one horizontal of stiffness δ (See Figure 7-2).

If p,q denote the tangential, transverse displacements respectively, T the dynamic tension and ϕ the dynamic angle, then:

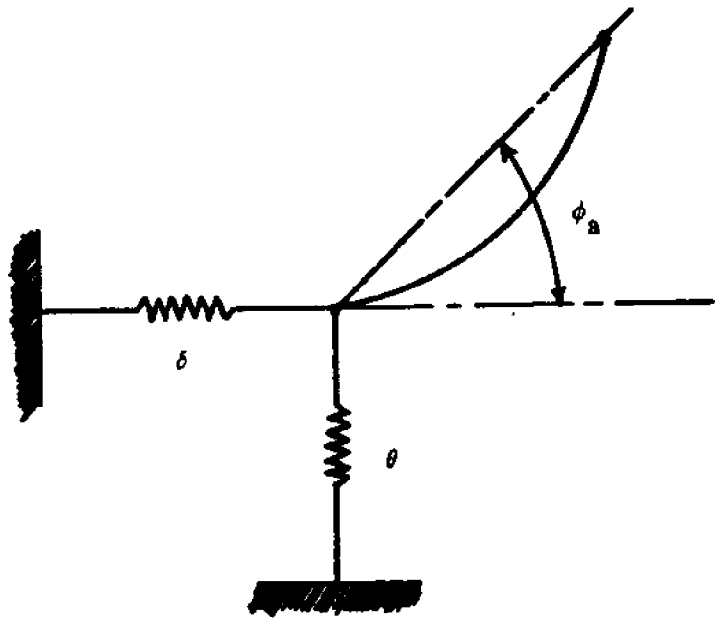

Figure 7-2: Spring Constants δ and θ

$$T_0 \phi = \theta \cdot q$$

$$T = \delta \cdot p \qquad \text{at } s = 0 \tag{7.8}$$

$$q = 0, \; p = 0 \qquad \text{at } s = L \tag{7.9}$$

are the linearized boundary conditions, with T_0 the static tension.

In order to acquire some understanding of dynamics, we consider the curvature as constant and equal to α (this is correct to first order for high tension to cable weight ratio). Then if E denotes Young's modulus and A the cross-sectional area, the first few natural frequencies are given by the equation (correct to first order in α):

$$2 - \cos(kL)\left\{2 - \frac{T_0}{\theta L}(kL)^2\left[\frac{(kL)^2}{\lambda^2}\left(1 - \frac{EA}{\delta L}\right) - 1\right]\right\} \tag{7.10}$$

$$+ \sin(kL)\cdot kL\{\frac{(kL)^2}{\lambda^2}\,[1+\frac{EA}{\delta L}] + \frac{T_0}{\theta L} - 1\} = 0$$

where ;

$$k = \frac{\omega}{\sqrt{T_0/m}} \tag{7.11}$$

$$\lambda^2 = \frac{E\,A}{T_0}\,(\frac{wL}{T_0})^2 \cos^2\phi_a \tag{7.12}$$

with T_0 an average tension of the static configuration (assumed constant with our simple derivation), ϕ_a the inclination angle, w the weight per unit length and m the mass per unit length.

The derivation of (7.10) follows the steps of our earlier derivations for the natural frequencies of cables, subject to the different boundary conditions (7.8), (7.9). We chose to assume the tension and curvature constant so (7.10) does not provide any hybrid modes as it should, but it will serve to illustrate important properties.

If we let θ and δ tend to infinity, then we derive the equation of Irvine and Caughey :

$$2\,(1-\cos kL) + kL \sin kL[\,(\frac{kL}{\lambda})^2 - 1\,] = 0 \tag{7.13}$$

If we let the vertical spring constant tend to infinity, then we derive :

$$2\,(1-\cos kL) + kL \sin kL[\,(\frac{kL}{\lambda})^2\,[1+\frac{EA}{\delta L}] - 1\,\} = 0 \tag{7.14}$$

We observe that if we define λ_* :

$$\lambda_*^2 = \frac{\Delta}{T_0}\,(\frac{wL}{T_0})^2 \cos^2\phi_a \tag{7.15}$$

with

$$\frac{1}{\Delta} = \frac{1}{EA} + \frac{1}{\delta L} \tag{7.16}$$

then (7.14) reverts to Irvine and Caughey's equation (7.13) with λ_* instead of λ.

As we have shown in our last year's study, the principal effect of drag is to increase the catenary stiffness to the point that the cable prefers to stretch rather than vibrate transversely. This happens at the higher frequencies when we would expect from our criterion to see possible impact forces. As a result, since all our excitation occurs at the top, we conclude that our modeling, in accordance with (7.10), must be as follows :

1. for transverse dynamics we may assume a large constnt θ, which makes use of the result that drag limits transverse motions substantially.

2. for longitudinal dynamics it is absolutely essential that we apply the modified boundary condition so as to ensure an accurate value of the elastic stiffness. Indeed, equation (7.14) indicates a substantial shift in dynamics due to the horizontal spring. Equation (7.14) indicates also that we can use instead of a new boundary condition (as in (7.8)) a modified stiffness EA directly in the dynamic equations. This is purely coincidental but of convenience to our numerical scheme.

In conclusion, our analysis has shown that the cable bottom interaction requires in the general case complete rewriting of the bottom boundary conditions. For cables in water, however, the principal effect is to alter the effective elastic stiffness, which is of paramount importance in determining the level of dynamic tension.

Conclusion and Summary

The basic conclusion from the previous phase of this study on mooring dynamics was that cables are subject to substantial tension amplification in deeper waters, because they are forced by the action of drag to employ the large elastic stiffness, instead of the small catenary stiffness, in response to oscillatory excitation in the wave frequency range.

The basic conclusion from the present, second phase of the effort is that multi-leg lines have a relatively small fatigue life in deeper waters, due to the basic amplification mechanism discovered during the first phase. [Triantafyllou 86] The finding makes the use of the present package very useful, because it allows a realistic estimate of the fatigue life at a reasonable small cost.

For most sea storms the linearization of drag, as it has been extended in the second phase to handle stochastic excitation, gives good results, compared to a fully nonlinear code. A method to account for "clipping" the dynamic tension when it reaches negative values exceeding in magnitude the static tension, and for accounting for the cable-bottom interaction has been provided. In both cases it has been assumed that these phenomena do not reach pathological levels. A badly designed system may exhibit such levels, which can be identified through the present analysis by checking the dynamic tension: Although the exact magnitude is not predicted accurately, the occurence of violent tension oscillation is identifiable, when, of course, fatigue calculation are not needed, since the danger for direct failure is greater.

However, for the cases tested the assumptions used were valid. The cases employed realistic sea data and a wide variety of storms. For most of these storms the dynamic amplification due to the drag action has been identified as the most important element of cable response.

In checking the various assumptions we found overall very good agreement between the stochastic linearization results and the predictions of fully nonlinear programs.

One item, however, deserves special attention : the boundary condition at the bottom.

As we explained in detail in the previous chapter, the basic change in the dynamics of a cable due to having part of the cable on the bottom is the additional spring constant introduced by the extensibility of the mooring line lying on the floor. It is very important, therefore, to introduce the equivalent elastic stiffness as explained in this report instead of the actual stiffness. This takes some engineering judgement, but it is well worth the effort.

For the same reason special attetion must be paid to selecting the proper value for the (equivalent) Young's modulus of the wire or chain, which can be different even by a factor of 10 from the value of Young's modulus for the material.

References

[Acaster 72] Acaster S.M.
Anchor Lines in the North Sea.
Offshore Technology Conference (OTC 1535), 1972.

[Alzheimer 81] Alzheimer J.M. and Anderson W.E.
Wire Rope Improvement Program.
Technical Report, Battelle Pacific Northwest Labolatory, 1981.

[API 84a] American Petroleum Institute.
API Specification for Mooring Chain.
American Petroleum Institute, 1984.

[API 84b] American Petroleum Institute.
API Specification for Wire Rope.
American Petroleum Institute, 1984.

[Berg 80] Berg A. and Taraldsen A.
Long-Term Mooring and Anchoring of Large Structure and Drilling Units -- Reliability and Safety of Anchor Chain Systems.
Offshore Technology Conference (OTC 3813), 1980.

[Bliek 84] Bliek, A.
Dynamic Analysis of Single Span Cables.
PhD thesis, MIT, 1984.

[Borgman 65a] Borgman L. E.
Random Hydrodynamic Forces on Objects.
Annuals of Mathematical Statistics 38(1), 1965.

[Borgman 65b] Borgman L. E.
Wave Forces on Piling for Narrow-band Spectra.
Journal of the Waterways and Harbors Division 91(WW3), 1965.

[Borgman 67] Borgman L. E.
Spectral Analysis of Ocean Wave Forces on Piling.
Journal of the Waterways and Harbors Division 93(WW2), 1967.

[Celander 72] Celander Ivar.
Preload Influence on Fatigue Characteristics of Chain Cable Exposed to Salt Water and AQtmospheric Conditions.
Offshore Technology Conference (OTC 1578), 1972.

[Crandall 63] Crandall S. and Mark W.
Random Vibration in Mechanical Systems.
Academic Press Inc., 111 Fifth Avenue, New York, NY. 10003, 1963.

[Davenport 65] Davenport, A. G. and Steels, G. N.
Dynamic Behavior of Massive Guy Cables.
Journal of the Structural Division, ASCE 91(ST2):43-70, April, 1965.

[Dowling 83] Dowling N.
Fatigue Life prediction for Complex load Versus Time Histories.
Journal of Engineering Materials and Technology 105, 1983.

[Fylling 82] Fylling I. and Larsen C.
Dynamic Behaviour of Anchor Lines.
In *Proceedings of BOSS '82*, pages 651-670. 1982.

[Hanzawa 81] Hanzawa M., Yokota H., Toda Y. and Yokoyama K.
Fatigue Behavior of Large-Diameter Wire Ropes.
Offshore Technology Conference (OTC 3999), 1981.

[Helvoirt 82] van Helvoirt L.C.
Static and Fatigue Tests on Chain Links and Chain Connecting Links.
Offshore Technology Conference (OTC 4179), 1982.

[Karadeniz 82] Karadeniz H., Manen S. and Vrouwenvelder A.
Probabilistic Reliability Analysis for the Fatigue Limit State of Gravity and Jacket-Type Structures.
In *Proceedings of BOSS '82*, pages 147-. 1982.

[Keller 69] Keller, H. B.
Accurate Difference Methods for Linear Ordinary Differential Systems Subject to Linear Constraints.
S.I.A.M. Journal of Numerical Analysis 6(1), March, 1969.

[Kenley 82] Kenley R.
Measurement of Fatigue Performance of Forties Bravo.
Offshore Technology Conference (OTC 4402), 1982.

[Lereim 85] Lereim J.
Summary of the 4-Year Research Project : Anchor Chain Cables Offshore.
Offshore Technology Conference (OTC 5060), 1985.

[Lucht 77] Lucht W.A. and Donecker F.W.
Factors Affecting Wire Rope in a Marine Environment.
Offshore Technology Conference (OTC 2924), 1977.

[Matanzo 72] Matanzo Frank.
Axial Fatigue of Wire Rope in Sea Water.
Offshore Technology Conference (OTC 1579), 1972.

[Paulling 79] Paulling, J.R.
Frequency Domain Analysis of OTEC CW Pipe and Platform Dynamics.
Offshore Technology Conference (OTC 3543), 1979.

[Prescott 46] Prescott J.
Applied Elasticity.
Dover Publications, New York, 1946.

[Ronson 80] Ronson K.T.
Ropes for Deep Water Mooring.
Offshore Technology Conference (OTC 3850), 1980.

[Savastano 67] Savastano F.
Seleting Wire Rope for Oceanographic Applications.
UnderSea Technology 8(2), 1967.

[Shin 85] Shin H.
Numerical Solution of the cable Dynamic Equations Using the Linearized Equivalent Damping Force.
Master's thesis, MIT, 1985.
Engineer's Thesis.

[Shoup 84] Shoup G.J. and Mueller R.A.
Failure Analysis of a Calm Buoy Anchor Chain System.
Offshore Technology Conference (OTC 4764), 1984.

[Stange 83] Stange W.F.
Laboratory Testing for Enhanced Undersea Cable Survivability.
In *Proceedings of the Second International Offshore Mechanics and Arctic Engineering Symposium*, pages 347. Jan-Feb, 1983.

[Stern 78] Stern I.L. and Wheatcroft.
Toward Improving the reliability of anchor chain and accessories.
Offshore Technology Conference (OTC 3206), 1978.

[Suhara 81] Suhara, T. et al.
Dynamic Behavior and Tension of Oscillating Mooring Chain.
Offshore Technology Conference (OTC 4053):415-418, 1981.

[Taraldsen 85] Taraldsen A.
Anchor Chain Fractures.
Offshore Technology Conference (OTC 5059), 1985.

[Thorpe 83] Thorpe T.W. and Rance Andrew.
the Tensile Fatigue of Wire Rope : a New Approach.
Offshore Technology Conference (OTC 4638), 1983.

[Triantafyllou 80]
Triantafyllou, M. S.
Mooring Lines
1980.
Class Notes.

[Triantafyllou 82]
Triantafyllou, M. S.
Preliminary Design of Mooring Systems.
Journal of Ship Research 26(1):25-35, March, 1982.

[Triantafyllou 85]
Triantafyllou M. S., Bliek A. and Shin H.
Dynamic Analysis as a Tool for Open-Sea Mooring System Design.
Transactions SNAME :303-324, 1985.

[Triantafyllou 86]
Triantafyllou M. S., Bliek A., Burgess J. and Shin H.
Mooring Dynamics for Offshore Applications.
Technical Report MITSG 86-1 and MITSG 86-2, Sea Grant College Program, January, 1986.

[Vidyasagar 78] Vidyasagar M.
Nonlinear Systems Analysis.
Prentice-Hall, Inc., Englewood Cliffs, New Jersey 07632, 1978.

[Waters 85] Waters D., Eggar D., and Plant H.
Develpments in Fatigue Assessments of Large-Diameter Wire Ropes used in Offshore Moorings.
Offshore Technology Conference (OTC 5000), 1985.

[Wirsching 73] Wirsching P. and Edward H.
Probabilistic Design for Random Fatigue Loads.
Journal of the Engineering Mechanics Division 99(EM6), 1973.

[Wirsching 80] Wirsching P. and Light M.
Fatigue under Wide Band Random Stresses.
Journal of the Structural Division 106(ST7), 1980.

Appendix for Chapter 5

Summary of References for Fatigue Data

Table of Contents

Summary of References on Fatigue of Cables

This report summarizes the findings on cable fatigue, as reported in the literature to date. It was prepared as part of the research effort to study the fatigue life of cables, supported by the M.I.T. Sea Grant Program and a consortium of offshore companies including Chevron Oil Field Research Co., Conoco Inc., Exxon Production research Co., and Shell Development Company.

The present report is an appendix to the main research report, where all theoretical and numerical results are reported.

The first part of the report contains data on wire cables, and the second part data on chains. The report contains all information from the open literature available to the authors, but the subject is by no means exhausted. On the contrary, data for large diameter cables and chains are very sparse and inconclusive. It is hoped that the present report will provide some basic understanding of the fatigue properties of cables, but, even more important, of the still unsolved problems that require further experimental and theoretical investigation.

1 Wire Rope

1.1 Selecting Wire Rope for Oceanographic Applications

[Savastano 67]

- What is Wire Rope ?

- Constrution : 7×variety, 6×variety, 3×variety and IWRC, etc

- Materials : Galvanized Aircraft Cable, Improved Plow Steel, a Plastic Jacketed

- Oceanographic Wire Rope

- Fatigue life of bare wire and plastic jacked wire rope

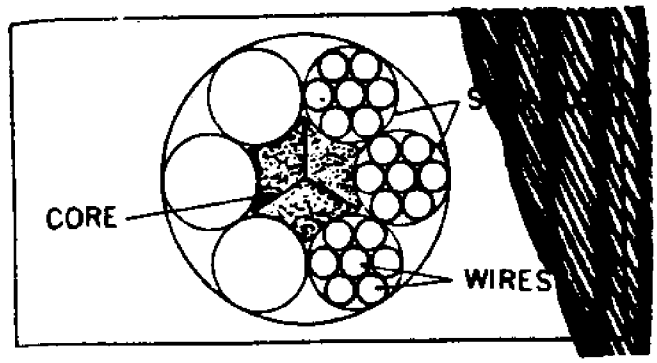

A "7x19" is further identified as 7 strands of 19 wires each. (6 strands of 19 wires over a core of 19 wires.)

There are three basic types of cores in wire rope: *steel, natural fibers* and *synthetic fibers.*

[savastano 67]

Strength, flexibility, corrosion resistance and cost are parameters around which most current oceanographic wire rope is designed. All these factors are inter-related with each parameter affecting the other

It is not surprising, therefore, to find that the most commonly used oceanographic ropes fall within the categories shown below.

B-T wire
for bathythermographic work
3/32 3x7 GAC*
3/32 7x7 GAC

Hydrographic or Hydrowire
3/16 3x19 GAC
3/16 3x19 GIP**

Coring Wire
1/2 6x19 IWRC GAC
1/2 7x19 GAC

*Galvanized Aircraft
**Galvanized Improved Plow Steel

Bergen Wire Rope

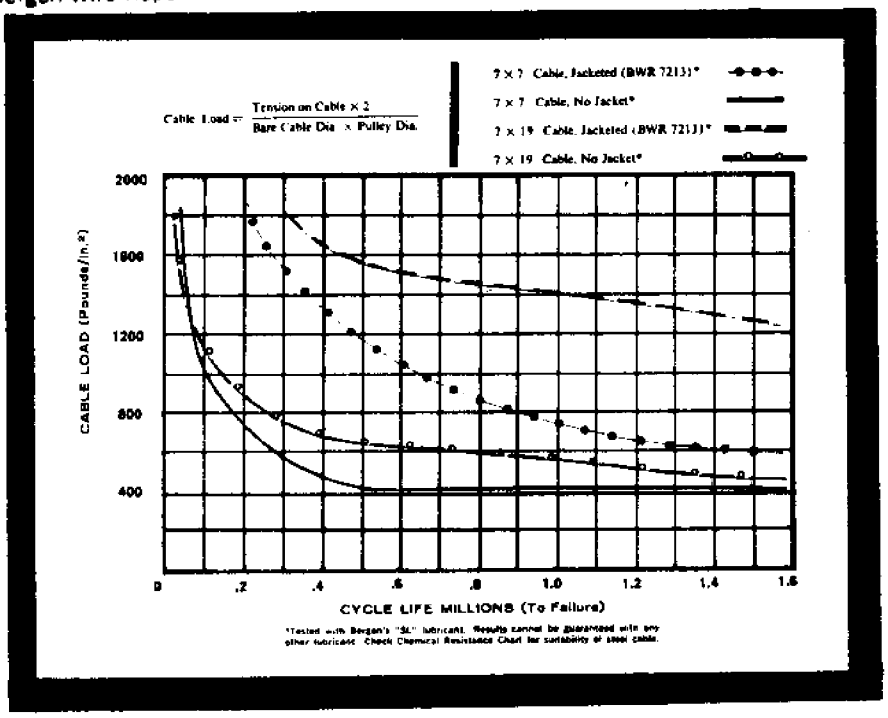

Curves showing fatigue life of bare wire rope and plastic jacketed wire rope. In these typical curves, cable load is defined as twice the cable tension, divided by the bare rope diameter, times the pulley diameter.

Savastano F.

NOMENCLATURE

AIPS	Aluminized Improved Plow Steel
Amp	Amplitude (Vibration)
D	Diameter of Test Sheave
d	Diameter of Cable
GAC	Galvanized Aircraft Cable
GHS	Galvanized High Strength (Steel)
GIPS	Galvanized Improved Plow Steel
GUHS	Galvanized Ultra High Strength (Steel)
GXIPS	Galvanized Extra Improved Plow (Steel)
IWRC	Independent Wire Rope Core
KEVLAR®	E. I. duPont Trademark for Aramid Fibers
NIT 50	Armco NITRONIC 50 Stainless Steel
RBS	Rated Break Strength
Phillystran®	Philadelphia Resins Impregnated Aramid Fiber's

1.2 Laboratory Testing for Enhanced Undersea Cable Survivability

[Stange 83]

- Cable testing experience and summaries of test results

- Experimental testing contributes to improved understanding of failure mechanisms and helps predict service life

- The Role of Laboratory Testing, Static and Dynamic Testing, Examples of Useful Testing (Axial Tension Cycling, Repeated Snap-Load Testing, Cycled Bending over Sheaves, Unsupported Bending, Strumming, Design Verification Testing), Conclusion

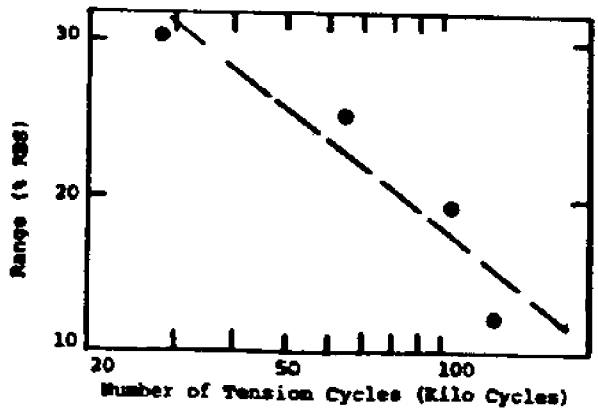

Figure 3: Endurance of 1 x 19 GAC Wire Rope Under Cyclic Axial Tension (Data from Table 3)

TABLE 3

ENDURANCE OF 0.25 INCH DIAMETER 1 x 19 GAC WIRE ROPE UNDER CYCLIC AXIAL TENSION

Tension (% RBS) Minimum	Maximum	Range (% RBS)	Number Of Tests	Average Cycles To Failure[1]
34	64	30	3	28,609
24	49	25	3	63,926
15	34	19	3	104,336
6	18	12	3	135,178[2]

1: Failure defined as two wire breaks in rope.
2: These tests stopped when one wire broke in rope.

[Stange 83]

TABLE 2

ENDURANCE OF SMALL WIRE ROPES UNDER CYCLIC AXIAL TENSION

Description	Manufacturer	Tension (% RBS) Minimum	Maximum	Range (% RBS)	Number Of Tests	Average Cycles To Complete Severance
1/4" 1 x 42 GIPS	A	27.5	52.5	25	5	46,413
1/4" 1 x 42 GUHS	A	27.5	52.5	25	5	46,878
9/32" 3 x 19 AIPS	B	27.5	52.5	25	5	103,840
5/16" 3 x 19 GIPS	C	27.5	52.5	25	2	622,207[1] 261,366[1]

1: One specimen was stopped at 622,207 cycles with no apparent damage. Another specimen was stopped at 261,366 cycles with no apparent damage.

1.3 Fatigue Behavior of Large-Diameter Wire Ropes

[Hanzawa 81]

- The factors that influence the tensile fatigue strength of large-diameter wire ropes and the effects of socket materials on wire breakage in sockets

- The possibility of extrapolation of fatigue data for small diameter wire ropes in order to predict the service life of large diameter wire ropes (Fig.4)

- A new wire breakage detector for the interal wire breakage, making use of acoustic emission and an accelerometer

Table 1 Specifications of Fatigue Tested Wire Ropes.

Code	9S6	9SL6*	6S9	MS9	LC6	6S7	6S8
Type	9 Strand		6 Strand	Multi Strand	Locked Coil	6 Strand	
Construction	37+(9×7)+ 9×WS(36) CFRC		7×7+ 6×{WS(38) +S(40)} CFRC	19×Ses {(7+6)+ (15+15)}	1+6+12+ 18+20Z	7+(6×7)+ 6×WS(36) CFRC	
Nominal Diameter(mm)	50	85	50		32	50	
Number of Wires (mm)	424		505	703	57	265	
Diameter of Wires (mm)	1.39 ~ 2.51	2.36 ~ 4.29	1.04 ~ 2.44	1.22 ~ 1.83	3.13 ~ 5.00	1.83 ~ 2.99	
Lay Length (mm)	462	833	402	452	378	400	
Nominal Cross Section Area (mm^2)	1380	4020	1279	1249	686	1300	
Tensile Strength of Wires (kgf/mm^2)	160		190		165	170	185
Breaking Strength of Wire Rope (kgf/mm^2)	150.0	151.3	171.2	171.7	152.3	156.4	165.4

[Hanzawa 81]

Table 2 Fatigue Test Conditions.

Code	Socketing* Material	Loading Conditions		Tested Frequency (rpm)
		Minimum Stress Smin (kgf/mm^2)	Stress Ratio R	
9S6	ZC	13.0	——	400
9SL6*		9.3~9.6 12.0		——
6S9	ZC. PE. EX	——	0.1. 0.4	400
MS9	PE			
LC6	ZC. EX		0.4	330
6S7	ZC	13.0	——	
6S8				

* ZC : Zn-Cu Alloy. PE : Polyester Resin. EX : Epoxy Resin

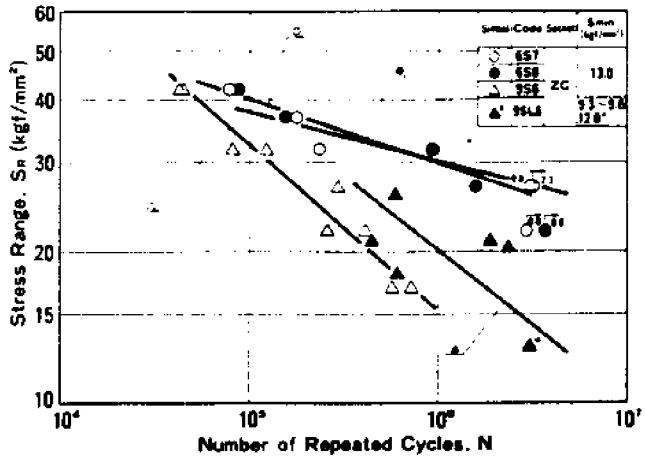

Fig. 4 S_R-N Curves at 5% Breakage Rate for Hanger Ropes.

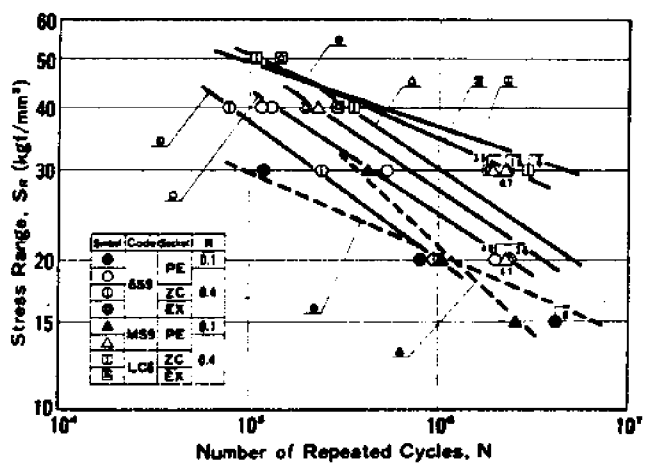

Fig. 5 S_R-N Curves at 5% Breakage Rate for Mooring Ropes.

1.4 Ropes for Deep Water Mooring

[Ronson 80]

- To guide the designers of deep mooring systems and to promote confidence in wire ropes, confidence based on the production, research, site experience

- Design, Fatigue, Corrosion, Mode of Failure, Further Techniques to Improve Corrosion Resistance, Performance Monitoring, Terminations, Handling

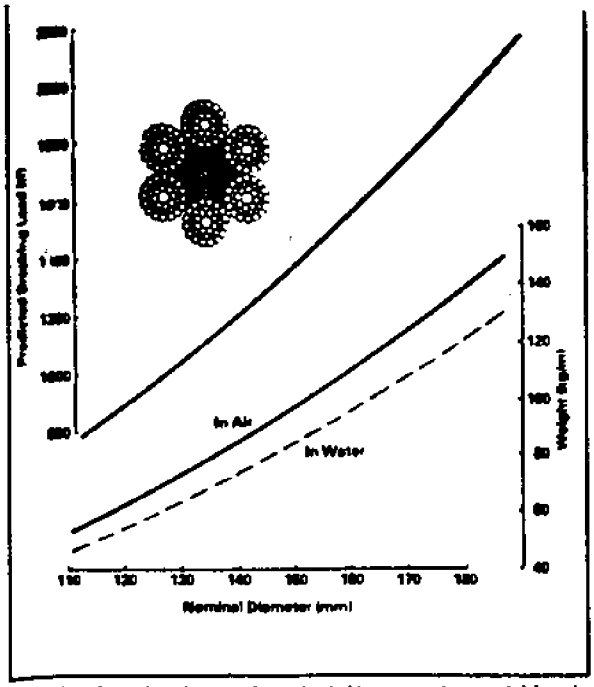

Fig. 1 - Six strand rope characteristics : - size, weight and breaking load relationship.

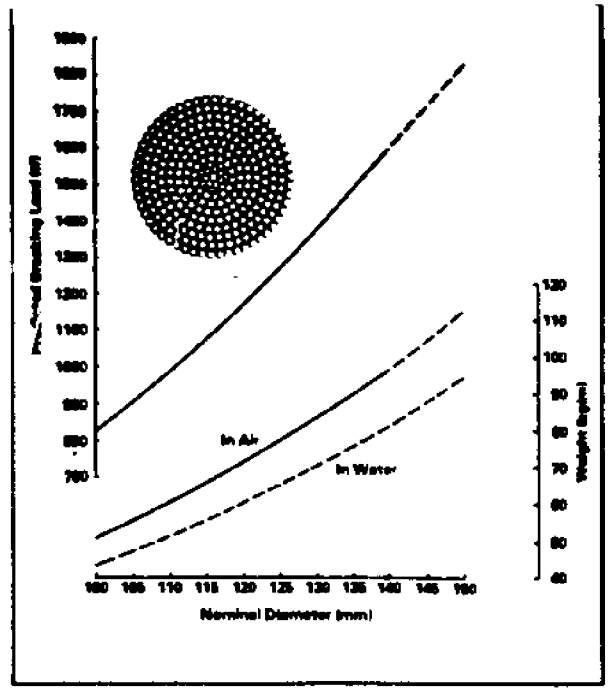

Fig. 2 - Spiral strand characteristics : - size, weight and breaking load relationship.

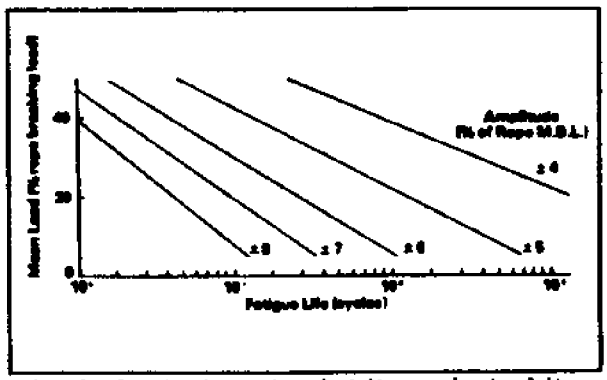

Fig. 3 - Six strand rope characteristics : - tension fatigue.

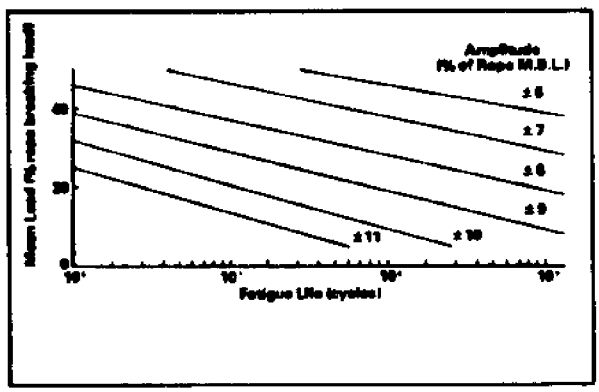

Fig. 4 - Spiral strand characteristics : - tension fatigue.

1.5 Develpments in Fatigue Assessments of Large-Diameter Wire Ropes used in Offshore Moorings

[Waters 85]

- Reviews some recent publications and outlines the results of various full and half cycle tests carried out in the United Kingdom since 1979

- Concluded that, through his collection of fatigue data from several published papers, the extrapolation of data has been shown to be inappropriate (Fig.1)

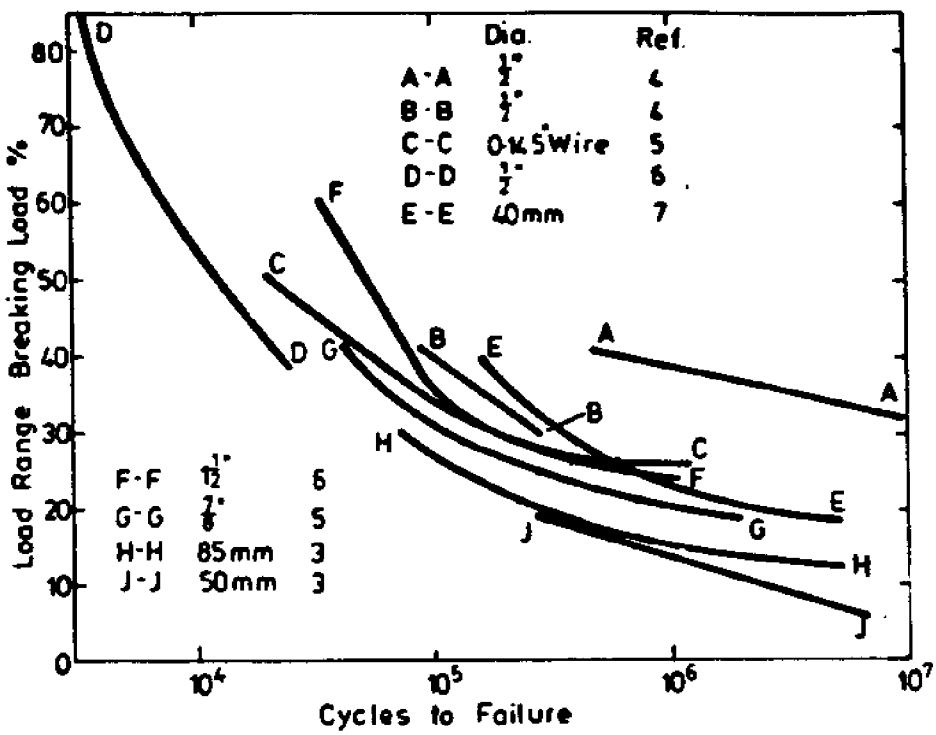

Fig 1 Axial Fatigue Results

the following parameters should be considered when developing a test programme:

Construction of the rope
Manufacturer of product
Size (sample length as well as diameter)
Sample termination
Lubrication and testing environment
(internal and external)
Mean load
Load ranges
Frequency of testing
Sheave/rope diameter ratio for bend tests
Angle of wrap for bend tests

1.6 The Tensile Fatigue of Wire Rope : a New Approach

[Thorpe 83]

- The fatigue behavior in air and seawater of zinc coated steel wire taken from a 40-mm diameter wire rope has been studied

- Experiments : corrosion, fatigue in air, corrosion-fatigue and fretting-fatigue

- Fretting in air has the most deleterious effect on fatigue life. This is supported by the single datum for air testing from the NEL wire rope tests, which lies on the extrapolation of the single wire fretting line (Fig.6)

- Synergistic interaction between corrosion and fretting can cause a substantial reduction in fatigue life for wire ropes in sea water (Fig.7)

- Fatigue endurance has a strong dependence on stress range, but no effect of the mean stress has been observed in air (Fig.3). Also [Matanzo 72], [Lucht 77] and [Ronson 80] derive the same conclusion

- Corrosion-Fatigue endurance is decreased with increasing mean stress (Fig.4). This observed trend is contradictory to the results of wire ropes reported in [Hanzawa 81]

TABLE 1

RESULTS OF FATIGUE TESTS ON SINGLE WIRES

COATING	ENVIRONMENT	TEST FREQUENCY (Hz)	MEAN STRESS (% UTS)
Hot-dipped	air	4.0	50
Hot-dipped	air	4.0	20
Hot-dipped	seawater	4.0	50
Hot-dipped	seawater	0.1	50
Hot-dipped	seawater	0.1	20
Hot-dipped	air + fretting	4.0	50
Hot-dipped (after removal of half coating thickness)	seawater	0.1	50
Electrogalvanised	air	4.0	50
"	seawater	4.0	50
"	seawater	0.1	50
" (after removal of half coating thickness)	seawater	0.1	50
Bare wire	seawater	0.1	50

TABLE 2

RESULTS OF TENSILE TESTS ON SINGLE WIRES (AVERAGE OF THREE TESTS ON EACH TYPE)

TYPE OF WIRE	UTS (MPA)
Hot-dipped	1840
Electrogalvanised	1831
Hot-dipped after removal of half the coating thickness	1826
Bare wire	1820
Hot-dipped after immersion in seawater for six months	1826

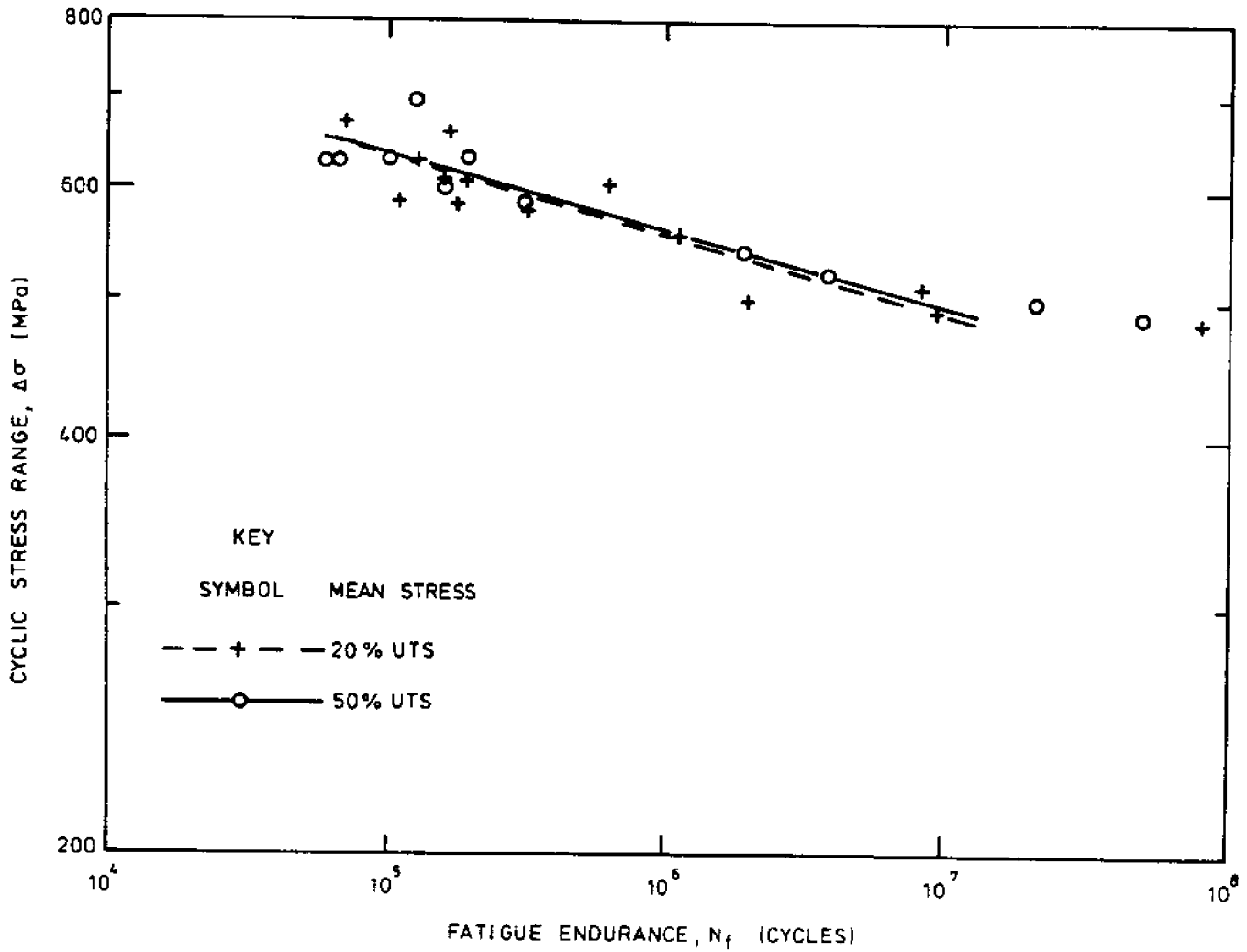

FIG.3. EXPERIMENTAL RESULTS FOR HOT-DIPPED WIRE IN AIR

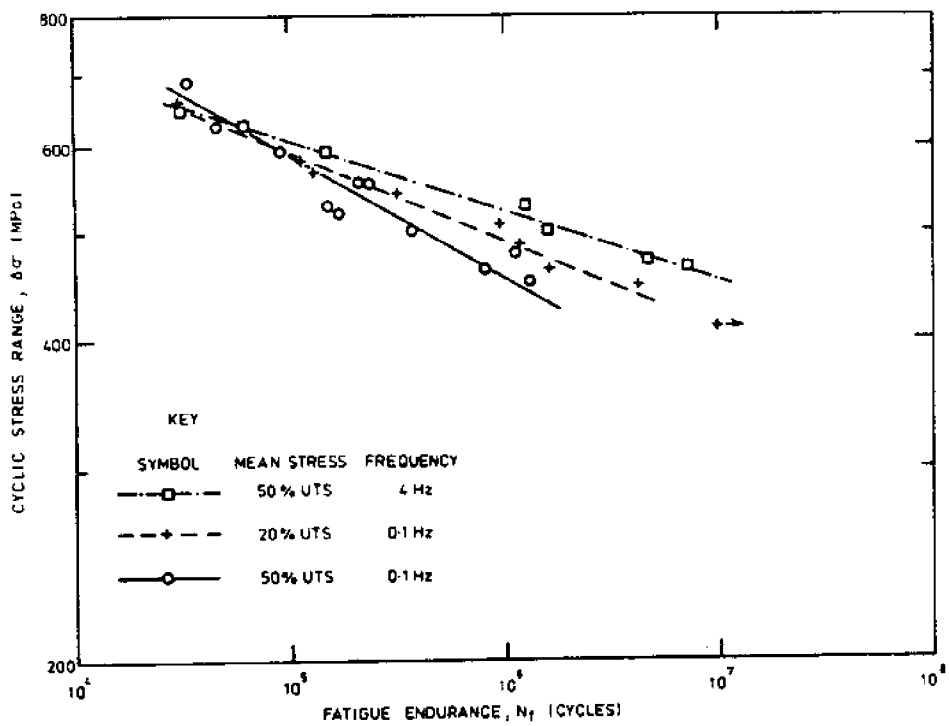

FIG. 4. EFFECT OF MEAN STRESS AND TEST FREQUENCY ON FATIGUE LIFE OF HOT-DIPPED WIRE IN SEAWATER

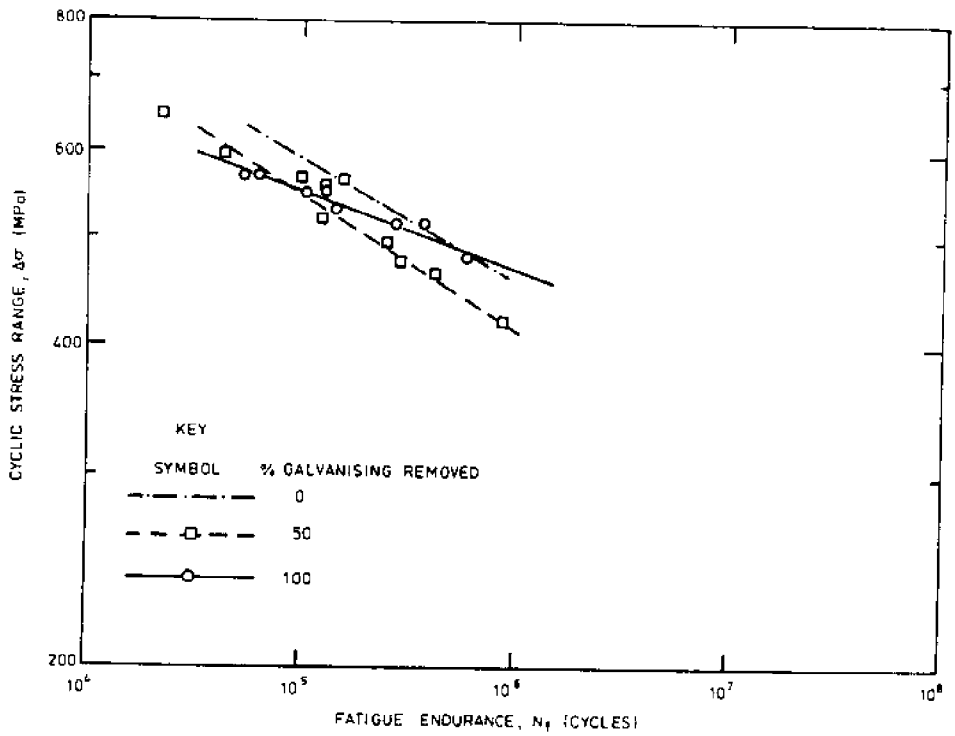

FIG. 5. EFFECT OF DECREASE OF AMOUNT OF GALVANISED COATING ON FATIGUE LIFE ON HOT-DIPPED WIRE IN SEAWATER AT 0·1 Hz WITH A MEAN TENSILE STRESS = 50 % UTS.

[Thorpe 83]

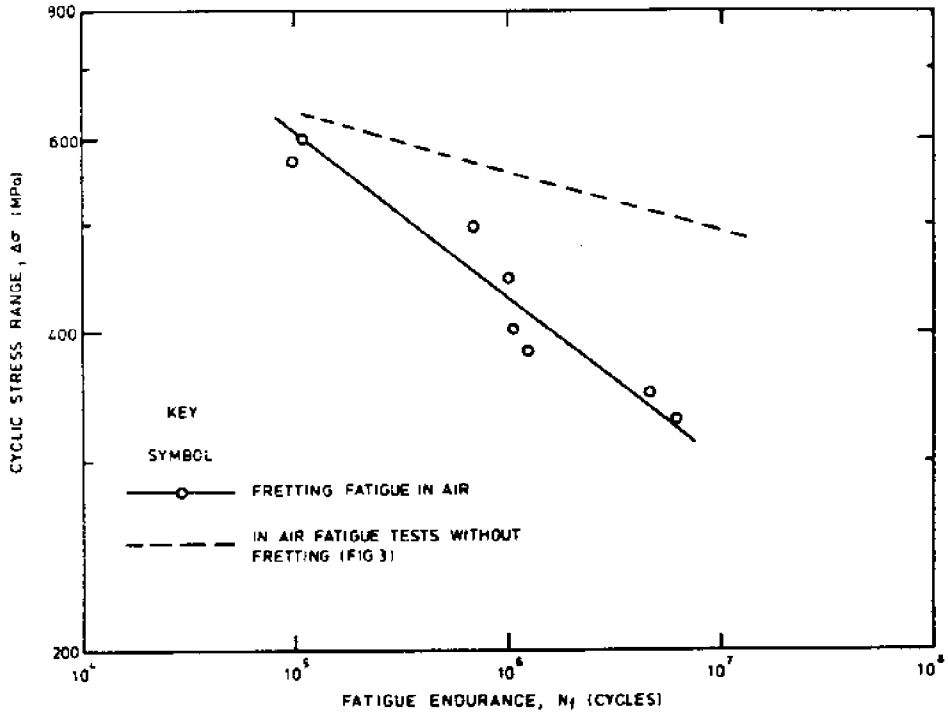

FIG. 6. EFFECT OF FRETTING ON FATIGUE LIFE OF HOT-DIPPED WIRE IN AIR WITH A MEAN TENSILE STRESS = 50% UTS

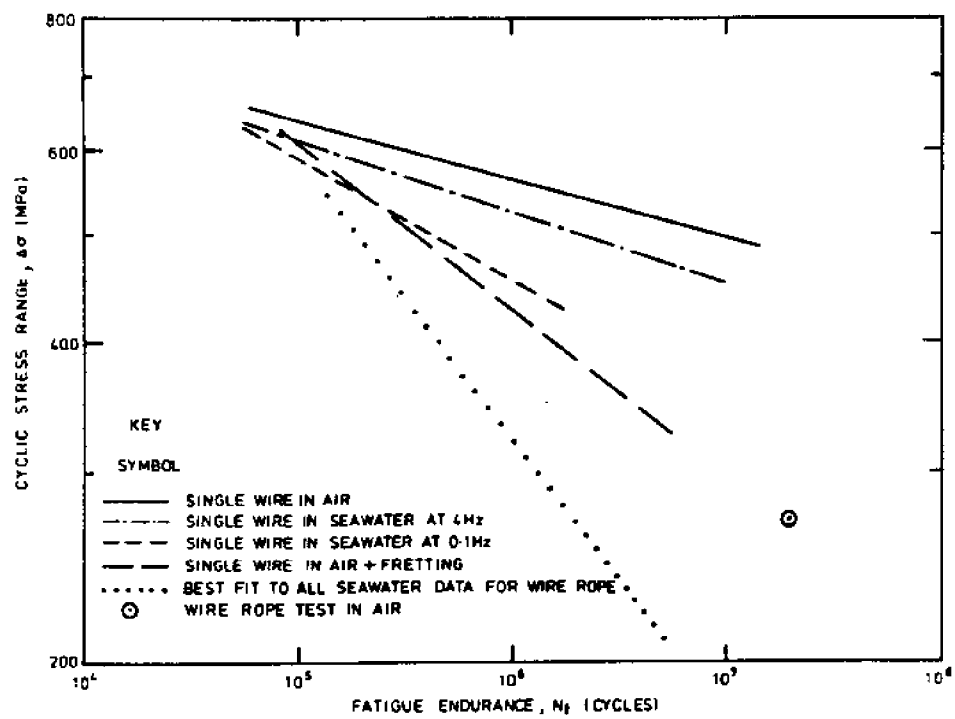

FIG. 7. SUMMARY OF SINGLE WIRE TESTING WITH MEAN STRESS = 50% UTS AND COMPARISON WITH RESULTS OF FATIGUE TESTS ON 40 mm. DIAMETER ROPE

[Thorpe 83]

1.7 Wire Rope

[Gibson 83]

- Figures are related to basic components of a wire rope, wire rope construction, lay, bending stress, Axial fatigue test data for steel rope,and Bending fatigue life

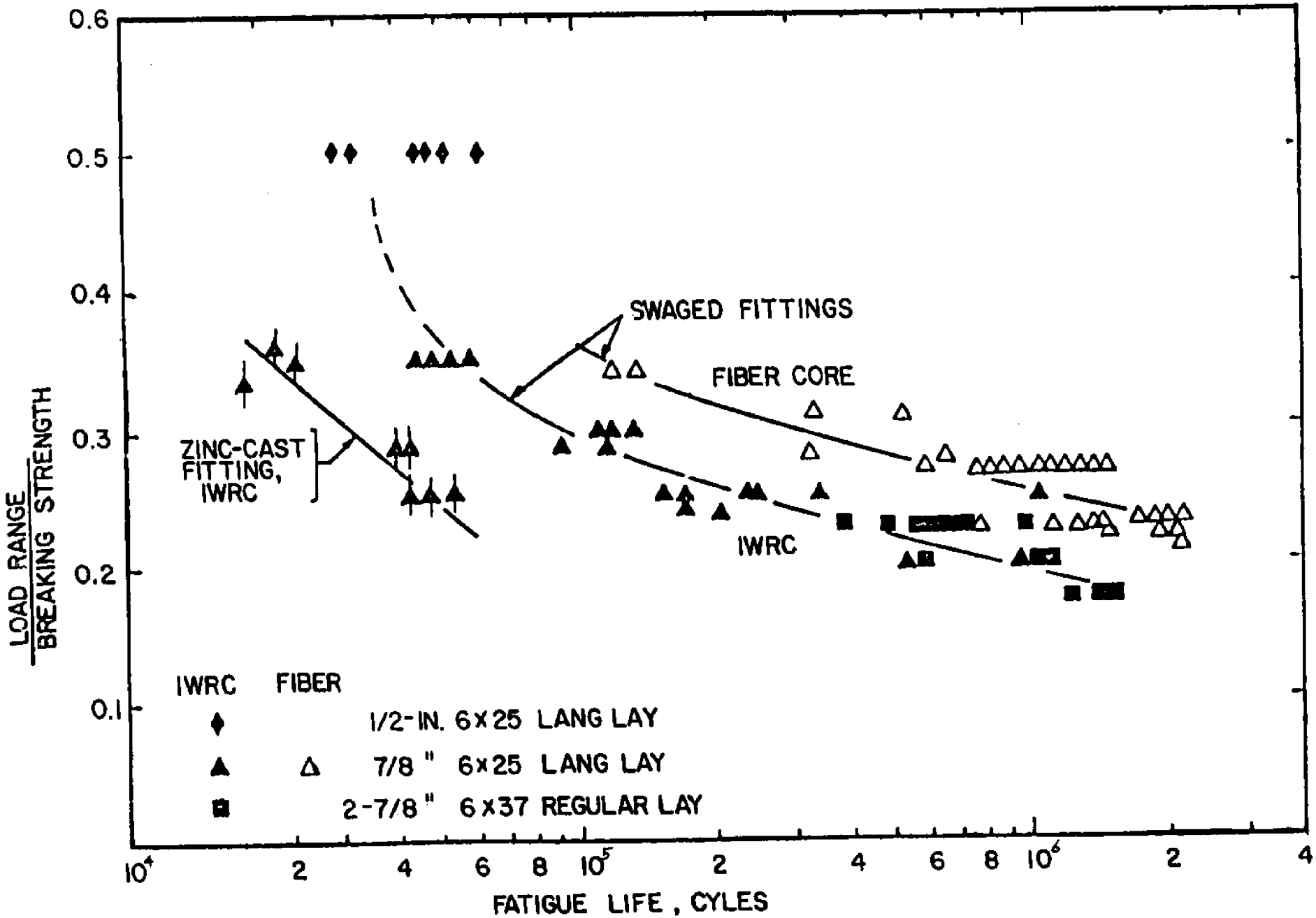

AXIAL FATIGUE TEST DATA FOR STEEL ROPE [Gibson 83a]

1.8 Factors Affecting Wire Rope in a Marine Environment

[Lucht 77]

- Wire rope life in a marine environment, affected by many factors, such as fatigue, corrosion, deployment methods and combinations of all three factors

- Fatigue tests by U.S. Steel Corporation plus experience in the Woods Hole Buoy Program

- Suggested that there may be a fatigue limit for wire ropes in axial tension fatigue (Fig.4)

- Concluded that plastic jacketed, drawn galvanized, torque balanced wire ropes with booted terminations provide performance superior to any other wire rope configuration

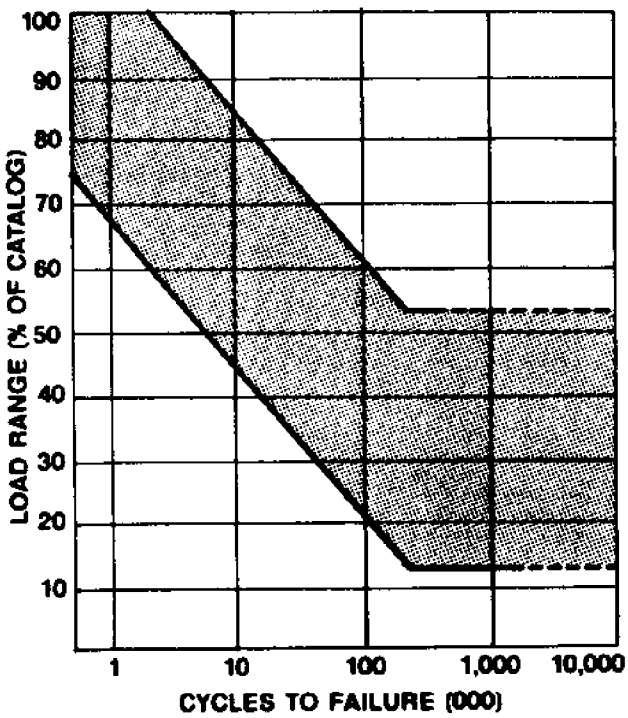

Fig. 4 - Axial tension fatigue.

Table II - Breaking Strengths of 5/16" 1 x 7 Galvanized Strand After Exposure For The Period Shown In A Severe Marine Atmosphere

Date	Exposure Period (Months)	Breaking Strength (Lbs.)
10/12/66 (Beginning of Test)	(Prior to exposure)	12,800
9/22/67	11	12,900
10/15/68	24	12,850
12/8/69	37	12,800
6/17/74	92	12,900
10/4/76	120	12,880

Table III - SEACON II - Rope Test Data

Description

1/2" Amgal Monitor AA Torque Balanced Rope Elevated Elastic Limit With Polyethylene Jacket

Breaking Strength (Pounds)	New	After 22 Months At Sea
	27,050	26,100
Fatigue Life*	46,400	72,700 (Avg. of 2)

* - Cycles to failure at load range 40% of Catalog Breaking Strength

TABLE I
RESULTS OF AXIAL TENSION FATIGUE TESTS

Wire Rope Size & Construction	Load Range (% Cat.)	Cycles To Failure	Termination Type
5/16" 3x19	50	123,000	S/B
Torque-Balanced	40	263,000	S/B
	35	287,000	S/B
	30	2,000,000	S/B
	25	2,000,000	S/B
1/2" 3x19	99	680	Z
Torque-Balanced	89	3,319	Z
	79	3,531	Z
	79	1,222	S
	69	7,432	S
	69	5,080	Z
	40	65,500	S
	40	21,798	Z
	40	46,000	S
	40	30,000	Z
	40	40,000	Z
	40	35,000	Z
	40	30,000	Z
7/8" 3x19	50	39,000	S
Torque-Balanced	40	27,000	S
	33	206,000	S
	25	729,000	S
	20	2,000,000	S
3/4" 3x46	60	26,785	E
Torque-Balanced	60	7,585	E
	40	92,000	E
	40	60,000	E
	20	2,000,000	E
1-1/2" 3x46	42	63,736	Z
Torque-Balanced	40	87,000	S
	40	95,000	S
	30	229,000	S
	20	1,413,000	S
	20	789,000	S
1-3/4" 3x46	50	40,000	S
Torque-Balanced	33	171,265	Z
	33	91,234	Z
	30	143,000	S
	25	251,000	S
	20	657,000	S
	15	1,564,000	S
3/4" 6x25 FW IWRC	70	13,000	Z
	52	15,000	Z
	35	73,000	Z
7/8" 6x25 FW IWRC	50	20,000	Z
	50	250,000	Z
	50	97,000	Z
	40	269,000	Z
	40	126,000	Z
	37	84,000	Z
	37	35,000	Z
	37	30,000	Z
	37	48,000	Z
	30	290,000	Z
	30	565,000	Z
	30	759,000	Z
	30	44,000	Z
	30	108,000	Z
	25	273,000	Z
	25	570,000	Z
	25	425,000	Z
	25	199,000	Z
	25	2,000,000	Z
	25	2,000,000	Z
	25	282,000	Z
1-3/8" 6x25 FW IWRC	45	450,000	S
	30	520,000	Z
	30	550,000	Z
	30	140,000	Z
	30	318,000	Z
	30	360,000	S
	30	193,000	S
1-1/2" 6x25 FW IWRC	60	33,000	Z
	60	34,000	Z
	45	63,000	Z
	37	85,000	Z
	30	148,000	Z
	30	460,000	Z
	24	1,600,000	Z
1-5/8" 6x25 FW IWRC	38	36,000	Z
	38	36,000	Z
2-1/4" 6x25 FW IWRC	45	64,000	Z
2-11/16" 6x32 (2-Op.)	13	1,696,000	Z
Strand Core	13	1,157,000	Z
(Used Rope from	13	1,183,000	Z
Golden Gate Bridge)	13	2,000,000	Z
	13	2,000,000	Z
	13	1,657,000	Z
	06	2,828,000	Z
1-5/8" 6x46 IWRC	38	158,000	Z
	38	74,000	Z

S = Swaged Socket
Z = Zinc Socket
E = Epoxy Filled Zinc Socket
S/B = Swaged Socket with Boot

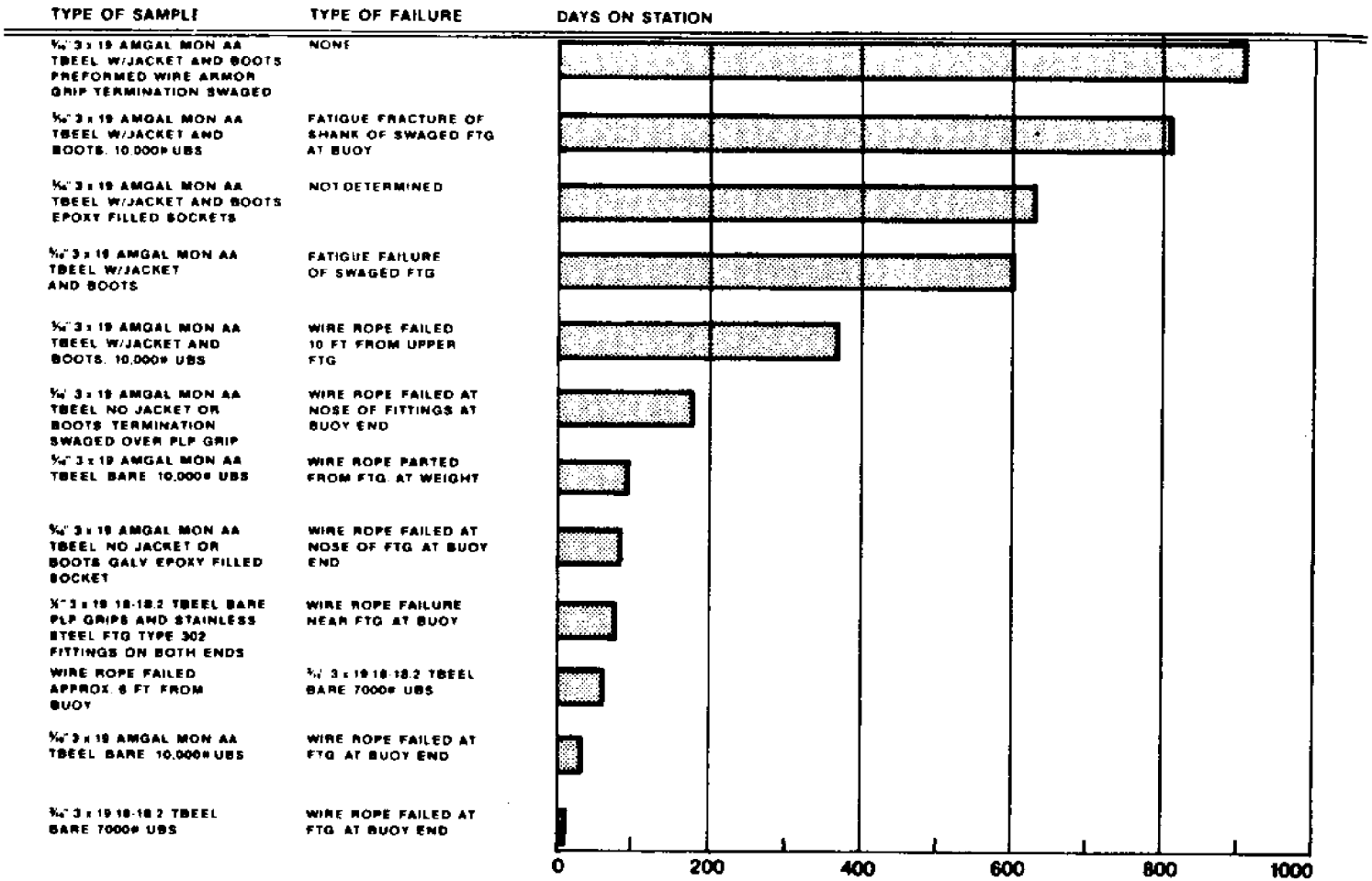

Fig. 5 - United States Steel Corp. mooring lines wire rope life at Woods Hole Buoy Farm.

1.9 Axial Fatigue of Wire Rope in Sea Water

[Matanzo 72]

- The axial fatigue resistance in air and seawater of wire rope measured in a laboratory experiment

- The effect of rope construction and core, as well as the effect of the applied mean load and load range

- Concluded that Lang, IWRC wire rope appeared to be the best for marine applications, although it suffered the greatest loss in fatigue life due to corrosion (Fig.4). This conclusion is, however, not in agreement with the API SPEC. [API 84a] and results from [Acaster 72]

- Acaster and API SPEC. recommend right lay, regular lay, IWRC, performed, galvanized or bright(bare) wire ropes for mooring systems. [Acaster 72] and [API 84a, 6.23]

TABLE 2 - AXIAL FATIGUE LIVES IN MILLIONS OF CYCLES OF 1/2 IN. DIAMETER, 6 X 25 w, IPS, BRT, FS WIRE ROPE

A Construction	LANG								REGULAR							
B Core	IWRC				POLY				IWRC				POLY			
C Load Range (%BL)	30		40		30		40		30		40		30		40	
D Mean Load (%BL)	20	30	20	30	20	30	20	30	20	30	20	30	20	30	20	30
AIR TESTS																
Two Replications	5.3	19.5	0.376	0.517	3.8	10.0	0.110	0.170	1.25	1.2	0.24	0.20	5.31	0.985	0.28	0.316
	16.1	10.0	0.481	0.600	3.5	2.4	0.190	0.258	1.5	2.5	0.291	0.291	13.6	4.79	0.97	0.280
Geometric Mean	9.45	13.96	0.425	0.557	3.64	4.9	0.144	0.208	1.37	1.73	0.264	0.241	8.50	2.17	0.521	0.298
Pooled Geometric Mean	11.358		0.487		4.227		0.174		1.540		0.252		4.296		0.351	
	2.351				0.858				0.623				1.228			
	1.420								0.875							
	1.115															
SEA WATER TESTS																
Two Replications	0.352	0.225	0.113	0.086	0.427	0.311	0.127	0.120	0.377	0.365	0.118	0.116	0.523	0.309	0.205	0.144
	0.274	0.210	0.085	0.101	0.217	0.325	0.150	0.157	0.390	0.257	0.124	0.159	0.389	0.232	0.173	0.119
Geometric Mean	0.310	0.212	0.098	0.093	0.304	0.318	0.138	0.137	0.383	0.306	0.121	0.136	0.451	0.268	0.189	0.131
Pooled Geometric Mean	0.257		0.095		0.311		0.136		0.343		0.128		0.347		0.157	
	0.157				0.205				0.210				0.233			
	0.179								0.221							
	0.199															

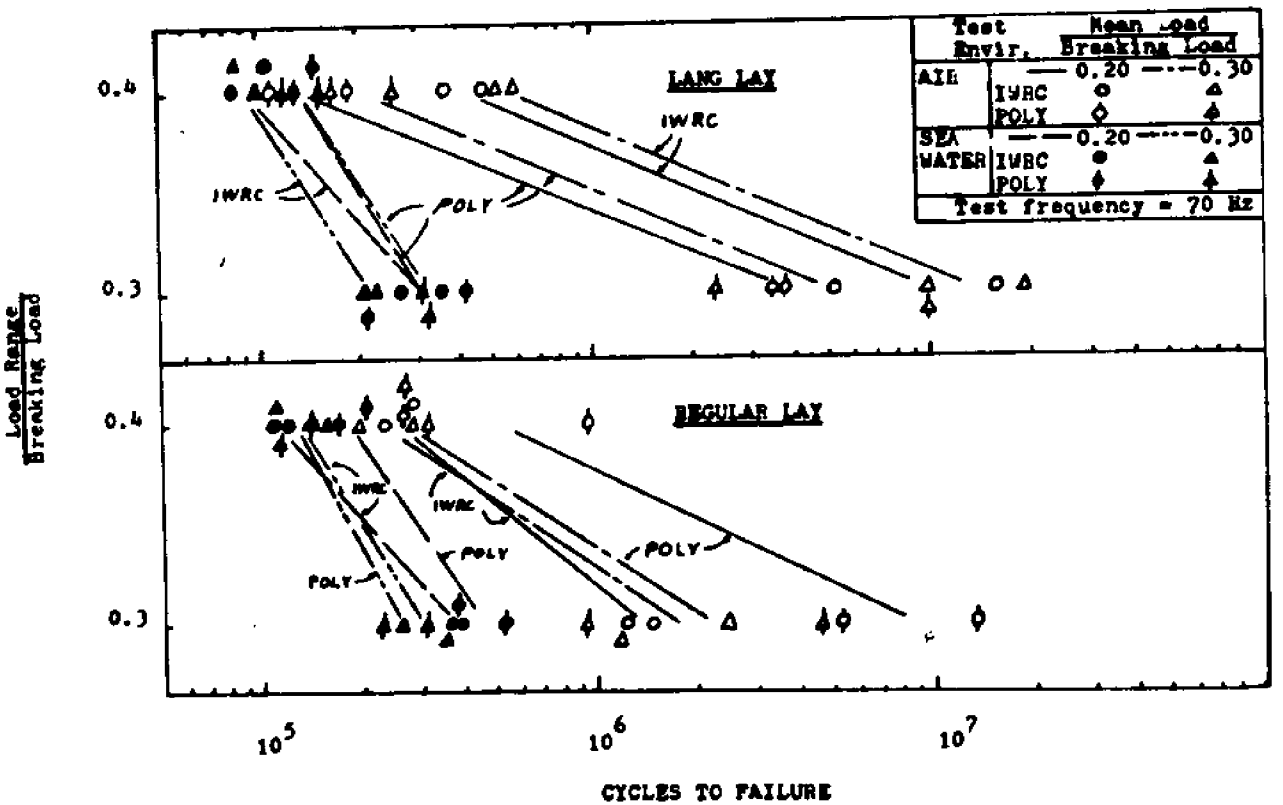

Fig. 4 - Axial fatigue life of 1/2-in. diameter, 6 X 25 W, IPS, BRT, FS rope.

[Matanzo 72]

2 Chain

2.1 Long-Term Mooring and Anchoring of Large Structure and Drilling Units -- Reliability and Safety of Anchor Chain Systems

[Berg 80]

- In the period 1976-80 more than 25 anchor chain failures have occured in the North Sea

- The initiation regions of the failures are associated with 4 different kinds of defects
    - o overheating defects in the link bend
    - o weld defect in or adjacent to the flash butt weld
    - o brittleness in the HAZ of study welds
    - o inferior impact properties in weld region and base material

Refer to [OTC 5059, 1985] by Taraldsen

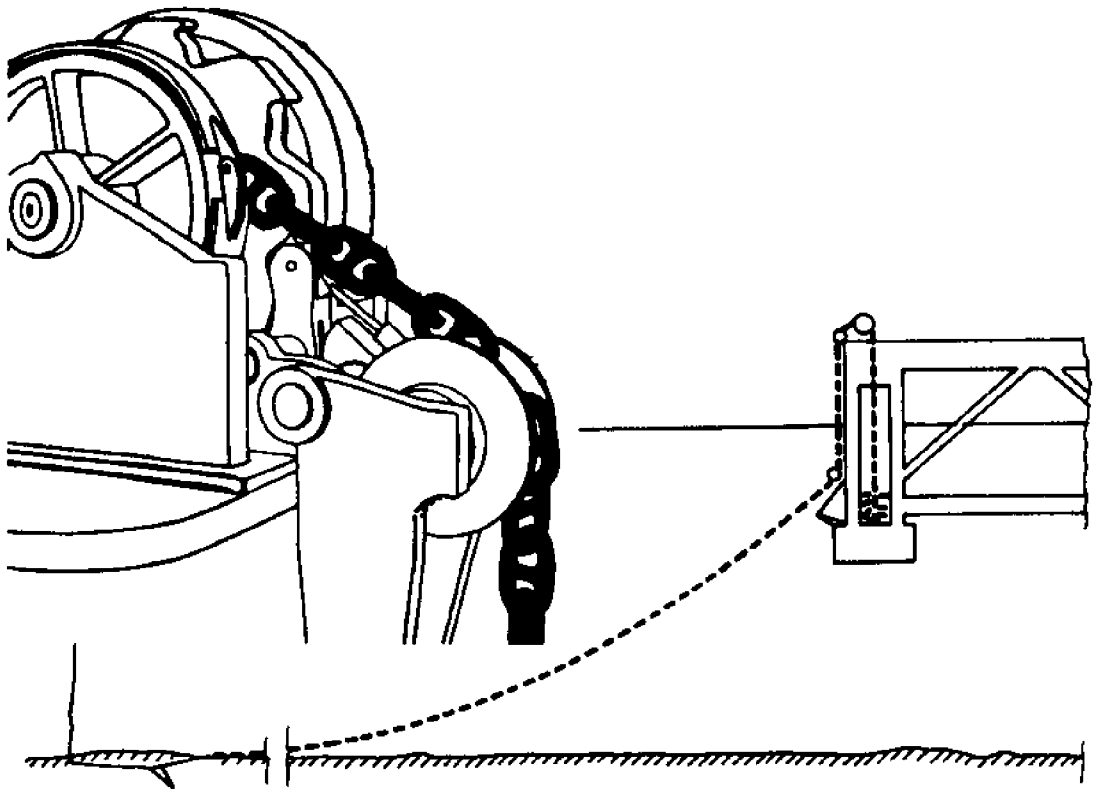

Fig. 1 - Anchor chain system - Fairlead.

TABLE 1

ANCHOR CHAIN FAILURES

Investigated by Det norske Veritas Aug 1976 – Jan. 1980

POSITION OF LINK	LINK REGION	TYPE OF DEFECT	DEFECT DEPTH	TOUGHNESS CHARPY-V at °C	FRATURE LOAD KIPS
AT SEA	BEND	OVERHEATING	40 mm		
AT FAIRLEAD	WELD	WELD DEFECT	6 mm	NLWELD 30 J	275
AT FAIRLEAD	NEAR WELD	CRACK	6 mm	140 J	275
AT SEA	BEND	OVERHEATING	20 mm		280
AT FAIRLEAD	WELD	WELD DEFECT	3 mm		150
AT FAIRLEAD	WELD	WELD DEFECT	5 mm	33 J	275
AT SEA	BEND	OVERHEATING	17 mm		430
AT SEA	BEND	OVERHEATING	–		–
AT SEA	BEND	OVERHEATING	16 mm		600
AT FAIRLEAD	STUD WELD	BRITTLE HAZ	.5 mm	16 J (15)	ca. 100
AT FAIRLEAD	←	LINK LOST	→	NL: 36 J	150
AT FAIRLEAD	←	LINK LOST	→	NL: 213 J	
AT FAIRLEAD	BEND	NO DEFECT	0	40 J	225
AT CHASER	STUD WELD	BRITTLE HAZ	.5 mm	13 J (10)	150
AT FAIRLEAD	WELD	WELD DEFECT	10 mm	63 J	280

NL = NEIGBOUR LINK

2.2 Failure Analysis of a Calm Buoy Anchor Chain System

[Shoup 84]

- A wear failure of a catenary anchor chain mooring used to moor a CALM type buoy

- Failure Hypothesis, Metallurgy and Wear, Wear Studies, Results of Wear Studies, Model Test Program, Model Test Results, Synthesis of Model Test and Wear Test Results

- The cause of wear failure was excessive wear generated by large values of interlink force and motion induced by the dynamic behaviour of the antisymmetric 4-leg mooring pattern (Fig.11)

TABLE 1

MAIN PARTICULARS OF MOORING THAT FAILED

Buoy type:	Calm 12m diameter
Mooring pattern:	Reference Figure 1
Anchor leg configuration:	140 ft 4-1/2 in U4 (off buoy) 1980 ft 5 in U3 (off pile)
Water Depth:	250 ft
Pretension angle:	60°
Hawser:	Double grommet nylon (4 lines) circumference = 20 in length = 51.2m
Tanker size:	100,000 DWT
Length between perpindiculars:	288m
Breadth:	34m
Depth:	19.7m
Draft at failure:	7.6m
Displacement weight at failure:	60,650 mt

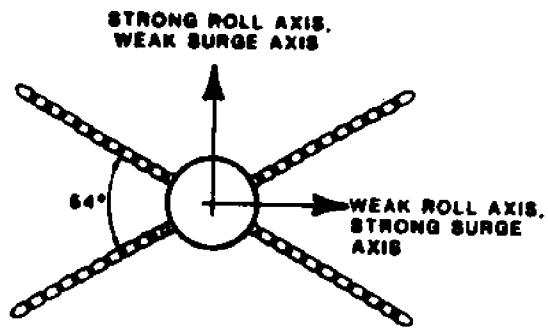

MATINLOC 4 LEG ANCHOR CHAIN PATTERN
THAT EXPERIENCED SEVERE WEAR

FIGURE 1

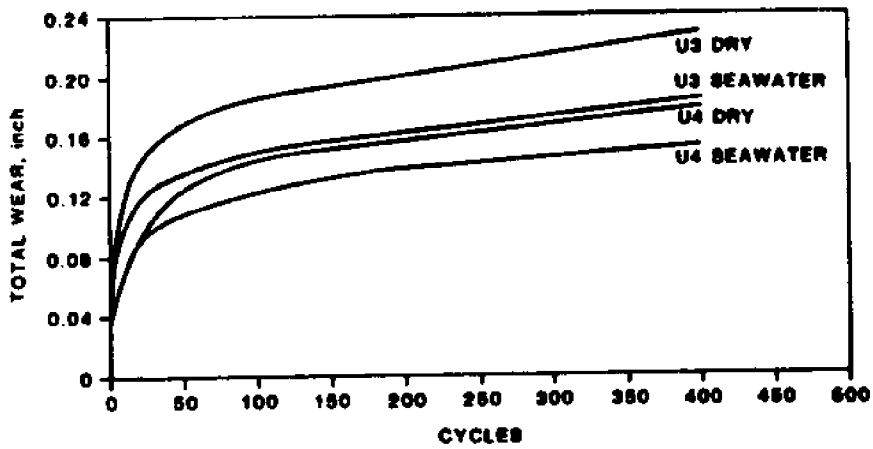

WEAR OF U4 AND U3 CHAIN LINK STEEL
AT 8170 LBS (300 metric ton equivalent)

FIGURE 6

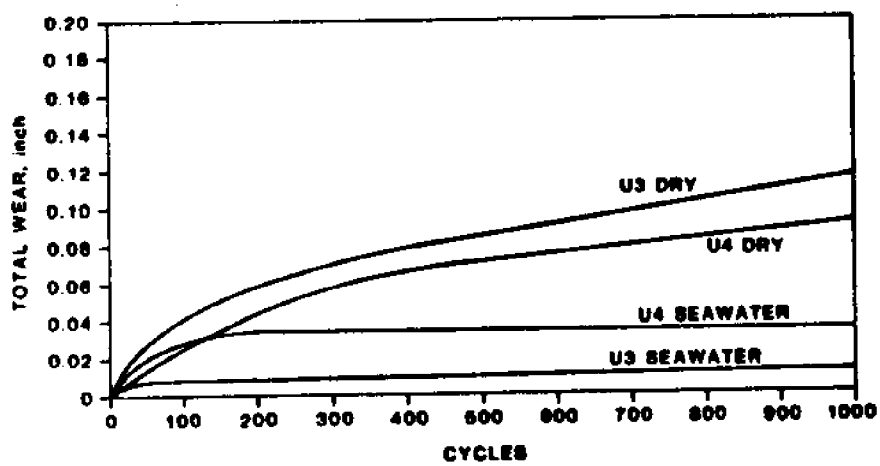

WEAR OF U4 AND U3 CHAIN LINK STEEL
AT 1360 LBS (50 metric ton equivalent)

FIGURE 7

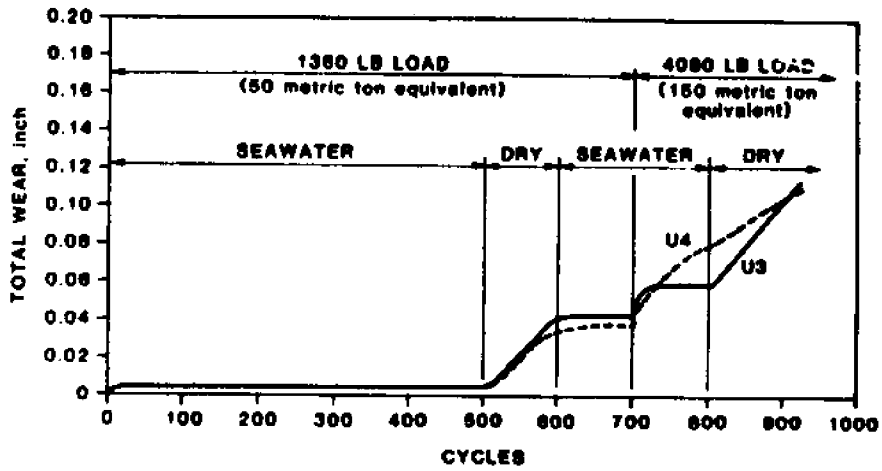

COMPARISON OF U4 AND U3 STEELS UNDER
DRY AND WET SLIDING AT TWO LOAD LEVELS

FIGURE 8

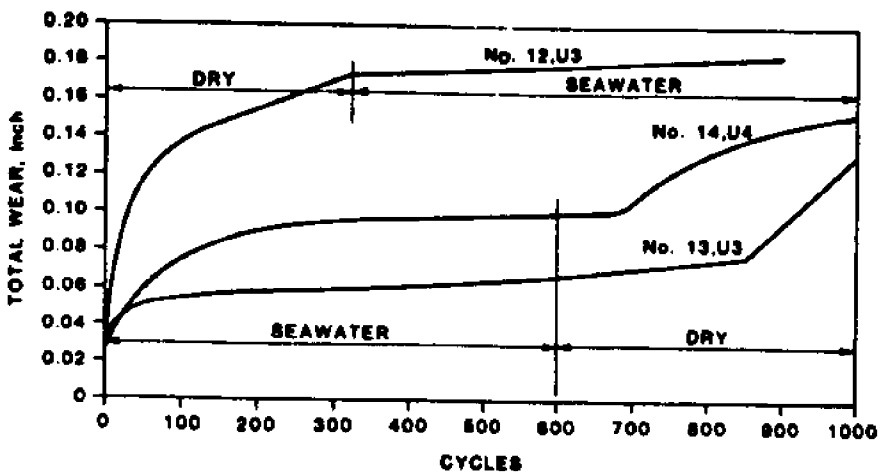

WEAR BEHAVIOR OF U4 AND U3 STEELS
AT A 4080 LB LOAD (150 metric ton equivalent)

FIGURE 9

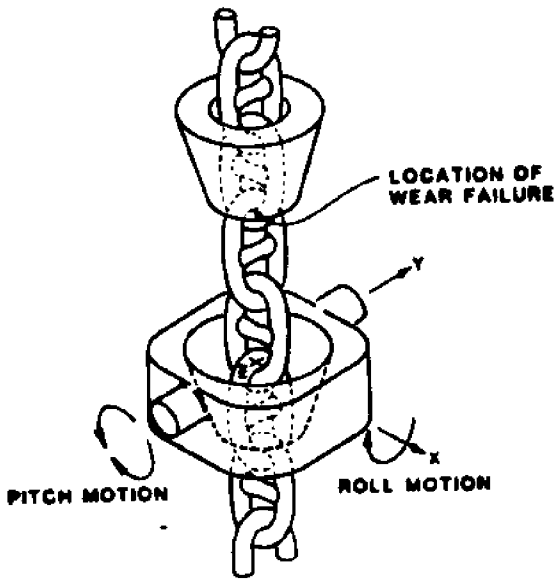

FIGURE 10

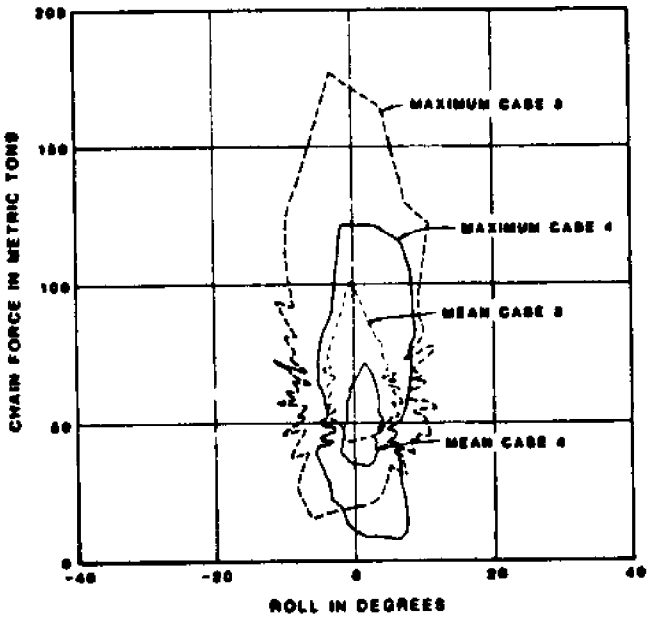

VECTOR DISTRIBUTION PLOT OF
ANCHOR CHAIN FORCE AND ROLL ANGLE

FIGURE 11

2.3 Toward improving the reliability of anchor chain and accessories

[Stern 78]

- Present an approach for improving the reliability of mooring systems for ships and mobile offshore drilling units

- Records of equipment failures on ABS classed vessels reported during two periods, 1965 - 1968 and 1973 - 1977

- Mooring system components : anchors, anchor shackle, connecting links, chain (common links)

- Cases of failure : internal unsoundness,weld unsoundness, brittle failures

- Minimizing failures

TABLE V

MOORING EQUIPMENT FAILURES[1]

Component	1965-1968		1973-1977		Total	
	No.	%	No.	%	No.	%
Anchor	19	21	75	21	94	21
Connecting Link[2]	35	38	143	40	178[4]	40
Chain Link	21	23	75	21	96	21
Bitter End[3]	16	18	66	18	82	18
Total	91	100%	359	100%	450	100%
Approx. No. of Ship Years	25,000		70,000		95,000	

1. All failures were associated with ships with the exception of two drilling unit failures (one connecting link and one chain common link failure).

2. Many reports did not clearly discriminate when the failure was reported as an "Anchor Shackle," between the anchor shackle and an adjacent joining shackle - therefore the category includes some anchor shackle (ring) failures.

3. Most bitter end failures were related to windlass malfunction or operator error.

4. A total of 67 of these failures were reported as Anchor Shackle failures, although it was apparent from examination of survey reports that many were actually failures of the first chain joining shackle.

TABLE VI

EQUIPMENT FAILURES WITH ANCHOR AND BITTER END EXCLUDED

Component	Failures		
	% of Total	% Excl. Anchor	% Excl. Anchor & Bitter End
Anchor	21	--	--
Bitter End	18	23	--
Chain	21	27	35
Connecting Link	40	50	65
Total	100	100	100

2.4 Preload Influence on Fatigue Characteristics of Chain Cable Exposed to Salt Water and Atmospheric Conditions

[Celander 72]

- Stress conditions of an anchor chain link

- Fatigue tests by the laboratories of Domnarverts Jernverk in Sweden

- Fatigue Characteristics of corroded and uncorroded links of special alloy Oil Rig Quality

- The fatigue tests show the negative effect of corrosion and the favourable effect of preload, as expected (Fig.4)

- The proof load, or preload, stiffens up the material and changes the stress picture in a favourably way, because a repeated load on a proof-loaded link must first overcome the negative stress at the most exposed point of the link (Fig.2)

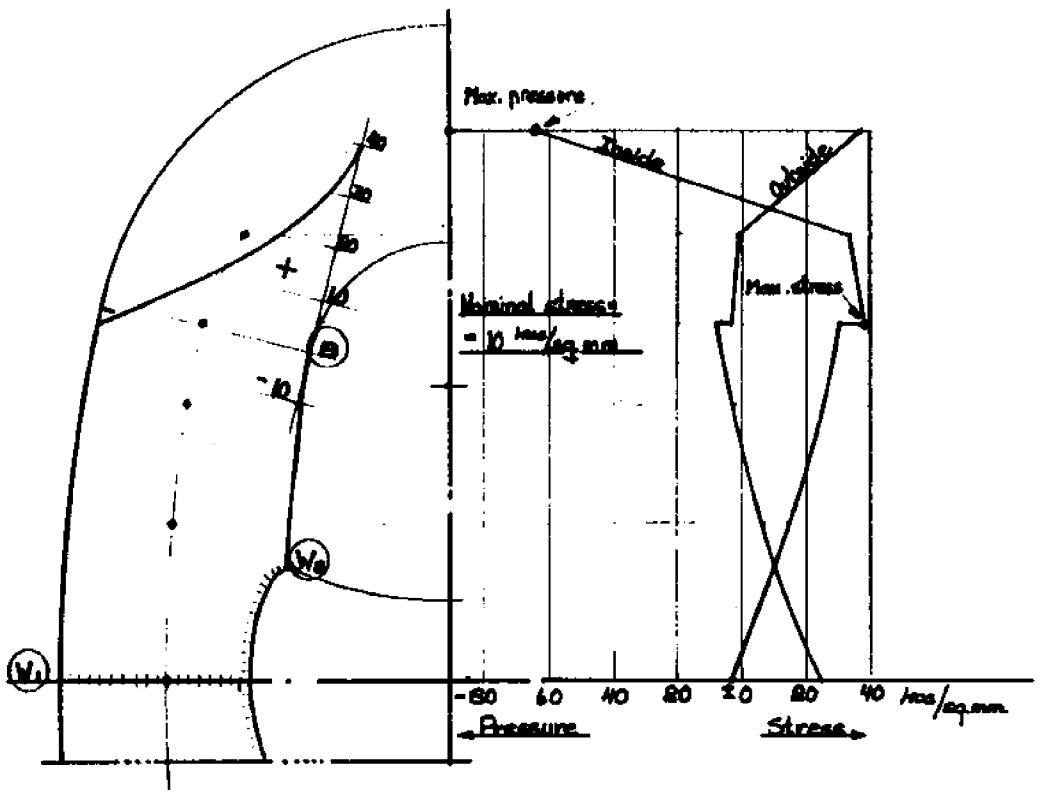
Max. pressure
Nominal stress
= 10 kms/sq.mm
Max. stress
-150
60
40
20
0
20
40
kms/sq.mm
Pressure
Stress
B
W1
W2

Fig. 1

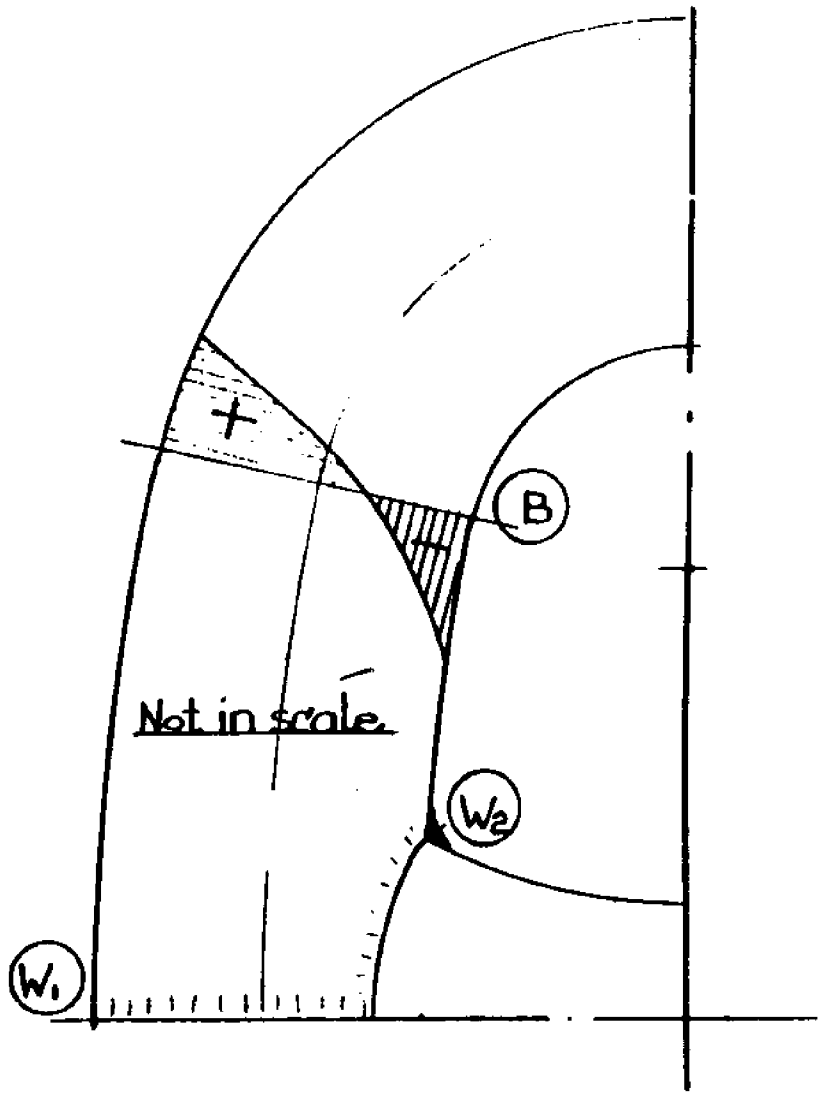
Not in scale.
B
W1
W2

Fig. 2

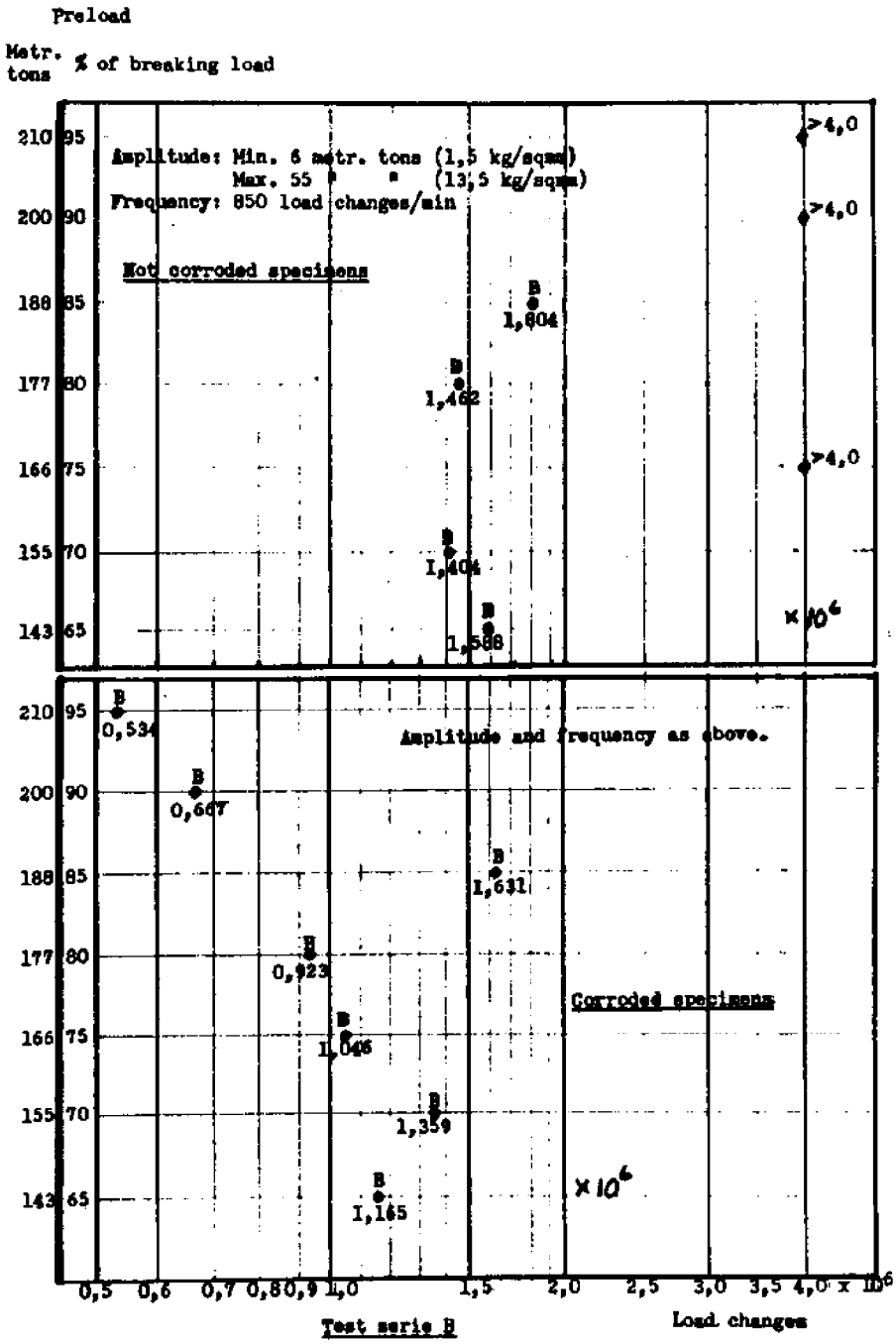
Preload
Metr. tons
% of breaking load
Amplitude: Min. 6 metr. tons (1,5 kg/sqmm)
Max. 55 " " (13,5 kg/sqmm)
Frequency: 850 load changes/min
Not corroded specimens
B 1,804
B 1,462
B 1,404
B 1,588
>4,0
>4,0
>4,0
x 10^6
Amplitude and frequency as above.
B 0,534
B 0,667
B 0,923
B 1,046
B 1,359
B 1,165
B 1,631
Corroded specimens
x 10^6
0,5 0,6 0,7 0,8 0,9 1,0 1,5 2,0 2,5 3,0 3,5 4,0 x 10^6
Test serie B
Load changes

Fig. 4

Quality	Number of load changes	Break at	Remarks	Serie No.
CRQ Grade 3 Grade 2	2271000 2610000 1789000	B B B	Only proofloaded Not corroded	1
CRQ Grade 3 Grade 2	10^7 3081000 10^7	- B -	Preloaded (95%) Not corroded	2
CRQ Grade 3 Grade 2	559400 340700 388500	B W_1 B	Only proofloaded Corroded	3
CRQ Grade 3 Grade 2	837100 871600 845800	W_1 W_2 W_1	Preloaded (95%) Corroded	4

Amplitude: Min. 11,5 metr. tons (1,5 kg/sqmm)
Max. 77,0 " " (10 kg/sqmm)

Frequency: 850 load changes/min

Proof load equal to 67% of breaking load

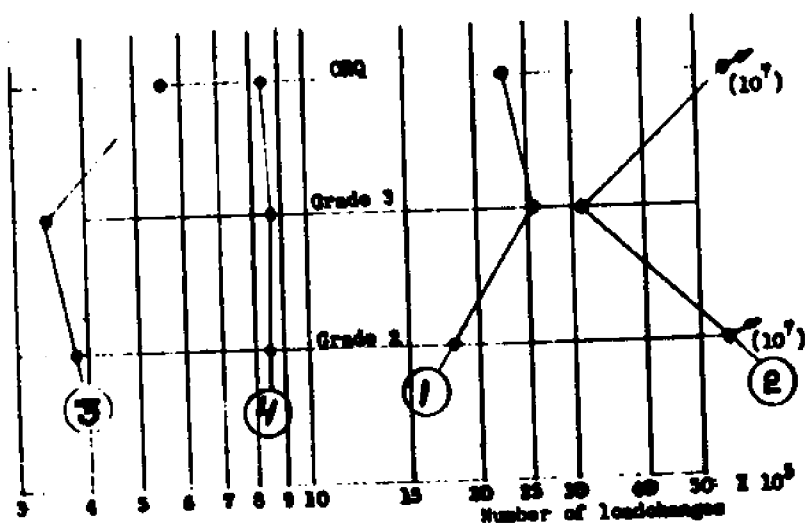

Test serie A

Celander

2.5 Anchor Chain Fractures

[Taraldsen 85]

- Statistics from 81 well-documented fractures are given

- Chain Quality, Fracture Appearance, Proof Load, Influence of Fairleads and Probability Aspects are discussed

- Unstable failure of a brittle manner is found to be the major failure mechanism preceded by little or no fatigue cracking

Anchor Chain Fractures

81 well-documented fractures

The fractures are mainly from the North Sea, mainly for the last 9 years and the bulk of them, about 2/3, is from Norwegian-owned rigs

AVAILABLE	NUMBER
FRACTURED CHAINS	81
LABORATORY REPORTS	66
FRACTURED LINKS	41

FIG. 2. Sources of Information

TYPE OF FRACTURE	NUMBER
FATIGUE	1
BRITTLE FRACTURE	39
DUCTILE OVERLOAD	2
SUM	42

FIG. 3. Number of different kinds of Fracture

[Taraldsen 85]

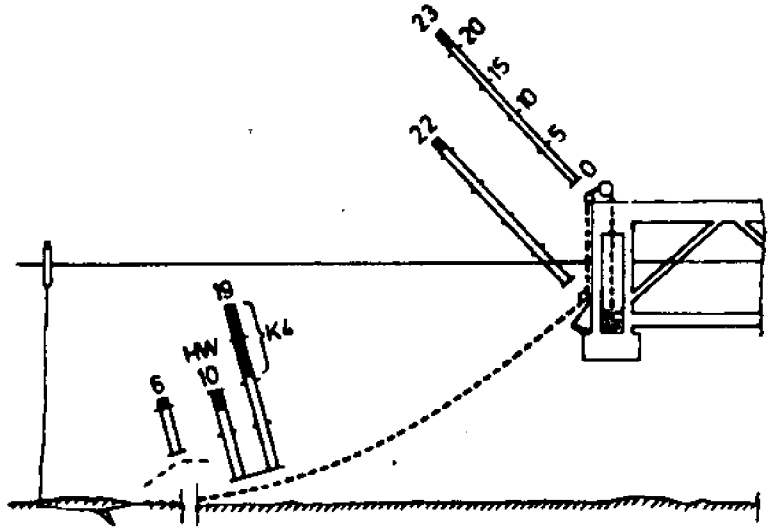

HW = HARD WEATHER - - - = CHASING ETC.

FIG 4 Location of 80 Chain Fractures (14 K4)

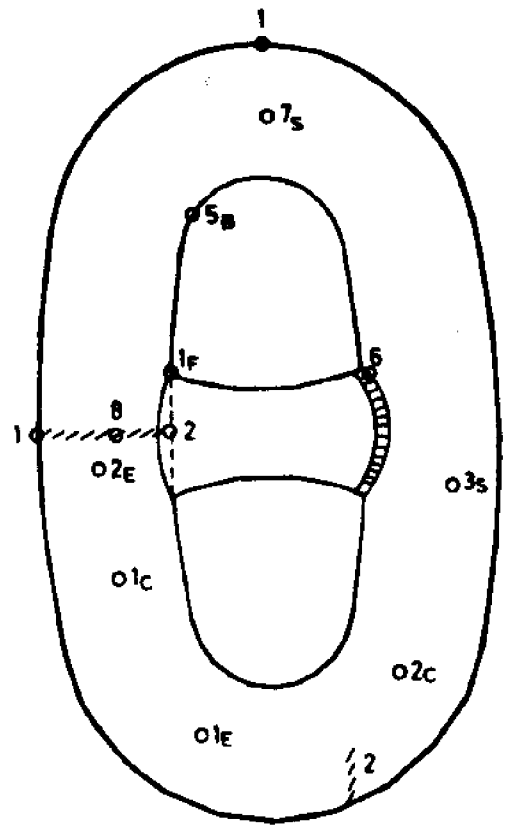

INDEX B= BURNT, C = CARBURIZED, E= ELECTRODE BURNMARK
F= FATIGUE, L= OVERLOAD, S= SMEAR OR SOOT MARK

FIG 5 Location of 42 Fractures

2.6 Summary of the 4-Year Research Project : Anchor Chain Cables Offshore

[Lereim 85]

- Aspects related to the reliability of offshore mooring chains of the grade Oil Rig Quality

- The Veritas Joint Industry research project was performed on 76 mm and 40 mm diameter chains of common links and connecting links at 3 cyclic load levels in air (Fig.3)

- Connecting links of Kenter type should be avoided in lines used for long-term permanent moorings, where fatigue considerations may become critical

- Fracture Strength and Toughness, Fatigue Strength, Stress Analysis and Line Tension Analysis, Reliability of Applied NDE Method

the Veritas Joint Industry Research Project

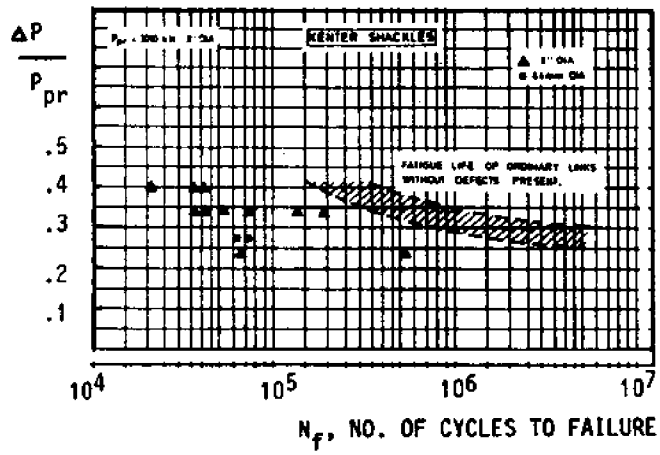

Fig. 3 Fatigue tests ORQ Chain.

Fatigue tests were performed on 76mm and 40mm diameter chains of ordinary links and connecting links. Testing was performed at 3 cyclic load levels only, and in air environment. Therefore, the experimental fatigue results should mainly be treated as reference test results and not as the typical real fatigue strength in corrosive environment.

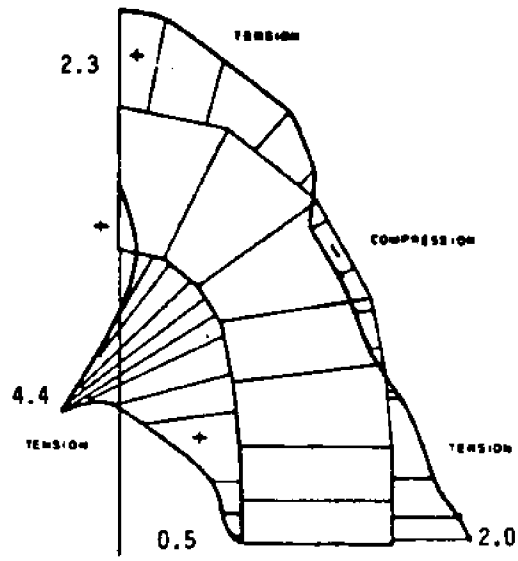

Fig. 6 Stress and SCF profile in midplane of link in pure tension loading.

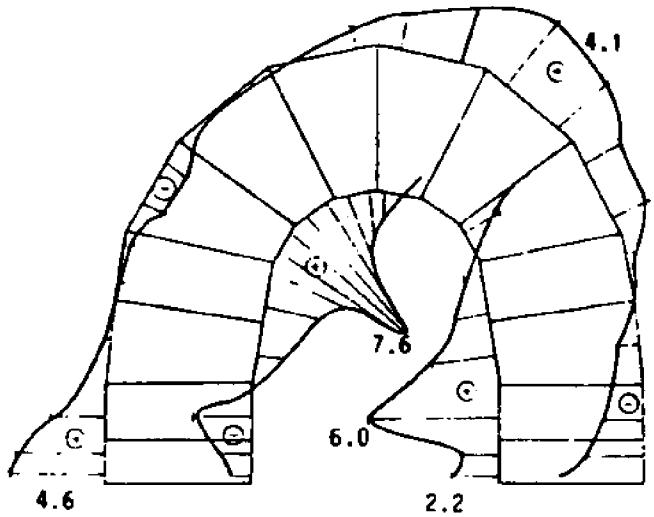

Fig. 7 Stress and SCF profile in mid plane for tension/bending loading of vertical link.

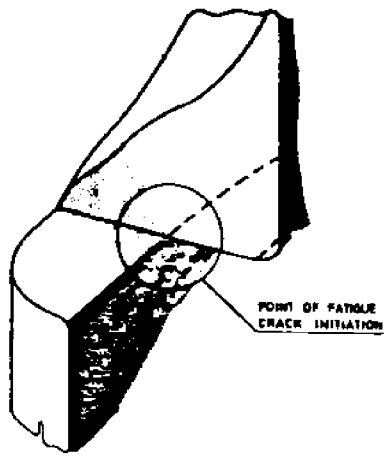

Fig. 4 Severe localized SCF in Kenter link.

the high local stress concentrations must be reduced, for example by increasing the minimum allowable groove radius and grinding the intersecting corners.

Lereim

2.7 Static and Fatigue Tests on Chain Links and Chain Connecting Links

[Helvoirt 82]

- The static strength and the fatigue strenth of common 3-inch stud-link chain and of various types of 3-inch conneting links

- The connecting elements have been found to be the weakest part in each mooring line

- Kenter-type connecting link, Baldt-type connecting link D-shackles

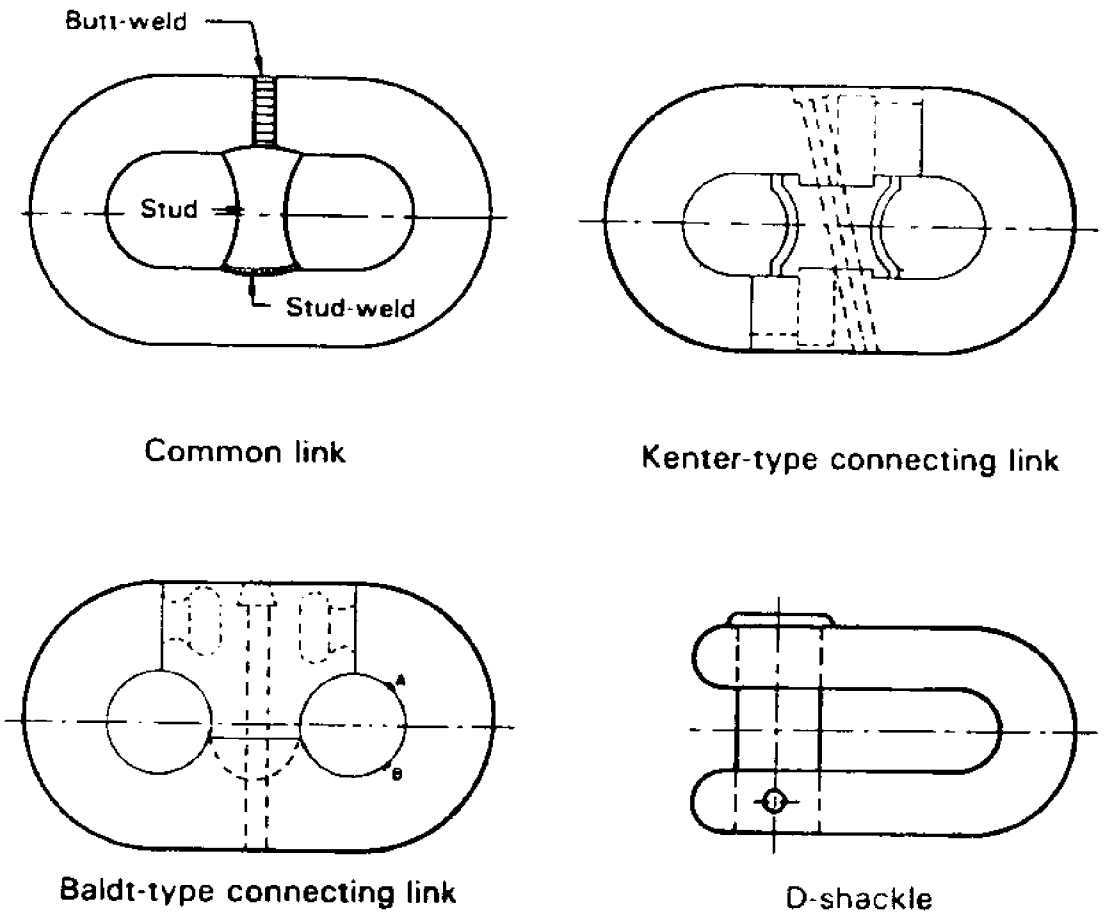

Fig. 1 MOORING ELEMENTS.

[Helvoirt 82]

alternating load was chosen between 800-1200 kN, because:

(a) a mean of 1.0 MN is realistic in 3-inch anchorline design,

(b) a range of 400 kN leads to an expected fatigue life of 1 - 2×10^6 cycles in the common links (according to AWS-AA).

Table 1

SUMMARY OF RESULTS OF FATIGUE TESTS

Type	Relative fatigue life
Common link	1
Kenter-type connecting link	0.2
Baldt-type connecting link	0.3-0.9
D-shackle	> 1

[Helvoirt 82]

References

[Berg 80] Berg A. and Taraldsen A.
Long-Term Mooring and Anchoring of Large Structure and Drilling Units -- Reliability and Safety of Anchor Chain Systems.
Offshore Technology Conference (OTC 3813), 1980.

[Celander 72] Celander Ivar.
Preload Influence on Fatigue Characteristics of Chain Cable Exposed to Salt Water and AQtmospheric Conditions.
Offshore Technology Conference (OTC 1578), 1972.

[Gibson 83] Gibson P.T.
Wire Rope.
1983.

[Hanzawa 81] Hanzawa M., Yokota H., Toda Y. and Yokoyama K.
Fatigue Behavior of Large-Diameter Wire Ropes.
Offshore Technology Conference (OTC 3999), 1981.

[Helvoirt 82] van Helvoirt L.C.
Static and Fatigue Tests on Chain Links and Chain Connecting Links.
Offshore Technology Conference (OTC 4179), 1982.

[Lereim 85] Lereim J.
Summary of the 4-Year Research Project : Anchor Chain Cables Offshore.
Offshore Technology Conference (OTC 5060), 1985.

[Lucht 77] Lucht W.A. and Donecker F.W.
Factors Affecting Wire Rope in a Marine Environment.
Offshore Technology Conference (OTC 2924), 1977.

[Matanzo 72] Matanzo Frank.
Axial Fatigue of Wire Rope in Sea Water.
Offshore Technology Conference (OTC 1579), 1972.

[Ronson 80] Ronson K.T.
Ropes for Deep Water Mooring.
Offshore Technology Conference (OTC 3850), 1980.

[Savastano 67] Savastano F.
Seleting Wire Rope for Oceanographic Applications.
UnderSea Technology 8(2), 1967.

[Shoup 84] Shoup G.J. and Mueller R.A.
Failure Analysis of a Calm Buoy Anchor Chain System.
Offshore Technology Conference (OTC 4764), 1984.

[Stange 83] Stange W.F.
Laboratory Testing for Enhanced Undersea Cable Survivability.
In *Proceedings of the Second International Offshore Mechanics and Arctic Engineering Symposium*, pages 347. Jan-Feb, 1983.

[Stern 78] Stern I.L. and Wheatcroft.
Toward Improving the reliability of anchor chain and accessories.
Offshore Technology Conference (OTC 3206), 1978.

[Taraldsen 85] Taraldsen A.
Anchor Chain Fractures.
Offshore Technology Conference (OTC 5059), 1985.

[Thorpe 83] Thorpe T.W. and Rance Andrew.
the Tensile Fatigue of Wire Rope : a New Approach.
Offshore Technology Conference (OTC 4638), 1983.

[Waters 85] Waters D., Eggar D., and Plant H.
Develpments in Fatigue Assessments of Large-Diameter Wire Ropes used in Offshore Moorings.
Offshore Technology Conference (OTC 5000), 1985.